2011

Single-molecule detection and microfluidics: generating systems for the in vitro diagnostics of stroke

Brandon M. Young
Louisiana State University and Agricultural and Mechanical College, byoun26@tigers.lsu.edu

SINGLE-MOLECULE DETECTION AND MICROFLUIDICS: GENERATING SYSTEMS FOR THE IN VITRO DIAGNOSTICS OF STROKE

A Thesis

Submitted to the Graduate Faculty of the

Louisiana State University and

Agricultural and Mechanical College

in partial fulfillment of the

requirements for the degree of

Master of Science

In

The Department of Chemistry

By

Brandon M. Young

B.S., Bowling Green University, 2007

December 2011

TABLE OF CONTENTS

List of Figures……..……...……...…iv

Abstract…….…….....viii

Chapter 1. Introduction to Single-Molecule Detection in Microfluidics…..……1
1.1. Gene Expression...…….……...…….…….……...1
1.2. Conventional Methods……...……...…...…2
1.3. Biomarkers……...……..…….....5
1.4. Genetic Analysis……...6
1.5. Single-Molecule Detection (SMD)…….…….…….....7
1.6. Molecular Probes/Molecular Beacons (MB)……...……..……8
1.7. Fluorescence Resonance Energy Transfer MBs……...……...11
1.8. Ligase Detection Reaction-based Assays (LDR)..…….……14
1.9. Ligase Detection Reaction Using Single-Pair FRET…...……...…….15
1.10. LDR-spFRET……..…...……..……17
1.11. Microfluidics……...……..……18
1.12. Microfluidics and Its Importance to SMD……...……...……...19
1.13. Objective of the Project……...……..……20
1.14. Report Outline…….……21
1.15. References……...……..……22

Chapter 2. Experimental for Single-Molecule Detection in Microfluidics. …….……..…32
2.1. Thesis Experimental…….……..32
2.2. Polymerase Chain Reaction (PCR) Amplification of Genomic DNA...…..…...……...34
2.3. Ligase Detection Reaction (LDR)……...……37
2.4. LDR Primers and Molecular Beacon Design ……...…….....38
2.5. Microfluidic Chip Design and Fabrication ……...……....…39
2.6. Instrument Design……..41
2.7. Microfluidic Chip Optimization……...……...……...….44
2.8. RT-PCR ……...…...……..48
2.9. LDR-spFRET via SMD Data...……...…….....51
2.10. References…..……..……53

Chapter 3. Design and Development of a Field-Deployable Single-Molecule Detector (SMD) for the Analysis of Molecular Markers ……56
3.1. Introduction……...……...…56
3.2. Experimental…...……..…61
3.3. Results and Discussion..…….....66
3.4. Conclusions ……...……77
3.5. References……...…78

Chapter 4 - Discussions, Conclusions and Future Works……83
4.1. Discussions……83
4.2. Conclusion……..…..……..…86
4.3. Future Work…….……..……..…86

Vita……90

LIST OF FIGURES

Figure 1.1 Transcription of DNA to RNA to protein forms the backbone of molecular biology and is represented by four major stages: 1) DNA replicates its information in **replication**, 2) DNA codes for messenger RNA (mRNA) in **transcription**, 3) mRNA is **processed** (essentially by splicing) and migrates from nucleus to cytoplasm. 4) mRNA carries coded information to ribosomes, which "reads" this information and uses it for protein synthesis in **translation…**……..……1

Figure 1.2 RT-PCR procedures via SYBR-Green, an intercalating dye that fluoresces upon light excitation when bound to double stranded DNA. The double stranded DNA is formed when adjusting conditions that promote the steps of denaturation, annealing and extension: 1) The reaction is first heated to **95ºC** to melt (**denaturation)** the **dsDNA** into separate strands. 2) The reaction is then cooled to **~50ºC**, the temperature at which the **primers** will find base-complementary regions in the **ssDNA**, to which they will stick (**annealing**). 3) The reaction is finally heated to **72ºC**, the temperature at which the ***Taq*** enzyme replicates the primed **ssDNA** (**extension**)……..3

Figure 1.3 The single-stranded oligonucleotides form a closed stem and loop structure in the absence of target DNA and open the stem when hybridized to the target DNA. These Molecular beacons in the closed form have a quencher in proximity to the fluorophore and emits no fluorescence. In the open form of the MB probe, the quencher and fluorophore are separated due to a conformational changes that result in the detection of fluorescent signal. …….9

Figure 1.4 Smart probes use a series of guanosines to quench the fluorophore in the closed DNA hairpin loop instead of a traditional quencher. This makes the fabrication of the DNA probe inexpensive and less labor intensive because only the 5' end is modified. The probe used here was designed to test for a SNP in TB responsible for rifampicin resistance.[133]…… ……..10

Figure 1.5 The fluorescent dyes Cy5 and Cy5.5 are a commonly used FRET pair. The Cy5 dye can be excited with a HeNe laser diode. The Cy5 dye will transfer its energy to Cy5.5 when they are in close proximity. For this dye pair R_0 distance is 61.7 Å..……...……..12

Figure 1.6 (A.) The schematic of spectral overlap (B.) The excitation/emission wavelength spectra of Cy5 and Cy5.5……...……..…13-14

Figure 1.7 Schematic of the LDR-spFRET assay in which two allele-specific primers are labeled at their 3'- and 5'-ends with fluorescent dyes and flank a SNP on the target template. An enzyme, Taq DNA ligase, covalently joins the two adjacent primers when perfectly matched to the template, forming a molecular beacon that can undergo FRET whereas mismatched primers remain unligated and do not show FRET. The detection temperature of the assay was maintained at 75ºC to melt the duplex formed between the target and LDR primers as well as stem sequences of unligated primers but not the stem of the fully formed beacon..……...……..14

Figure 2.1 Gene expression profiles of biomarkers that are characteristic of stroke…..……...……..32

Figure 2.2 RT-PCR Thermal Profile. ……..…….....35

Figure 2.3 LDR Thermal Profile. ……..……...36

Figure 2.4 LDR Primers and reverse Molecular Beacon Designed to undergo FRET. ……...……..…..37

Figure 2.5 Microfluidic chip AutoCAD Design that illustrates a chip model that has multiple detection zones in the dimensions of 100µm x 100µm, 50µm x 50µm, 25µm x 25µm, and 15µm x 15µm respectfully..……..38

Figure 2.6 Plot illustrating the measuring of the amount of energy needed to melt the COC polymer sample to identify the T_g. ……...……..39

Figure 2.7 The employed polymer is a cyclo olefin copolymer (COC) copolymerized from norbornene and ethylene using a metallocene catalyst. This polymer has a very low auto-fluorescence, which is the natural emission of light by biological entities. COC has a high moisture barrier, excellent chemical resistance, high heat resistance and long shelf life, which makes it a perfect subtract for this work.. ……..…...……40

Figure 2.8 (a) Picture of the compact SMD instrument connected to a mini-computer for data collection and instrument control. (b) Access panel for loading sample into the microfluidic chip and connecting the collection fiber optic to the fiber U-bench, which contained optical fibers and was interfaced to the SPAD. (c) Inside the compact SMD instrument showing the arrangement of the VCSEL, SPAD, FPGA and other peripheral electronics. (d) Schematic of the FPGA that was used for data acquisition and single-photon processing. The FPGA counted signals from the SPAD and output information to the first-in first-out (FIFO) memory. (1) – USB interface cable to the controlling computer; (2) – microfluidic chip sitting atop a mounting stage, which is accessed through a drawer that slides out from the main instrument case; (3) – controlling computer; (4) – fiber bench with optical cable connected to the fluidic chip; (5) – SPAD with integrated fiber optic; (6) – cooling fan for the FPGA, which is located underneath this fan; (7) – various power supplies; (8) – fiber bench with optical filters; (9) – VCSEL with integrated fiber; and (10) – electrophoresis power supply to actuate fluids electronkinetically…….41

Figure 2.9 Graph shows the increase of fluorescent events and their intensity, in equivalent LDR-spFRET product dilutions, which have been subjected to SMD methodology ...……...……....44

Figure 2.10 Graph shows an increase of fluorescent events and their intensities, in equivalent LDR-spFRET product dilutions for channel dimensions 50 µm to 100 µm via SMD, but decreases when sample is detected in 25µm……44

Figure 2.11 The calculated angle shown is determined by the interactions across the three interfaces. This test is illustrated with a small liquid droplet resting on a flat horizontal solid surface. The Young's relation or Wetting, which observes the ability of a liquid to maintain contact with a solid surface, determines the droplets shape…….46

Figure 2.12 (A.) The surface activation is characterized by the modification of chemical surface properties which is based on chain scission, the formation of functional groups, and cross-linking on the surface based on plasma generated components mainly UV radiation, charged particles (ions), and radicals, which in turn reacts using an oxygen molecule to producing hydro-peroxides, ketones, aldehydes, carboxyls, hydroxides, and ester groups. (B.) O2 plasma modification - The reaction is initiated with atomic oxygen, which abstracts a hydrogen atom from the surface. This result in a free radical on the surface, which in turn can react with an oxygen molecule to producing hydro-peroxides, ketones, aldehydes, carboxyls, hydroxides, and ester groups. The plasma oxidation results furthermore in breaking the polymer chains and material removal. A specific surface functionalisation is possible under precise control of the reaction conditions……...47

Figure 2.13 Agarose gel electrophoresis using 1.8% TBE (Tris-Borate-EDTA) for sample injection well; to confirm the Human genomic DNA and probing primer assembly to form PCR products (152 bp)……...…….....47

Figure 2.14 RT-PCR Amplification plot of Human genomic DNA diluted in a 10-fold dilution series (copy numbers 0; 22.8; 45.6; 91.2; 228; 456; 912; 2280; 4560; 9120) and amplified using SYBR Green I. ……...……..48

Figure 2.15 (a.) Above. A calibration plot showing the various fluorescence intensities in correlation to the genomic DNA (copy number dilutions) employed (i.e. 0; 22.8; 45.6; 91.2; 228; 456; 912; 2280; 4560; 9120).....49

Figure 2.15 (b.) Below. A standard curve was derived from the serial dilutions in a customary manner. Relative concentrations were expressed in arbitrary units. Logarithms (base 10) of concentrations were plotted against crossing points. Least square fit was used as the standard curve……...……..49

Figure 2.16 Optimized microfluidic chip, which put to use Polymer COC; 25X25 μm channel detection window; Pumping injection method; O_2 plasma modification……...…….50

Figure 2.17 Beckman Coulter GenomeLab Plot of LDR-spFRET products. The above graph is showing at ladder marker labeled for 20 nucleotides, we see large peaks characteristic of the non-ligased primers. Furthermore, the data illustrates peaks between 1600-1700 time (min) characteristic of ligased products……..…...……....51

Figure 2.18 Calibration plot of channel dimensions at various copy numbers dilutions presented by plotting the number of photon events versus the copy number……...…….....52

Figure 3.1 (a) Picture of the compact SMD instrument connected to a mini-computer for data collection and instrument control. (b) Access panel for loading sample into the microfluidic chip and connecting the collection fiber optic to the fiber U-bench, which contained optical fibers and was interfaced to the SPAD. (c) Inside the compact SMD instrument showing the arrangement of the VCSEL, SPAD, FPGA and other peripheral electronics. (d) Schematic of the FPGA that was used for data acquisition and single-photon processing. The FPGA counted signals from the SPAD and output information to the first-in first-out (FIFO) memory. (1) – USB interface cable to the controlling computer; (2) – microfluidic chip sitting atop a mounting stage, which is accessed through a drawer that slides out from the main instrument case; (3) – controlling computer; (4) – fiber bench with optical cable connected to the fluidic chip; (5) – SPAD with integrated fiber optic; (6) – cooling fan for the FPGA, which is located underneath this fan; (7) – various power supplies; (8) – fiber bench with optical filters; (9) – VCSEL with integrated fiber; and (10) – electrophoresis power supply to actuate fluids electronkinetically……...……..61

Figure 3.2 (a) Design of the polymer-based microfluidic chip with integrated fiber optics for delivering excitation light to the chip and collecting the resulting emission. The fibers were placed in guide channels embossed into the chip to allow exact placement during chip assembly and were oriented at 90° with respect to each other. The chip also contained a backside heater to control the temperature for hybridization-based assays. (b) Fluorescence image of the field-of-view of the excitation and emission fibers showing the intersection of the optical paths, which defined the probe volume, which was determined to be 98 pL in this case. The chip was filled with Alexa Fluor 660 dye to generate the necessary image……...…….....64

Figure 3.3 (a) Simulation of the flow velocities and flow vectors of the fluid as it moved from the input channel into the detection zone (units are m/s). The simulation was run using Fluent software with quad elements meshing and 80,000 nodes performed in Gambit. An outline of the probe volume as determined from Figure 1 (b) is shown as well (black dotted line). (b) 3D surface plot of the detection zone versus the irradiance experienced by single fluorescent entities as they traverse through the probe volume. The irradiance decreased as the beam expanded and thus, single fluorescent entities traveling along the edges of the Gaussian intensity profile show reduced photon fluxes……...…….68

Figure 3.4 Photon burst data collected using the compact, field deployable SMD instrument. The red trace shows the blank and the black trace is the data with fluorescent beads or dye seeded into the buffer. (a) Plot of photon bursts generated from fluorescent microspheres. (b) Single Alexa Fluor 660 dye molecule burst data. ……69

Figure 3.4 (c) Autocorrelation analysis was performed on the blank, fluorescent spheres and Alexa Fluor 660 dye molecule solutions. The fluorescent microspheres and the Alexa Fluor dye molecules showed transit times of 49 ms and 53 ms, respectively, using the same flow rate……...…….....70

Figure 3.5 (a) Trace data of photon bursts detected using a confocal LIF setup. A threshold level of 3,000 cps was set to discriminate true single particle events against background fluorescence fluctuations. (b) Trace data of photon burst data detected using the compact SMD instrument. In this case, a threshold level of 40,000 cps was set to discriminate single particle events against background fluorescence fluctuations. (c) Histogram of photon burst intensity constructed from data set in (a) using the confocal LIF setup. The accepted photon bursts were compiled into bins of 5,000 cps. (d) Histogram of photon burst intensity from data set in (c) using the compact SMD instrument. The data in this case were accumulated into bins of 20,000 cps……...……...72

Figure 3.6 Complementary DNA was mixed with 0.5 nM of the MBs and pumped through the microfluidic chip at 0.01 mL/h. The target concentrations used in this case were; (a) 5.0 x 10^{-16} M; (b) 1.0 x 10^{-15} M; (c) 5.0 x 10^{-15} M; and (d) 1.0 x 10^{-14} M……...…….76

Figure 3.7 (a) Calibration plot generated from the data shown in Figure 6. The data points were fit to a linear function; y = 3 x 10^{15} x – 0.9291, with R^2 = 0.97. (b) rDNA extracted from 2,000 *S. aureus* cells (Gram (+)) and mixed with the 0.5 nM MB solution. As a control, DNA from *E. coli* (Gram(-)) was extracted and mixed with the MB solution as well. The *S. aureus* showed 3 events above the discrimination level whereas the *E. coli* showed no events above this level……...……...77

Figure 4.1 (A., B.) Calibration plots for the merit comparing of methods LDR-spFRET and RT-qPCR. The probing primers are both located in the same 152 (bp) gene sequence succession of the AMPH biomarker target. The biological samples were both at copy number concentration between 0-10,000. The experiment tests were replicated three times and plotting at their means...……...……..83-84

Figure 4.2 Proposed SMD microfluidic devise using LDR-spFRET methods for the diagnostic of stroke....…….88

Figure 4.3 Proposed SMD microfluidic devise using LDR-spFRET design for the diagnostic of stroke....…...……89

ABSTRACT

Key words: Stroke, Single-Molecule Detection, Microfluidics, Biomarkers

There is currently no available molecular diagnostic test for stroke; the common modality for diagnosis consists of computed tomography or magnetic resonance imaging. Unfortunately, the use of these diagnostic regimens can delay proper therapeutic treatment, which requires administration within the first 3 h of a stroke event. We are developing a molecular assay that can report, in near real time and at the point-of-care, the presence or absence of biomarkers specifically targeted for the diagnosis of ischemic or hemorrhagic stroke. The proposed strategy uses blood-borne mRNAs that are either under-expressed or over-expressed as a result of tissue damage within the brain. The ability to report on these diagnostic markers is enabled through the use of a fluidic bio-processor fabricated in polymers via micro-replication to provide autonomous sample processing. This bio-processor comprises a fluidic motherboard that possesses task-specific modules for the selection of white blood cells from a blood sample, cell lysis and solid-phase extraction of the mRNA markers, ligase detection reaction to identify the mRNA markers and an optical module for multiplexed detection. The sample-processing pipeline was streamlined to generate a rapid assay turn-around-time by employing single-molecule detection. The output of the clinical sample processing hardware are molecular beacons undergoing single pair Fluorescence Resonance Energy Transfer (spFRET) that are digitally counted to provide exquisite analytical sensitivity for the expression profiling of the relevant mRNA markers. The presentation will discuss the use of spFRET for mRNA expression profile with comparisons made to quantitative real-time PCR.

CHAPTER 1 - INTRODUCTION

1.1 Gene Expression

The significance of gene expression profiling is evident in an array of clinical, pharmaceutical and industrial applications. [4,27-28,50,52,53,63,74,84] Researchers have just begun to understand the importance of manipulating and quantifying the relative activity of target genes, which have been emphatically identified. Even more, studies have substantiated their important real world medical employments, for example in the case of cancer and HIV.[85] The advent of next-generation sequencing/gene expression analysis is an increasingly popular science, making "digital" alternatives to microarrays and other sequence identification technology novel.

Gene expression is the process by which information from a gene is used in the synthesis of a functional gene product; this then utilizes the central dogma of molecular biology, which includes: transcription, RNA splicing, translation, and post-translational modification of a protein.

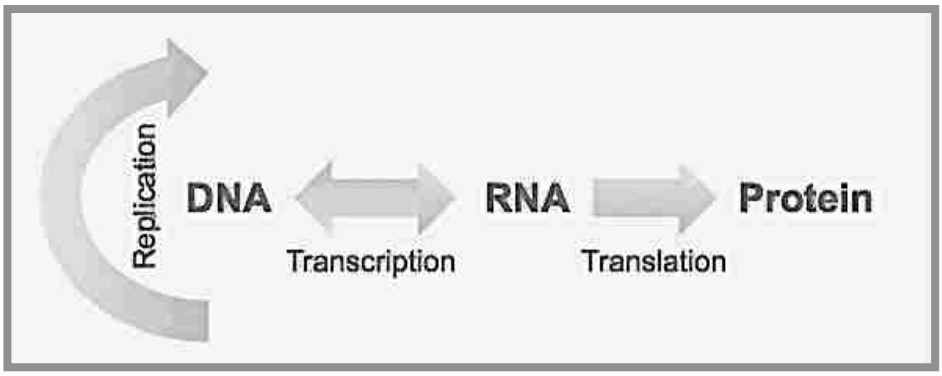

Figure 1.1 Transcription of DNA to RNA to protein forms the backbone of molecular biology and is represented by four major stages: 1) DNA replicates its information in **replication**, 2) DNA codes for messenger RNA (mRNA) in **transcription**, 3) mRNA is **processed** (essentially by splicing) and migrates from nucleus to cytoplasm. 4) mRNA carries coded information to ribosomes, which "reads" this information and uses it for protein synthesis in **translation**.

The process of gene expression is used by all known life to generate the macromolecular machinery for life: eukaryotes, including multicellular organisms; prokaryotes, including bacteria, archaea, and viruses. Regulation of gene expression (or gene regulation) is the function that controls the way information in genes is turned into gene products, in turn giving the cell control over structure and function; it is the basis for cellular differentiation, morphogenesis, and the versatility and adaptability of any organism to their environment and/or physiological events. For instance, changes are prevalent where disease, external stimuli, injury, or changes in normal anatomy have occurred. Gene expression serves as a substrate or biomarker for change due to the process of gene regulation and the function incurred to control the timing, location, and amount of gene expression. This has been observed to have a profound effect on the behavior/activity of the gene in a cell or in a multicellular organism.[94] Therefore, through studies of a specific gene activity (over expression or under expression) and its expression profile, the diagnoses of various physiological events can be realized.

1.2 Conventional Methods

There are many methods in molecular biology for gene expression profiling and measuring quantities of target nucleic acid sequences like biomarkers. The conventional methods include, but are not limited to, Southern blotting, [90] serial analysis of gene expression (SAGE), [86] DNA microarrays, [87] and RT-qPCR. [4, 88] However, most of these methods exhibit one or more shortcomings. It is often the case that conventional methods prove to be time consuming, laborious, insensitive, non-quantitative, use dangerous radioactivity, or have substantial probability of cross contamination. [4, 86,87,88,90] In recent years, it has become evident among the science community that the Quantitative Real-Time PCR (RT-PCR) approach is seemingly the most accurate, sensitive and simple method of gene expression level analysis (Figure 1.2). RT-

qPCR, with the use of Sybr Green I intercalating fluorescent dye, is said to provide the most economical and easy-to use application of real-time technology.[93] This method combines the nucleic acid amplification and detection steps into one homogeneous assay and obviates the need for gel electrophoresis to detect amplification products. With the use of the appropriate chemistries and data analysis, the need for Southern blotting or DNA sequencing for amplicon identification is eliminated.[89]

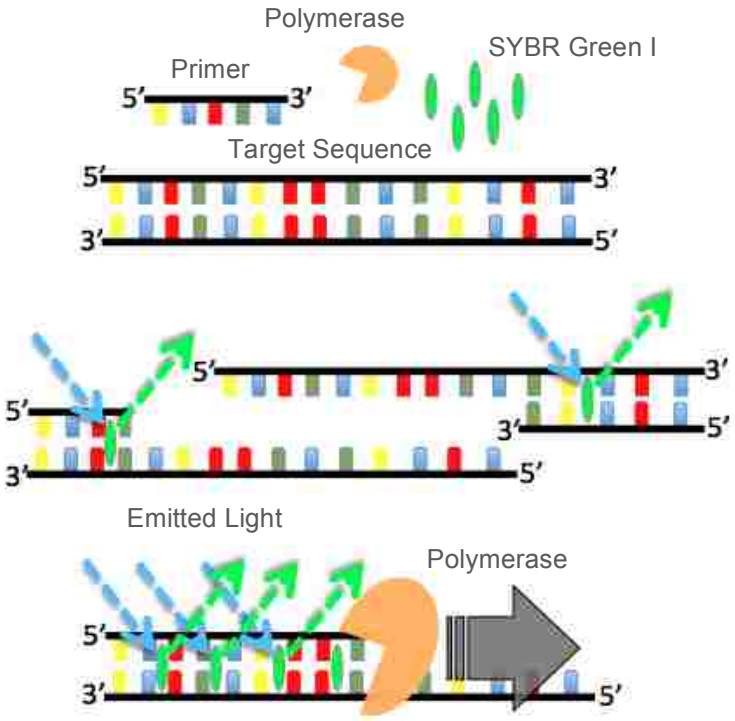

Figure 1.2 RT-PCR procedures via SYBR-Green, an intercalating dye that fluoresces upon light excitation when bound to double stranded DNA. The double stranded DNA is formed when adjusting conditions that promote the steps of denaturation, annealing and extension: 1) The reaction is first heated to **95ºC** to melt (**denaturation)** the **dsDNA** into separate strands. 2) The reaction is then cooled to **~50ºC**, the temperature at which the **primers** will find base-complementary regions in the **ssDNA**, to which they will stick (**annealing**). 3) The reaction is finally heated to **72ºC**, the temperature at which the ***Taq*** enzyme replicates the primed **ssDNA** (**extension**).

Quantitative Real-Time PCR's desired simplicity, specificity and sensitivity, with the potential for high throughput and the versatile design to procure new chemistries, has deemed qPCR the benchmark technology for the detection and/or comparison of gene expression profiling (Figure 1.2). PCR has several disadvantages that must be addressed, despite its

influence in genomics-based analyses. The first issue that must be confronted is that of time; typically, PCR is carried out using protocols requiring 30 cycles of 2 hours processing time (240 seconds per cycle).[55, 56] In addition to the issue of time, there are drawbacks with the amplification process. It has been discovered that reproducible quantification of any low abundance target (< 1000 copies) is problematic due to the inherent limitation of PCR amplification of small amounts of template contained within a complex nucleic acid mixture (Monte Carlo effect).[91] The process is highly susceptible to misinterpretation of sequences due to contamination, mis-priming and formation of artifacts. This is largely due to a lack of normalization strategy to control for the amount of starting material, variation of amplification efficiencies and differences between complex biological samples. But yet, RT-PCR has held true against high quality samples to produce quantification results that are biologically relevant, commonly proven using internal controls such as reference genes, sometimes also called "housekeeping genes".[89,57,92] Secondly, since many biological samples contain inhibitors of the RT and/or the PCR step, it is crucial to assess the presence of any inhibitors of polymerase activity in RT and PCR. The design of PCR primers employed also causes unforeseen problems/constraints; some targeted gene sequence regions are difficult to amplify using PCR, regions that include highly repetitive regions and/or DNA regions with high GC content. Therefore, in consideration of these matters, it would be advantageous to develop a genomics-based analysis technique to improve the biological validity of quantitative data.

With the recent interest and understanding for the analysis of gene expression, the novel technique of Single-Molecule Detection or SMD, has become extremely relevant to gene quantification analysis. This is due to the sensitivity necessary for gene expression analysis because of limited sample volumes. The progressive method, SMD, will be the detection

technique under investigation, in respect to this studies theory, and will be integrated with microfluidic devices. In this study, SMD measured gene expression of targeted biomarkers will be employed to render reliable, quantitative and reproducible data.

1.3 Biomarkers

A biomarker is a biological molecule, which can be found in blood, urine, and other bodily fluids; biomarkers also manifest in tissues that are modified by a particular disease state, as well as tissues verified to be an indicator for a particular state of an organism. Biomolecules such as lipids, carbohydrates, proteins, and nucleic acids have key cellular roles, which make them ideal and important biomarkers for measuring the response to external stimuli. Additionally, biomarkers signal normal or abnormal processes to tell how well the body responds to treatment for a disease or condition. Consequently, the biomarkers' functional interaction makes the discovery and use of them as medical diagnostic and/or prognostic indicators valuable. However, studies have shown that biomarker analysis exhibits challenging analytical obstacles due to the employment of limited sample sizes, the complex matrices of applied samples, and the low abundance of targeted biomarkers/genes.

Single-molecule detection (SMD) offers an attractive approach for identifying and quantifying the presence of biomarkers that show promise in respect of in-vitro molecular diagnostics in near-real time, due to the ability to eliminate sample-processing steps (for example, eliminating the need for amplification steps, such as PCR). The ability to monitor biomarkers using this simple and portable instrument will have a number of important applications, such as strain-specific detection of pathogenic bacteria and the molecular diagnosis

of diseases requiring rapid turn-around-times directly at the point-of-use by means of a portable instrument, which will be outlined in Chapter 3.[27]

1.4 Genetic Analysis

Analysis of genetic material such as DNA or RNA, in a clinical laboratory for diagnostics involves a number of critical molecular processing steps that include: 1) sample collection, 2) DNA extraction and purification, 3) target enrichment/amplification, 4) scanning or identification of molecular alterations or sequence-specific reporters, and 5) detection of the products generated as a result of step four. First, samples are collected from bodily fluids and/or tissues. The targeted molecules contained within those samples are then isolated from potential interferences by the selective extraction and purification of the sample, which is normally accomplished through procedures such as ultracentrifugation, liquid-liquid extraction, precipitation, or solid-phase extraction. Following this extraction, selected genes of interest are amplified for further molecular analyses. Finally, the target DNA is analyzed or detected by a number of formats, for example fluorescence.[4] As illustrated in studies when SMD is coupled to biological analyses, the high sensitivity enables the detection of target sequences in limited biological samples without amplification. Therefore, SMD holds promise for the analysis of biomolecules and biomarkers (over expression or under expression) by streamlining the steps required in the assays, potentially creating the possibility for near real-time results.[1.8]

DNA analysis is being harnessed for a number of diagnoses, such as detection of infectious agents, paternity testing and many more.[58] However, when these types of analyses are coupled with SMD, there is the potential to eliminate processes such as PCR. Previously, it was described that there are several disadvantages to using PCR. However, it has been studied that

when SMD is used for the same process analysis, there is immediate improvement. It is evident that there is increased analysis speed due to the nullification of limitation set forth by PCR instrumentation. Additionally, it has been realized that SMD is highly sensitive due to the use of fluorescence, which is utilized by using Ligase Detection Reaction via Single-Pair FRET. It is also notable, that SMD provides for the direct sequencing of DNA as seen for example, Castro's work demonstrating a technique for the rapid detection of specific nucleic acid sequences in unamplified DNA samples from *Bacillus anthracis*.[28] Through these improvements, single-molecule detection (SMD) of DNA would be highly beneficial in determining gene expression level and identifying of an array of targeted sequences.[46-49, 51,59-67] Therefore, the focus of this thesis will be on the advantages gained by using SMD with genomics-based analysis.

1.5 Single-Molecule Detection (SMD)

The potential of SMD in liquids has been realized and shows promise in an array of applications. For example, the Soper research group has shown the ability to distinguish between molecules of Texas red and Rhodamine 6G using fluorescence coupled with SMD.[1] Furthermore, detection of other single rhodamine molecules have also been distinguish using hydrodynamic flow cells.[2, 3] When pursuing this technique further, DNA has been sequenced through the detection of isolated fluorescently tagged mononucleotides.[4] The work illustrated by Hirschfield in 1976, describing detection of a single antibody molecule that was labeled using 80-100 fluorophores, is noted to be the origin of the development of the SMD technique. Keller and coworkers later used hydrodynamically focused flows of molecules to show the decreasing limit-of-detection in terms of molecule numbers and thus reported their ability to detect individual florescent molecules in 1990.[2-3]

SMD begins with the photon burst; a photon burst results when a single molecule is resident in a laser beam, where it can be cycled between the excited state and ground state with subsequent emission of a single fluorescent photon. The continued cycling process produces a burst of photons. Fundamentally, as the fluorophore is excited, several pieces of information can be gathered. These characteristics include their relative brightness, fluorescence lifetime, concentration, and even electrophoretic drift.[12] Due to the capability to deduce this variety of information, single-molecule spectroscopy (SMS), is currently used to quantitatively measure single molecule properties, including gene expression via fluorescence resonance energy transfer (FRET), as seen in this study. Essentially this method for analysis has allowed for protein, DNA-based and RNA-based analysis, while demonstrating a level of detection that is thought to be currently unparalleled.[1-5,7-11,28] Through this process, individual molecules can be detected with highly accurate and quantitative measurements.

1.6 Molecular Probes/Molecular Beacons (MB)

Molecular beacons are oligonucleotide probes that can report the presence of specific nucleic acid sequences in homogenous solution. The term more often used is "molecular beacon probes." In the presence of the target sequence, they unfold, bind and fluoresce. Molecular beacon (MB) probing is one of the chemistries used to carry out many real-time experiments as shown in work by Kramer and Tyagi.[70] Essentially, MBs are oligonucleotide molecular probes, which recognize and signal the presence of specific sequences.[70] MBs contain a section that is complementary to the target DNA sequence that is bound on either side by bases that are also complementary to target sequence. This target DNA sequence is termed the "Loop" region, while the complementary bases describes the "Stem" region. The relationship between the stem and loop regions in the MB gives high specificity despite a large amount of interfering DNA.

MBs are typically labeled with a fluorescent dye at the terminus of the stem region. The stem is formed when the two complementary arms, which flank the probe sequence, are hybridized (1.3). However, when the stem region does not come into contact with any target DNA, a hairpin structure forms, bringing the fluorophore and quencher at the ends of the stem region closer. This results in energy transfer to the quencher, rather than fluorescence emission from the fluorophore. If the probe or loop sequence comes into contact with the complementary DNA of the loop sequence, hybridization results, thus opening the hairpin structure, and subsequently, restoring fluorescence.[71]

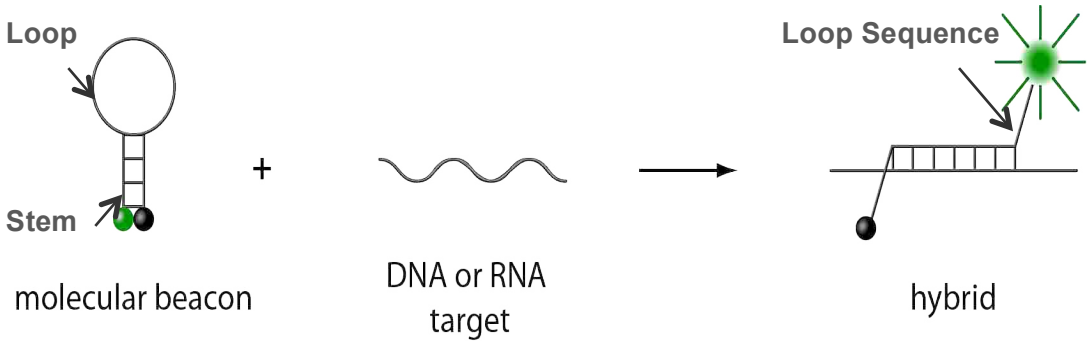

Figure 1.3 The single-stranded oligonucleotides form a closed stem and loop structure in the absence of target DNA and open the stem when hybridized to the target DNA. These Molecular beacons in the closed form have a quencher in proximity to the fluorophore and emits no fluorescence. In the open form of the MB probe, the quencher and fluorophore are separated due to a conformational changes that result in the detection of fluorescent signal.

MBs have illustrated their improvement to target sequence probing through increase in quantum yield, which also shows sensitivity in the detection of single nucleotide polymorphisms (SNPs).[72-74] A disadvantage in previous work of MBs stem from their inability to attach different fluorophores or quenchers to opposite ends of the probe, which does not allow for versatility in terms of reaction yield. In order to increase yield, more probe was needed, which calls for additional cost.[76] Work to better this probe assembly was done by Knemeyer, who developed a 25-mer single-stranded oligonucleotide containing an 18-base recognition sequence.[76] An oxazine dye, JA242, is the fluorescent energy donor. In respect, the other end contained

guanosine residues, which quenched the signal. As seen in figure 1.4, when the cytosines and guanines do not have a target DNA sequence to bind to, a hairpin structure forms, bringing the cytosines and guanines in close proximity. This insures that when the hairpin structure comes into contact with target DNA, there is hybridization, thus opening the hairpin structure, and the MB binds to the target. This forces the cytosines and guanines apart, causing a strong fluorescence emission. Knemeyer was able to detect DNA at a very low concentration: 10^{-12} M.[76]

It the literature, we see the method of using MBs or a "smart probe" to probe for bacterial SNPs. Marme and colleagues applied fluorescently labeled DNA-hairpin structures in combination with SMD. The MBs were hybridized to target DNA sequences, thus causing a conformational change, as illustrated in Figure 1.4.[77]

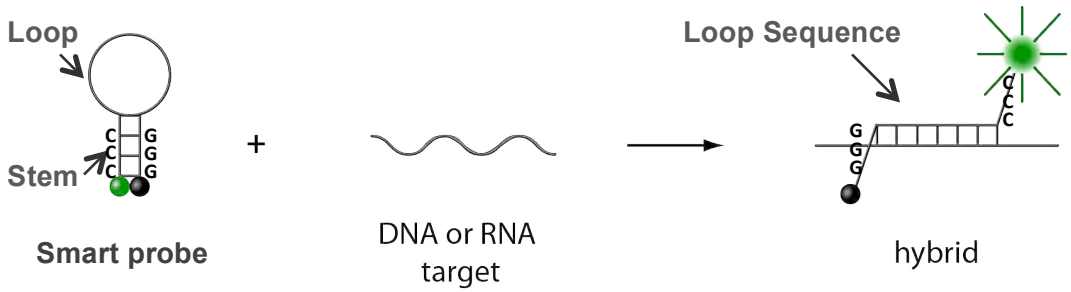

Figure 1.4 Smart probes use a series of guanosines to quench the fluorophore in the closed DNA hairpin loop instead of a traditional quencher. This makes the fabrication of the DNA probe inexpensive and less labor intensive because only the 5' end is modified. The probe used here was designed to test for a SNP in TB responsible for rifampicin resistance.[133]

Marme's methodology was improved for several reasons. Their use of unlabeled oligonucleotides, called "cold" sequences, prevented the formation of secondary structures within the target sequence. The "cold" sequence also proved to be a disadvantage to the assay, adding complexity and decreasing the limit-of-detection LOD. When compared, the process used by Marme and colleagues to identify SNPs in only 10^{-11} M solutions, versus the 10^{-12} M concentrations used by Knemeyer, it is apparent that they achieved a time improvement, evident

by the hybridization only lasted 100 seconds. The PCR for this experimentation added between one and two hours of analysis time, and as discussed in previous sections, PCR will add substantial assay time to genomics-bases analysis techniques.[76-78]

The work of Zhang and colleagues illustrated the use of QDs to improve fluorescence detection in these biological assays. Zhang also developed a two-MB SMD system for quantification of NAs. This work, too, was innovative, in that this was the first use of two differently colored MBs. This work consisted of the development of a comparative hybridization assay as well as simultaneous determination of target and control strands. The fluorescent dyes used in this work were Oregon green 488 and Cy5. Compared to other methods, there was a decrease in the probe consumption. The disadvantages of their system were mostly cost related, as two lasers had to be used, PCR was needed to amplify target molecules, and using unrelated organic dyes, made the system more complicated. Using these organic dyes also proved to be an issue due to their broad emission profiles.[78]

1.7 Fluorescence Resonance Energy Transfer MBs

Fluorescence Resonance Energy Transfer (FRET) is a special technique to gauge the distance between two chromophores, called a donor-acceptor pair. The limitation of FRET is that this transfer process is effective only when the separating distance of donor-acceptor pair is smaller than 10 nanometers. However, FRET is a highly distance-dependent phenomenon and thus has become a popular tool to measure the dynamic activities of biological molecules within nanoscale. The Förster energy transfer is the phenomenon that an excited donor transfers energy (not an electron) to an acceptor group through a non-radiative process. This process is highly distance-dependent, thus allowing one to probe biological structures. One common application is

simply to measure the distance between two positions of interest on a big molecule, generally a biological macromolecule, by attaching appropriate donor-acceptor groups to the big one. If the big molecule only involves one donor and one acceptor group, the distance between the donor and the acceptor can be easily measured if there is no conformational change within this process. Besides, if the molecule has a huge conformational change, one may also measure the dynamical activities between two sites on this macromolecule such as protein interactions1 . Today, this technique is widely applied in many fields such as single-molecule experiments2 , molecular imaging3 , molecular motors4 , biosensors5 and DNA mechanical movements6 . The FRET is also called the "Spectroscopic Ruler"7 because of its intrinsic convenience. In Figure 1.4, the work of Knemeyer, Zhang, and Marme illustrated the effect of energy transfer in the realm of creating a MB through the hairpin structure. Using fluorescence resonance energy transfer (FRET) will differ by using a fluorophore and a molecule that can accept energy (donor-acceptor pair), which will then fluoresce. The sections herein will describe, in detail, the process of FRET.

Fluorescent Resonance Energy Transfer (FRET), also known as Förster Resonance Energy Transfer, is a process that was described over fifty years ago. It is the non-radio active transmission of energy from a fluorophore (e.g. donor molecule) to an acceptor molecule through distance-dependent interactions. This process has no conversion to thermal energy that may have been caused by some sort of thermal collision.[81] Wabuyele and colleagues conducted this work using two cyanine dyes, Cy5 and Cy5.5, as a FRET pair for SMD of products generated from a Ligase Detection Reaction (LDR).[27] The cyanine dyes were attached to LDR primers and brought into close proximity due to hybridization of the stem structures of MBs. The calculated Förster distance (R_0) for these cyanine dyes was 61.7 angstroms (Figure 1.5).[27]

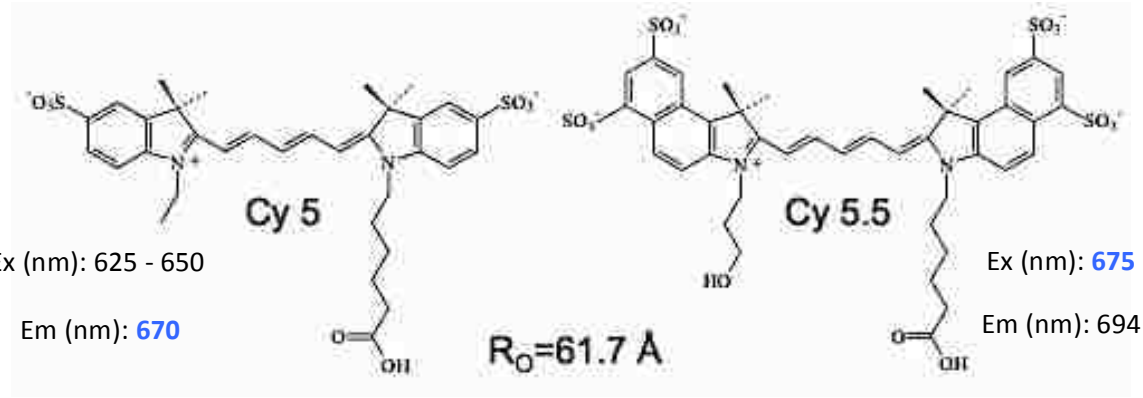

Figure 1.5 The fluorescent dyes Cy5 and Cy5.5 are a commonly used FRET pair. The Cy5 dye can be excited with a HeNe laser diode. The Cy5 dye will transfer its energy to Cy5.5 when they are in close proximity. For this dye pair R_0 distance is 61.7 Å.

To enhance the FRET efficiency, the donor group should have good abilities to absorb photons and emit photons. That means the donor group should have a high extinction coefficient and a high quantum yield. The overlap of emission spectrum of the donor and absorption spectrum of the acceptor means that the energy lost from excited donor to ground state could excite the acceptor group. The energy matching is called the resonance phenomenon. Thus, the more overlap of spectra, the better a donor can transfer energy to the acceptor. The overlap integral, J(λ), between the donor and the acceptor stands for the overlap of spectra, as shown in Figure 1.6.

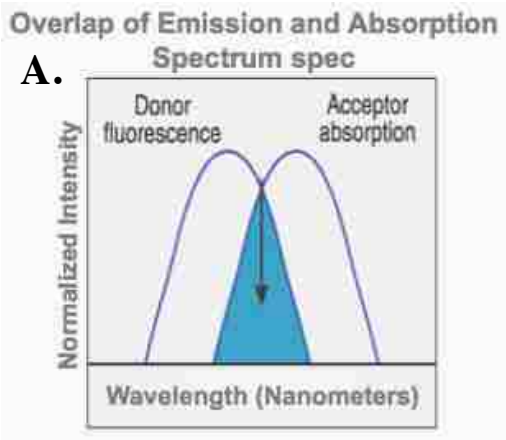

Figure 1.6 (A.) The schematic of spectral overlap

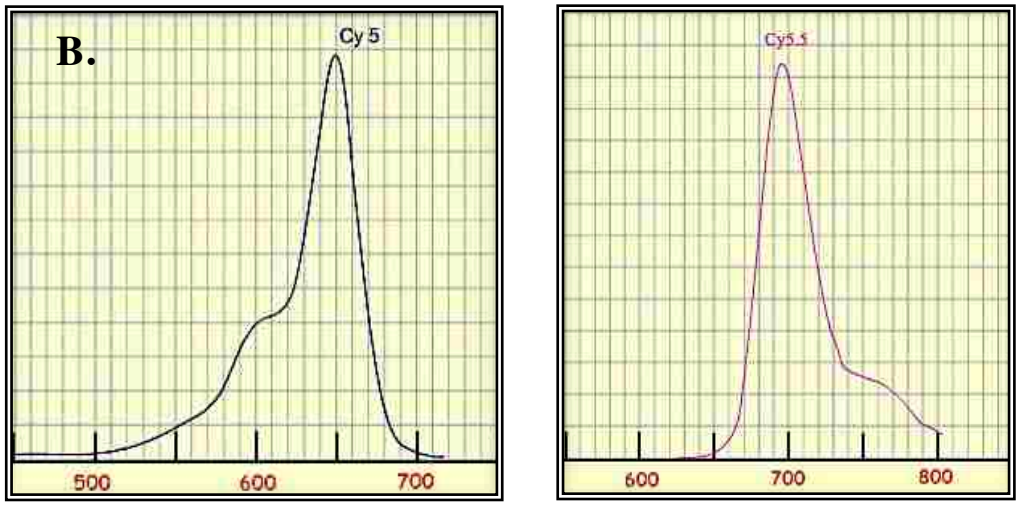

Figure 1.6 (B.) The excitation/emission wavelength spectra of Cy5 and Cy5.5

1.8 Ligase Detection Reaction-based Assays (LDR)

LDR-based assays are generally compared to assays based on the ligase chain reaction (LCR).[83] The difference between the two is LDR works in a single DNA strand, which LCR works on also, like PCR. The LDR flanks the target material and thus linearly amplifies the target material containing the desired sequence. A DNA ligase enzyme can be used to distinguish between normal and mutant DNA. Primers are synthesized to be complementary to the target sequence, allowing for selective amplification of the mutant allele. LDR has shown much promise in medicine, by screening for T-cell receptor polymorphisms and sickle cell anemia.[82] Due to the chemistry of the LDR primers and target sequences; LDR products can also be labeled with fluorescent molecules like the MBs making results easily quantifiable.

LDR also can be used with reverse molecular beacons, or rMBs. Previously, the use of MBs illustrated the use a fluorescent dye and a quencher. In using rMBs, the stems are labeled with two different dyes forming a FRET pair. For this assay, the melting temperature of the stem section, T_m, is higher than the melting temperature of both the LDR primers and of the unligated stem section. LDR can be performed after PCR amplification of template DNA or of genomic

DNA directly.[27] LDR is also advantageous as it can quickly identify multiple sites of mutations or, as mentioned previously, screen large populations for disease polymorphisms.[83]

1.9 Ligase Detection Reaction Using Single-Pair FRET

Wabuyele used an LDR assay to detect SNPs for colorectal cancer diagnostic mutations. The assay used SMD and did not use PCR. Without the PCR step, the assay time was greatly reduced.[27] The assay used two allele-specific primers labeled at their 3' and 5' ends with fluorescent dyes. The primers flanked a single base mutation of the target template and each primer had a complementary arm sequence. The two primers were bound covalently using DNA ligase only when the mutation was present, which formed an rMB that could then undergo FRET. Wabuyele detected the fluorescence emission in a microfluidic channel using a confocal optical system. Using this assay, the K-ras oncogene (codon 12) mutations, which are highly associated with colorectal cancer, were detected with a sensitivity of 1:1,000 mutants-to-wild-type alleles. In order to achieve these results, analysis times of less than five minutes were required. LDR allowed for linear amplification of the rMB by increasing the number of thermal cycles and thus, illustrated its potential as being compared with PCR.[52,53] This process, known as LDR single-pair fluorescence resonance energy transfer (LDR-spFRET), is illustrated in Figure 1.7.

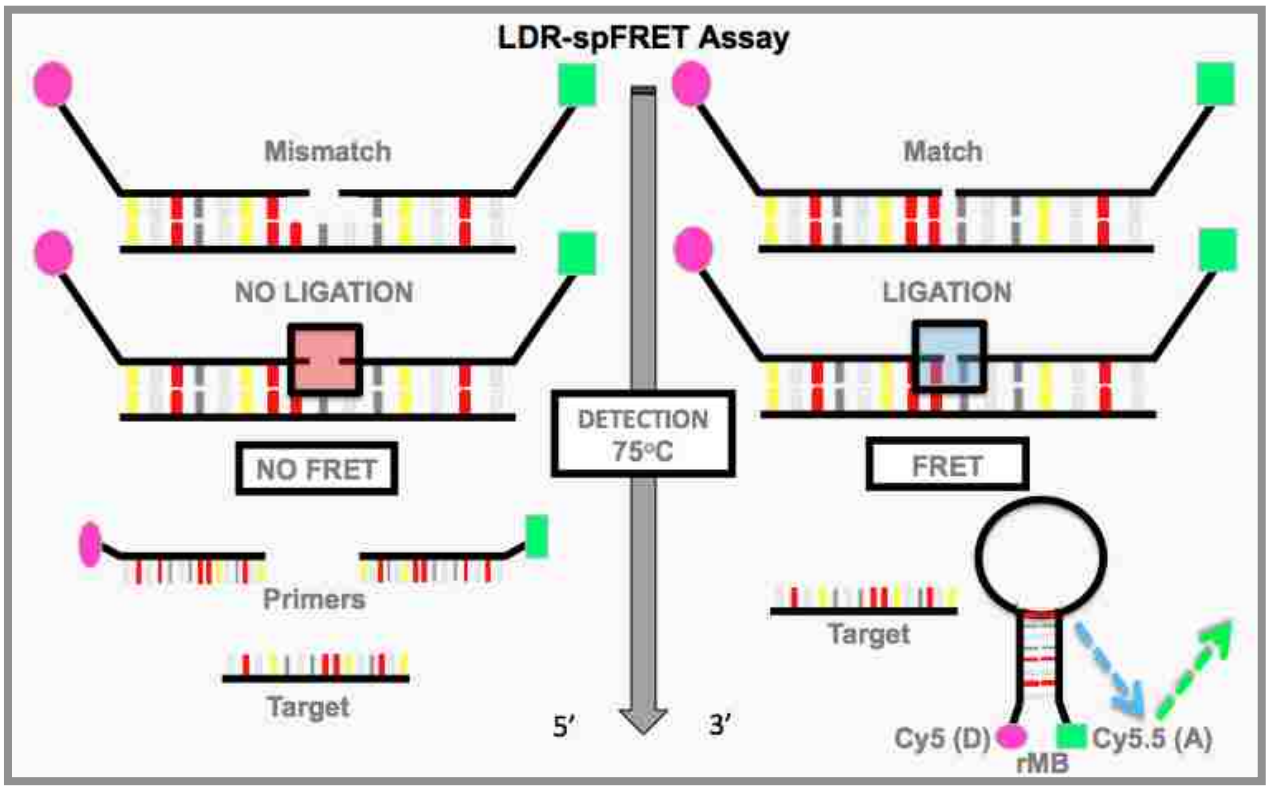

Figure 1.7 Schematic of the LDR-spFRET assay in which two allele-specific primers are labeled at their 3'- and 5'-ends with fluorescent dyes and flank a SNP on the target template. An enzyme, Taq DNA ligase, covalently joins the two adjacent primers when perfectly matched to the template, forming a molecular beacon that can undergo FRET whereas mismatched primers remain unligated and do not show FRET. The detection temperature of the assay was maintained at 75ºC to melt the duplex formed between the target and LDR primers as well as stem sequences of unligated primers but not the stem of the fully formed beacon.

1.10 LDR-spFRET

Using the combination of a reverse molecular beacon (rMBs) with LDR has proven to be increasingly efficient in developing new assays to detect point mutations in genomic DNA.[5] This combination is known as LDR-spFRET and several assays have been named in the completion of this work. The strategy, however, involves the use of two primers that forms a MB after ligation of the two primers with attach fluorophores (Donor and Acceptor) and melting from the target DNA. The complementary target gene sequence is termed the "loop" region, while the ten complementary bases are described as the "stem" region. The relationship between the stem and loop regions in the rMB gives high specificity despite a large amount of interfering unwanted gene sequences. When the stem region comes into contact with any target DNA, the two primers hybridize/ligate and the primers labeled with fluorophores are brought into close proximity, and in turn they undergo fluorescence resonance energy transfer (FRET). If the probe or loop sequence comes into contact with a sequence where the primers are not specific, hybridization does not result and primers remain unligated, resulting in no fluorescence and no FRET. Once the primers are ligated, the solution temperature is then higher than the melting temperature (T_m) of the DNA duplex formed by the loop structures, and the target sequence is separated from the LDR-spFRET product. The stem of the rMB was designed to have a higher T_m than that of the ligated primers to the template at the concentrations used for the molecular assay. It is important to consider that the primers will not be ligated if the DNA target is not complementary to the primers. Because of this, an rMB cannot form (Figure 1.7). Only one thermal cycle for LDR is needed to form the rMB, but multiple cycles can be used to linearly increase the number of rMBs to aid in detection. Single-pair FRET coupled with LDR is quite superior to other methods. Single-pair FRET is highly specific, which illustrates the fact that pathogenic information at the

strain level can be obtained. In light of the single-pair FRET's highly specific nature, it is thought that the sample volume tested can be of low-targeted gene concentration; this being realized gives way to the idea of coupling rMB probing with the use of microfluidic devices. The rMB products can then be directly interrogated in a microfluidic channel by a laser-induced fluorescence (LIF) system at the single-molecule level that will then be able to report the presence of certain pathogens with high sensitivity, reliability, and time efficiency.

1.11 Microfluidics

Microfluidics deals with designing and manufacturing devices and processes for the manipulation of extremely small volumes of liquid samples. Microfluidics has become an integral element of many-advanced diagnostic and screening technologies. For example, work done by TED's Senior Fellow Frederick Balagadde, shows the ability to build an HIV kit in a microfluidic system, so with one microfluidic chip, can diagnose one hundred patients at the same time. For each of the patients, shows that physicians will be able to do up to one hundred different viral loads per patient and this is only done in four hours, which is fifty times faster than the current state of the art, at a cost that will be five to five hundred times cheaper than the current options. The impact of microfluidics on the biological and pharmaceutical industries continues to expand; yet the basic principles of microfluidics can be found in the earliest treatise on fluid dynamics. The basics include fluid flow at the microscale and the forces and mechanisms, which may be used for directed transport of fluids and/or particles through microscale systems. Research in the field of microfluidics is aimed at minimizing the time and cost associated with routine chemical and biological analysis, which in-turn improves reproducibility, accuracy and reliability. It is proposed that the use of microfluidic devices in-conjunction with detection via Single-Molecule Detection (SMD) will demonstrate attractive

benefits for gene expression profiling and measuring quantities of target nucleic acid sequences. Some of its benefits include enhanced processing speed by eliminating processing steps, elimination of ensemble averaging and single-molecule sensitivity.

1.12 Microfluidics and Its Importance to SMD

Microfluidic devices for genomic assays play a very important role due to fully automated sampling and short analysis times. Based on these two components, there is a higher cost efficiency, due to the shorter run-time and lower volume of reagents necessary for analysis. Earlier methods of microfluidic devices by Craighead,[29] Ramsey and Mathies,[30,31] used glass-based microfluidics.[30, 32,33] Craighead's DNA fragment sizing device consisted of micro/nano-structured fluidic channels, which defined the effective probe volume and can enhance the sampling throughput for SMD. Ramsey and Mathies used glass-based microfluidic devices using organic chromophores and DNA molecules. In using both types of molecules, it was demonstrated that SMD coupled with microfluidics is possible.[30, 31]

It is important to consider the type of material used as the microfluidic channel. Craighead, Ramsey, and Mathies used glass-based microfluidics. Glass is a good material due to its favorable optical properties, mostly due to the auto-fluorescence and low background produced. However, using glass also has several disadvantages, such as the cost of manufacturing, its low aspect ratio associated with wet etching, and the elevated temperature necessary for bonding the coverslip to enclose the channels.[34] In recent years, polymers have been developed to improve upon the glass-based microfluidic channels.[34] Polymers may prove to be adequate alternatives due to their cost efficiency, multi-solvent compatibility, biocompatibility, tunable surface properties, and the capability to be manipulated for various

fabrication designs.[35-38] Microfabrication of devices in polymers has been done using injection molding, imprinting, embossing,[40] X-ray lithography,[35] and laser ablation.[40] The use of polymers in microfluidics has been applied in the life sciences, which can be illustrated through several reviews in the literature. Some of the applications include, PCR amplification,[41-44] DNA sequencing and separations,[46-49] even cell culture and handling.[50]

1.13 Objective of the Project

We will develop a simple flow-through modular fluidic bio-processor made from polymeric materials via replication micro-technologies to analyze the molecular content of PBMCs for the expression level of mRNAs that provide diagnostic information for ischemic and/or hemorrhagic stroke in a turn-around-time (TAT) less than 20 min. The fluidic bio-processor accepts the input sample (whole blood), clears the blood of RBCs, neutrophils and platelets to produce the PBMC fraction, thermally and/or chemically lysis the PBMCs, isolates the total RNA using SPE, reverse transcribes the mRNAs into cDNAs, performs an LDR on the cDNAs using primers that carry reporter sequences for the target and readout of successful ligation events using spFRET. The use of spFRET obviates the need for a PCR step, which not only reduces processing time, but also produces exquisite analytical sensitivity.

1.14 Report Outline

A summary of the theory, techniques and methods in this report is presented:

Chapter 2. Experimental

This chapter provides experimental methods and optimization applications for the microfluidic device. This chapter presents the methods of device fabrication and the devices role in gene expression profiling using LDR-spFRET.

Chapter 3. Design and Development of a Field-Deployable Single-Molecule Detector (SMD) for the Analysis of Molecular Markers

This chapter reports a simple and compact fluorescence single-molecule instrument that is straightforward to operate, consisting of fiber optics directly coupled to a microfluidic device. It is seen that with this integration of fiber optics, it simplifies the optical requirements associated with traditional SMD instruments by eliminating the need for optical alignment and simplification of the optical train.

Chapter 4. Discussions, Conclusions and Future Work

This chapter provides experimental results, conclusion and a discussion of the future/current work propelling project goals.

1.15 References

1. Soper, S. A.; Davis, **L.** M.; Shera, E. B., Detection and Identification of Single Molecules in Solution. *Journal of the Optical Society of America B-Optica/ Physics* **1992,** *9* (10),1761-1769.

2. Nguyen, D. C.; Keller, R. A.; Jett, J. **H.;** Martin, J. C., Detection of Single Molecules of Phycoerythrin in Hydrodynamically Focused Flows by Laser-Induced Fluorescence. *Anal Chem* **1987,** 59 (17), 2158-2161.

3. Nguyen, D. C.; Keller, R. A.; Trkula, M., Ultrasensitive Laser-Induced Fluorescence Detection in Hydrodynamically Focused Flows. *Journal of the Optical Society of America B-Optical Physics* **1987,** 4 (2), 138-143.

4. Sauer, M.; Angerer, B.; Ankenbauer, W.; Foldes-Papp, Z.; Gobel, F.; Han, K. **T.;** Rigler, R.; Schulz, A.; Wolfrum, **J.;** Zander, C., Single Molecule DNA Sequencing in Submicrometer Channels: State of the Art and Future Prospects. *Journal of Biotechnology* **2001,** 86 (3), 181-201.

5. Hirschfeld, T., Optical Microscopic Observation of Single Small Molecules. *Appl Opt,* (12), 2965-2966.

6. Tamara, P .; Maali, A.; Lounis, B.; Orrit, M., Ten Years of Single-Molecule Spectroscopy. *J Phys Chem A* **2000,** 104 (1), 1-16.

7. Deniz, A. A.; Dahan, M.; Grunwell, J. R.; Ha, T. J.; Faulhaber, A. E.; Chemla, D. S.; Weiss, S.; Schultz, P. G. In *Single-Pair Fluorescence Resonance Energy Transfer on Freely Diffusing Molecules: Observation of Forster Distance Dependence and Subpopulations,* 1999; pp 3670-3675.

8. Deniz, A. A.; Laurence, T. A.; Beligere, G. S.; Dahan, M.; Martin, A. B.; Chemla, D. S.; Dawson, P. E.; Schultz, P. G.; Weiss, S., Single-Molecule Protein Folding: Diffusion Fluorescence Resonance Energy Transfer Studies of the Denaturation of Chymotrypsin Inhibitor 2. *Proc Nat/ Acad Sci USA* **2000,** 97 (10), 5179-5184.

9. Ha, T.; Enderle, T.; Ogletree, D. F.; Chemla, D. S.; Selvin, P.R.; Weiss, S., Probing the Interaction between Two Single Molecules: Fluorescence Resonance Energy Transfer between a Single Donor and a Single Acceptor. *Proc Nat/ Acad Sci US A* **1996,** 93 (13), 6264-6268.

10. Jares-Erijman, E. A.; Jovin, T. M., Fret Imaging. *Nat Biotechnol* **2003,** 21 **(II)**, 1387-1395.

11. Schuler, B.; Lipman, E. A.; Eaton, W. A., Probing the Free-Energy Surface for Protein Folding with Single-Molecule Fluorescence Spectroscopy. *Nature* **2002**, 419 (6908), 743-747.

12. Mathies, R. A.; Peck, K., Optimization of High-Sensitivity Fluorescence Detection. *Anal. Chem.* ***1990,62,*** 1786-1791.

13. Zander, C., Single-Molecule Detection in Solution: A New Tool for Analytical Chemistry. *Fresenius Journal of Analytical Chemistry* **2000,** 366 (6-7), 745-751.

14. Nie, S. M.; Chiu, D. T.; Zare, R. N., Real-Time Detection of Single-Molecules in Solution by Confocal Fluorescence Microscopy. *Anal. Chem.* **1995,** 67 (17), 2849-2857.

15. Shera, E. B.; Seitzinger, N. K.; Davis, L. M.; Keller, R. A.; Soper, S. A., Detection of Single Fluorescent Molecules. *Chem. Phys. Lett.,* **1990,** 174 (6), 553-557.

16. Eigen, M.; Rigler, R., Sorting Single Molecules - Application to Diagnostics and Evolutionary Biotechnology. *Proc Natl Acad* Sci *USA* **1994**, 91 (13), 5740-5747.

17. Dickson, R. M.; Norris, D. J.; Tzeng, Y. L.; Moemer, W. E., Three-Dimensional Imaging of Single Molecules Solvated in Pores of Poly (Acrylamide) Gels. *Science* **1996**, 274 (5289), 966-969.

18. Fister, J. C.; Jacobson, S.C.; Davis, L. M.; Ramsey, J. M., Counting Single Chromophore Molecules for Ultrasensitive Analysis and Separations on Microchip Devices. *Anal. Chem.* **1998**, 70 (3), 431-437.

19. Barnes, M. D.; Ng, K. C.; Whitten, W. B.; Ramsey, J. M., Detection of Single Rhodamine-6g Molecules in Levitated Microdroplets. *Anal. Chem.* **1993**, 65 (17), 2360-2365.

20. Mertz, J.; Xu, C.; Webb, W. W., Single-Molecule Detection by Two-Photon-Excited Fluorescence. *Opt. Lett.* **1995**, 20 (24), 2532-2534.

21. Wabuyele, M. B.; Ford, S.M.; Stryjewski, W.; Barrow, J.; Soper, S. A., Single Molecule Detection of Double-Stranded DNA in Poly (Methylmethacrylate) and Polycarbonate Microfluidic Devices. *Electrophoresis* **2001**, 22 (18), 3939-3948.

22. Soper, S. A.; Nutter, H. L.; Keller, R. A.; Davis, L. M.; Shera, E. B., The Photophysical Constants of Several Fluorescent Dyes Pertaining to Ultrasensitive Fluorescence Spectroscopy. *Photochemistry And Photobiology* **1993**, 57 (6), 972-977.

23. Soper, S. A.; Mattingly, Q. L.; Vegunta, P., Photon Burst Detection of Single near-Infrared Fluorescent Molecules. *Analytical Chemistry* 1993, *65* (6), 740-747.

24. Zander, C., Single-Molecule Detection in Solution: A New Tool for Analytical Chemistry. *Fresenius Journal of Analytical Chemistry*. **2000,** 366 (6-7), 745-751.

25. Unger, M.; Kartalov, E.; Chiu, C. S.; Lester, H. A.; Quake, S. R., Single-Molecule Fluorescence Observed with Mercury Lamp Illumination. *BioTechniques*. **1999**, 27 (5), 1008.

26. Li, L. Q.; Davis, L. M., Single-Photon Avalanche-Diode for Single-Molecule Detection. *Rev Sci Ins/rum*. **1993**, 64 (6), 1524-1529.

27. Wabuyele, M. B.; Farquar, H.; StrY.iewski, W.; Hammer, R. P.; Soper, S. A.; Cheng, Y. W.; Barany, F., Approaching Real-Time Molecular Diagnostics: Single-Pair Fluorescence Resonance Energy Transfer (Spfret) Detection for the Analysis of Low Abundant Point Mutations in K-Ras Oncogenes. *J. Am. Chem. Soc*. **2003**, 125 (23), 6937-6945.

28. Castro, A.; Williams, J. G. K., Single-Molecule Detection of Specific Nucleic Acid Sequences in Unamplified Genomic DNA. *Anal. Chem.* **1997**, *69* (19), 3915-3920.

29. Foquet, M.; Korlach, J.; Zipfel, W.; Webb, W. W.; Craighead, H. G., DNA Fragment Sizing by Single Molecule Detection in Submicrometer-Sized Closed Fluidic Charmels. *Anal. Chem*. **2002,** 74 (6), 1415-1422.

30. Fister, J. C.; Jacobson, S. C.; Ramsey, J. M., Ultrasensitive Cross Correlation Electrophoresis on Microchip Devices. *Anal. Chem.* **1999**, *71* (20), 4460-4464.

31. Betzig, E.; Chichester, R. J., Single Molecules Observed by near-Field Scanning Optical Microscopy. *Science*. **1993**, 262 (5138), 1422-1425.

32. Chou, H. P.; Spence, C.; Scherer, A.; Quake, S., A Microfabricated Device for Sizing and Sorting DNA Molecules. *Proc Nat/ Acad Sci USA*. **1999,** 96 (1), 11-13.

33. Haab, B. B.; Mathies, R. A., Single-Molecule Detection of DNA Separations in Microfabricated Capillary Electrophoresis Chips Employing Focused Molecular Streams. *Anal. Chem*. **1999,** 71 (22), 5137-5145.

34. Fan, Z. H.; Harrison, D. J., Micromachining of Capillary Electrophoresis Injectors and Separators on Glass Chips and Evaluation of Flow at Capillary Intersections. *Anal. Chem*. ***1*994**, 66 (1), 177-184.

35. Ford, S. M.; Davies, J.; Kar, B.; Qi, S. D.; McWhorter, S.; Soper, S. A.; Malek, C. K., Micromachining in Plastics Using X-Ray Lithography for the Fabrication of Micro- Electrophoresis Devices. *Journal Of Biomechanical Engineering-Transactions Of The Asme* **1999**, 121 (1), 13-21.

36. Becker, H.; Gartner, C., Polymer Microfabrication Methods for Microfluidic Analytical Applications. *Electrophoresis 2000,21* (1), 12-26.

37. Becker, H.; Locascio, L. E., Polymer Microfluidic Devices. *Talanta* **2002**, 56 (2), 267-287.

38. McDonald, J. C.; Duffy, D. C.; Anderson, J. R.; Chin, D. T.; Wu, H. K.; Schueller, 0. J. A.; Whitesides, G. M., Fabrication of Microfluidic Systems in Poly (Dimethylsiloxane). *Electrophoresis* **2000**, 21 (1), 27-40.

39. Effenhauser, C. S.; Bruin, G. J. M.; Paulus, A.; Ehrat, M., Integrated Capillary Electrophoresis on Flexible Silicone Microdevices: Analysis of DNA Restriction Fragments and Detection of Single DNA Molecules on Microchips. *Anal Chem* **1997**, 69 (17), 3451-3457.

40. McCormick, R. M.; Nelson, R. J.; AlonsoAmigo, M. G.; Benvegnu, J.; Hooper, H. H. In *Microchannel Electrophoretic Separations of DNA in Injection-Molded Plastic Substrates*. **1997**, 2626-2630.

41. Beer, N. R.; Hindson, B. J.; Wheeler, E. K.; Hall, S. B.; Rose, K. A.; Kennedy, I. M.; Colston, B. W., On-Chip, Real-Time, Single-Copy Polymerase Chain Reaction in Picoliter Droplets. *Anal Chern* **2007,** *79* (22), 8471-8475.

42. Koh, C. G.; Tan, W.; Zhao, M. Q.; Ricco, A. J.; Fan, Z. H., Integrating Polymerase Chain Reaction, Valving, and Electrophoresis in a Plastic Device for Bacterial Detection. *Anal Chern* **2003,** 75 (17), 4591-4598.

43. Liu, P.; Seo, T. S.; Beyor, N.; Shin, K. J.; Scherer, J. R.; Mathies, R. A., Integrated Portable Polymerase Chain Reaction-Capillary Electrophoresis Microsystem for Rapid Forensic Short Tandem Repeat Typing. *Anal. Chem.* **2007,** 79 (5), 1881-1889.

44. Ottesen, E. A.; Hong, J. W.; Quake, S. R.; Leadbetter, J. R., Microfluidic Digital Per Enables Multigene Analysis of Individual Environmental Bacteria. *Science* **2006,** 314 (5804), 1464-1467.

45. Liu, Y. J.; Ganser, D.; Schneider, A.; Liu, R.; Grodzinski, P.; Kroutchinina, N., Microfabricated Polycarbonate Ce Devices for DNA Analysis. *Anal. Chem.* **2001**, 73 (17), 4196-4201.

46. Eid, J.; Fehr, A.; Gray, J.; Luong, K.; Lyle, J.; Otto, G.; Peluso, P.; Rank, D.; Baybayan, P.; Bellman, B.; Bibillo, A.; Bjornson, K.; Chaudhuri, B.; Christians, F.; Cicero, R.; Clark, S.; Dalal, R.; Dewinter, A.; Dixon, J.; Foquet, M.; Gaertner, A.; Hardcnbol, P.; Heiner, C.; Hester, K.; Holden, D.; Kearns, G.; Kong, X. X.; Kuse, R.; Lacroix, Y.; Lin, S.; Lundquist, P.; Ma, C. C.; Marks, P.; Maxham, M.; Murphy, D.; Park, I.; Pham, T.; Phillips, M.; Roy, J.; Sebra, R.; Shen, G.; Sorenson, J.; Tomaney, A.; Travers, K.; Trulson, M.; Vieceli, J.; Wegener, J.; Wu, D.; Yang, A.; Zaccarin, D.; Zhao, P.; Zhong, F.; Korlach, J.; Turner, S., Real-Time DNA Sequencing from Single Polymerase Molecules. *Science* **2009**, 323 (5910), 133-138.

47. Clarke, J.; Wu, H. C.; Jayasinghe, L.; Patel, A.; Reid, S.; Bayley, H., Continuous Base Identification for Single-Molecule Nanopore DNA Sequencing. *Nature Nanotechnology* **2009**, 4 (4), 265-270.

48. Harris, T. D.; Buzby, P. R.; Babcock, H.; Beer, E.; Bowers, J.; Braslavsky, I.; Causey, M.; Coloncll, J.; Dimeo, J.; Efcavitch, J. W.; Giladi, E.; Gill, J.; Healy, J.; Jarosz, M.; Lapen, D.; Moulton, K.; Quake, S. R.; Steinmann, K.; Thayer, E.; Tyurina, A.; Ward, R.; Weiss, H.; Xie, Z., Single-Molecule DNA Sequencing of a Viral Genome. *Science* **2008,** 320 (5872), 106-109.

49. Branton, D.; Deamer, D. W.; Marziali, A.; Bayley, H.; Benner, S. A.; Butler, T.; Di Ventra, M.; Garaj, S.; Hibbs, A.; Huang, X. H.; Jovanovich, S. B.; Krstic, P. S.; Lindsay, S.; Ling, X. S. S.; Mastrangelo, C. H.; Meller, A.; Oliver, J. S.; Pershin, Y. V.; Ramsey, J. M.; Riehn, R.; Soni, G. V.; Tabard-Cossa, V.; Wanunu, M.; Wiggin, M.; Schloss, J. A., The Potential and Challenges of Nanopore Sequencing. *Nat Biotechnol* **2008,** 26 (I 0), 1146-1153.

50. Lin, Y. C.; Jen, C. M.; Huang, M. Y.; Wu, C. Y.; Lin, X. Z., Electroporation Microchips for Continuous Gene Transfection. *Sensors and Actuators B-Chemical* **2001**, 79 (2-3), 137-143.

51. Dittrich, P. S.; Manz, A., Single-Molecule Fluorescence Detection in Microfluidic Channels -the Holy Grail in Mu Tas. *Anal Bioanal Chern* **2005,** 382 (8), 1771-1782.

52. Hashimoto, M.; Barany, F.; Soper, S. A., Polymerase Chain Reaction/Ligase Detection Reaction/Hybridization Assays Using Flow-through Microfluidic Devices for the Detection of Low-Abundant DNA Point Mutations. *Biosensors & Bioelectronics* **2006,** 21 (10), 1915-1923.

53. Hashimoto, M.; Barany, F.; Xu, F.; Soper, S. A., Serial Processing of Biological Reactions Using Flow-through Microfluidic Devices: Coupled Pcr /Ldr for the Detection of Low-Abundant DNA Point Mutations. *Analyst* **2007,** 132 (9), 913-921.

54. Hashimoto, M.; Chen, P. C.; Mitchell, M. W.; Nikitopoulos, D. E.; Soper, S. A.; Murphy, M. C., Rapid Per in a Continuous Flow Device. *Lab on a Chip* **2004,** 4 (6), 638-645.

55. Wittwer, C. T.; Fillmore, G. C.; Garling, D. J., Minimizing the Time Required for DNA Amplification by Efficient Heat-Transfer to Small Samples. *Analytical Biochemistry* **1990,** 186 (2), 328-331.

56. Wittwer, C. T.; Garling, D. J., Rapid Cycle DNA Amplification- Time and Temperature Optimization. *Biotechniques* **1991,** 10 (1), 76-&.

57. Bej, A. K.; Mahbubani, M. H.; Atlas, R. M., Amplification of Nucleic Acids by Polymerase Chain-Reaction (Per) and Other Methods and Their Applications. *Crit Rev Biochem Mol Biol* **1991**, 26 (3-4), 301-334.

58. Asseline, U., Development and Applications of Fluorescent Oligonucleotides. *Curr. Org. Chem.* **2006,** 10 (4), 491-518.

59. Yeh, H. C.; Chao, S. Y.; Ho, Y. P.; Wang, T. H., Single-Molecule Detection and Probe Strategies for Rapid and Ultrasensitive Genomic Detection. *Curr Pharm Biotechnol* **2005,** *6* (6), 453-461.

60. Marziali, A.; Akeson, M., New DNA Sequencing Methods. *Annu Rev Biomed Eng* **2001,** 3, 195-223.

61. Franca, L. T. C.; Carrilho, E.; Kist, T. B. L., A Review of DNA Sequencing Techniques. *Q Rev Biophys* 2002, *35* (2), 169-200.

62. Meldrum, D., Automation for Genomics, Part Two: Sequencers, Microarrays, and Future Trends. *Genome Res* **2000**, 10 (9), 1288-1303.

63. Davis, L. M.; Fairfield, F. R.; Harger, C. A.; Jett, J. H.; Keller, R. A.; Hahn, J. H.; Krakowski, L.A.; Marrone, B. L.; Martin, J. C.; Nutter, H. L.; Ratliff, R. L.; Shera, E. B.; Simpson, D. J.; Soper, S. A., Rapid DNA Sequencing Based Upon Single Molecule Detection. *Genetic Analysis-Biomolecular Engineering* **1991**, 8 (1), 1-7.

64. Chan, E. Y., Advances in Sequencing Technology. *Mutation Research-Fundamental and Molecular Mechanisms of Mutagenesis* **2005**, 573 (1-2), 13-40.

65. Bennett, S. T.; Barnes, C.; Cox, A.; Davies, L.; Brown, C., Toward the $1000 Human Genome. *Pharmacogenomics* **2005**, 6 (4), 373-382.

66. Astier, Y.; Braha, 0.; Bayley, H., Toward Single Molecule DNA Sequencing: Direct Identification of Ribonucleoside and Deoxyribonucleoside 5 '-Monophosphates by Using an Engineered Protein Nanopore Equipped with a Molecular Adapter. *J Am Chem Soc* **2006**,128 (5), 1705-1710.

67. Krieg, A.; Ruckstuhl, T.; Seeger, S., Towards Single-Molecule DNA Sequencing: Assays with Low Nonspecific Adsorption. *Anal Biochem* **2006**, 349 (2), 181-185.

68. D'Antoni, C. M.; Fuchs, M.; Harris, J. L.; Ko, H. P.; Meyer, R. E.; Nadel, M. E.; Randall, J. D.; Rooke, J. E.; Nalefski, E. A., Rapid Quantitative Analysis Using a Single Molecule Counting Approach. *Anal Biochem* **2006**, 352 (1), 97-109.

69. Zhang, C. Y.; Johnson, L. W., Homogenous Rapid Detection of Nucleic Acids Using Two-Color Quantum Dots. *Analyst* **2006**, 131 (4), 484-488.

70. Tyagi, S., and Kramer,F.R., Molecular Beacons: Probes That Fluoresce Upon Hybridization. *Nat. Biotechnol.,* **1995,** 14, 303-308.

71. Knemeyer, J. P., Marme, N., and Sauer,M., Probes for Detection of Specific DNA Sequences at the Single-Molecule Level. *Anal. Chem.* **2000,** 72, 3717-3724.

72. Szemes, M.; Schoen, C. D., Design of Molecular Beacons for Amplidet Rna Assay - Characterization of Binding Stability and Probe Specificity. *Anal Biochem* **2003,** 315 (2), 189-201.

73. Wu, Z. S.; Jiang, J. H.; Shen, G. L.; Yu, R. Q., Highly Sensitive DNA Detection and Point Mutation Identification: An Electrochemical Approach Based on the Combined Use of Ligase and Reverse Molecular Beacon. *Human Mutation* **2007**, 28 (6), 630-637.

74. Yang, L.; Coo, Z. H.; Lin, Y. M.; Wood, W. C.; Staley, C. A., Molecular Beacon Imaging of Tumor Marker Gene Expression in Pancreatic Cancer Cells. *Cancer Biology & Therapy* **2005**, 4 (5), 561-570.

75. Venkatesan, N.; Seo, Y. J.; Kim, B. H., Quencher-Free Molecular Beacons: A New Strategy in Fluorescence Based Nucleic Acid Analysis. *Chern Soc Rev* **2008**, 37 (4), 648-663.

76. Knemeyer, J.P.; Manne, N.; Sauer, M., Probes for Detection of Specific DNA Sequences at the Single-Molecule Level. *Anal Chem* **2000**, 72 (16), 3717-3724.

77. Manne, N.; Friedrich, A.; Muller, M.; Nolte, 0.; Wolfrum, J.; Hoheisel, J.D.; Sauer, M.; Knemeyer, J. P., Identification of Single-Point Mutations in Mycobacterial 16s Rrna Sequences by Confocal Single-Molecule Fluorescence Spectroscopy. *Nucleic Acids Res* **2006**, 34 (13).

78. Zhang, C. Y.; Chao, S. Y.; Wang, T. H., Comparative Quantification of Nucleic Acids Using Single-Molecule Detection and Molecular Beacons. *Analyst* **2005**, 130 (4), 483-488.

79. Puleo, C. M.; Wang, T. H., Microfluidic Means of Achieving Attomolar Detection Limits with Molecular Beacon Probes. *Lab Chip* **2009**, 9 (8), 1065-1072.

80. Lakowicz, J. R., Principles *of Fluorescence Spectroscopy*. 2nd Edition ed.; Kluwer Academic/Pelnum Publishers: New York, **1999**.

81. Held, P. Introduction to Fluorescence Resonance Energy Transfer (FRET) Technology and its Application in Bioscience. *BioTek White Paper*. **2005**.

82. Barany, F.; Widmann, M.; Wilson, W. J.; Czajka, J.; Luo, J.; Batt, C. A., Ligase Chain Reaction (Lcr)-- Overview and Applications. *PCR Methods and Applications* **1994**, S51-S64.

83. Khanna, M., Park, P., Zirvi, M., Cao, W., Picon, A., Day, J., Paty, P. and Barany, F., Multiplex Pcr /Ldr for Detection of K-Ras Mutations in Primary Colon Tumors. *Oncogene* **1999**, 18, 27-38.

84. Neely, L.A.; Patel, S.; Garver, J.; Gallo, M.; Hackett, M.; McLaughlin, S.; Nadel, M.; Harris, J.; Gullans, S.; Rooke, J., A Single-Molecule Method for the Quantitation ofMicrorna Gene Expression. *Nat Methods* **2006,** 3, 41-46.

85. Khan, J; Jun S; Wei1, S; Ringer, M.; Lao, H.; Sail, Litany, M.; Wassermann, F.; Berthold, F.; Schwab, M.; Antonescu, C. R.; Peterson, C.; Meltzer, P. S. Classification and diagnostic prediction of cancers using gene expression profiling and artificial neural networks *Nature Medicine* **2001**, 7, 673 – 679.

86. Hanriot, L; Keime, C; Gay, N. A combination of Long SAGE with Solexa sequencing is well suited to explore the depth and the complexity of transcriptome. *BMC Genomics* **2008**, 9, 418.

87. Wheelan, S. J.; Martínez-Murillo, F.; Boeke, J.D.. The incredible shrinking world of DNA microarrays. *Mol Biosyst 4* **2008**, 7, 726–32.

88. Hierro, N; Esteve-Zarzoso, B.; González, A; Mas, A.; Guillamón, J. M. Real-time quantitative PCR (QPCR) and reverse transcription-QPCR (RT-QPCR) for the detection and enumeration of total yeasts in wine. *Appl. Environ. Microbiol.* **2006,** AEM.00388-06

89. Bustin, S. A.; Benes, V.; Nolan, T.; Pfaffl, M. W. Quantitative real-time RT-PCR – a perspective. *Journal of Molecular Endocrinology* **2005,** 34**,** 597–601

90. Slots, J.; Liu, Y. B.; DiRienzo, J. M.; Chen, C.; Evaluating two methods for fingerprinting genomes of Actinobacillus actinomycetemcomitans. *Oral Microbiology and Immunology* **1993**, 8, 337–343.

91. Karrer, E.E.; Licioln, J.E.; Hogenhout, S.; Bennett, A.B.; Bostoek, R.M; Martinau, B.; Lucas, W.J.; Gilchrist, D.G.; Alexander, D.; *In situ* isolation of mRNA from individual plant cells: creation of cell-specific cDNA libraries. *PNAS* **1995,** 92, 3814–3818.

92. Hruz.T; Wyss, M.; Docquier, M.; Pfaffl, M. W.; Masanetz, S.; Borghi, L.; Verbrugghe, P.; Kalaydjieva, L.; Bleuler, S.; Laule, O.; Descombes, P.; Gruissem, W.; Zimmermann, P. RefGenes: identification of reliable and condition specific reference genes for RT-qPCR data normalization. *BMC Genomics* **2011**, 12, 156

93. Micheal W. Pfaffl., A new mathematical model for relative quantification in real-time RT–PCR. *Nucleic Acids Research,* **2001**, 29 (9).

94. Schwanhäusser B, Busse D, Dittmar G, Schuchhardt J, Wolf J, Chen W, Selbach M.,"Global quantification of mammalian gene expression control". *Nature* **2011,** 473.

95. Boone, T.; Fan, Z. H.; Hooper, H.; Ricco, A.; Tan, H. D.; Williams, S., Plastic Advances Microfluidic Devices. *Anal Chern* **2002**, *74* (3), 78A-86A.

Chapter 2 - Experimental

2.1 Thesis Experimental

Biomarkers are biological molecules that are found in blood, other bodily fluids, and tissues. Research indicates that biomarkers are signatures of a normal or abnormal process, even biological conditions or disease.[1, 2, 3] A biomarker may be used to see how well or poorly the body responds to a treatment; it is also indicative of the presence of a disease or condition. For this reason, biomarkers are also noted in medical/scientific literature as molecular markers and signature molecules. To potentially harness the body's capability to render such information makes this study, the utility of biomarkers, and the detection of them not only a novel endeavor, but also one of necessity.

As with current studies, the employment of biomarkers is a significant factor in current and future research initiatives. An array of biomarkers will be derived and applyed as a distinction method for an applied biomarker panel as well as for identifying stroke and its class. Our partnering institution, Downstate Medical Center, first disclosed the biomarkers of research and detection interest, after identifying their over or under gene expression regulation behavior.[2] With the information shared by Downstate, the desired PCR and LDR primers were synthesized to have high specificity for gene sequences, which have been identified as biomarker for the stroke event/condition.

As seen in figure 2.1, by means of Real-time PCR expression profiling, the study and data recovered of various genes that include Amphiphysin (AMPH), Interleukin (IL1R2), and Spectrin alpha chain (SPTAN1) were accomplished and the differentially expressed genes between ischemic stroke (labeled in blue) and hemorrhagic stroke (labeled in red) can be clearly

realized. The data illustrated by Downstate was carried out on blood samples from patients clinically diagnosed with the respective stroke condition via Real-Time PCR. The disparity in this plot (e.g. Hem vs. Isc) shows that the gene regulation of an identified gene type can serve as a viable biomarker in a diagnostic scheme for the stroke condition. In light of the work done previously by Downstate and the large differentiation in gene expression of Amphiphysin (AMPH), which is known to be the gene that encodes for a protein which is associated with the cytoplasmic surface of synaptic vesicles, the biomarker identified as AMPH was chosen for this thesis study.

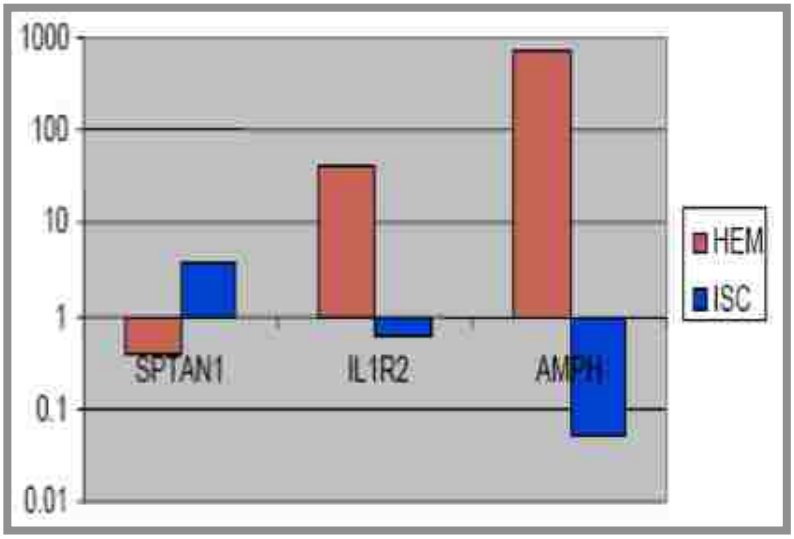

Figure 2.1 Gene expression profiles of biomarkers that are characteristic of stroke. The differentially expressed genes between ischemic which are labeled in (blue) and hemorrhagic stroke in contrast are labeled in (red) are shown. Real time PCR was carried out on blood samples from patients clinically diagnosed with the respective stroke condition. Looking at the figure we can visualize the disparity in expression of a gene type during a diagnosed stroke condition.

For gene expression profiling in this works proposed method and conventional method the biomarker will be synthesized too double-stranded cDNA from mRNA (Reverse Transcription). This reaction utilizes a short oligo(dT) chain is hybridized to the poly(A) tail of an mRNA strand. The oligo(dT) segment serves as a primer for the action of reverse transcriptase, which uses the mRNA as a template for the synthesis of a complementary DNA

strand. The resulting cDNA ends in a hairpin loop. When the mRNA strand has been degraded by treatment with NaOH, the hairpin loop becomes a primer for DNA polymerase I, which completes the paired DNA strand. The loop is then cleaved by S1 nuclease (which acts only on the single-stranded loop) to produce a double-stranded cDNA molecule (From J. D. Watson, J. Tooze, and D. T. Kurtz, Recombinant DNA: A Short Course. Copyright © 1983 by W. H. Freeman and Company.) .

Analyzing mRNA in white blood cells circulating throughout the cardiovascular system, which are recruited to repair tissue damage in the brain, characterizes this gene expression profiling. The blood-brain barrier, which is formed by tight bonds between endothelial cells that restricted the passage of solutes, mandates the use of recruited cells this is due to the fact that the cells at the stroke event location in the brain are not accessible for gene expression profiling. The limited amount of sample advocates the use of mRNA for exploitation due to its potential to be reverse transcribed and amplified for quantification analysis, unlike protein biomarkers.

2.2 Polymerase Chain Reaction (PCR) Amplification of Genomic DNA

For this work, gene expression profiling's most practiced conventional method of RT-PCR was also studied. The method was engineered to probe and quantify for the biomarker AMPH, which then was used to serve as a benchmark to determine the validity of the novel gene expression profiling method proposed in this chapter. There are several steps involved in PCR techniques, which were presented in Section 1.1 and illustrated in Figure 1.2. The overall concepts of this profiling method mainly consist of the replication and amplification of the biological materials DNA or RNA at an exponential rate.

This work's use of human genomic cDNA made reverse transcription unnecessary to create complimentary DNA for the PCR primers; this reverse transcription step is done when RNA is the target molecule, due to the fact that the *Taq* enzyme will not preform on RNA (only DNA). The DNA was first denatured; the strands and primer are annealed, and then extended. This amplification of sequences is taken through repetitive thermal cycling. This process is manipulated through the use of thermal controls as seen in Figure 2.2. Following the thermal profile programed into the Stratagene Mx4000 interface (Figure 2.2), it is seen that denaturation of the DNA takes place at 95ºC for this assay. This causes the double helix to unwind and form single stranded DNA making the target sequence readily accessible for primer hybridization. The annealing step takes place between 54ºC and 72ºC (Figure 2.2) making primers readily available for complementary sequence, taking into account that both utilized primer's T_m should be between 55ºC and 88ºC, to alleviate the assembly of self priming and self–dimer structures.[7, 8] In addition, the primer length should be 17-28 bases long, should end 3' in a G or C or GC or GC, and should be composed of 50-60% G-C to T-A to create a higher priming efficiency due to Watson-Crick G-C base pair bond strength. When the correct primer design parameters are followed, we see in this step that PCR primers, short oligonucleotides designed to complement a specific sites, bind to the template DNA (which was created in the denaturing step) and define the region to be amplified (check primer fabrication via http://www.ncbi.nlm.nih.gov/). In the last step, extension, the temperature is set at 72ºC. The deoxyribonucleotide triphosphates (Adenine, dATP; Cytosine, dCTP; Thymine, dTTP; Guanine, dGTP) are polymerized from the PCR primer in a 3' to 5' direction and subsequently inserted according to Watson-Crick base paring from the target DNA strand. These steps are repeated in an exponential amplification process, see section 1.1 and figure 1.2 for more details.

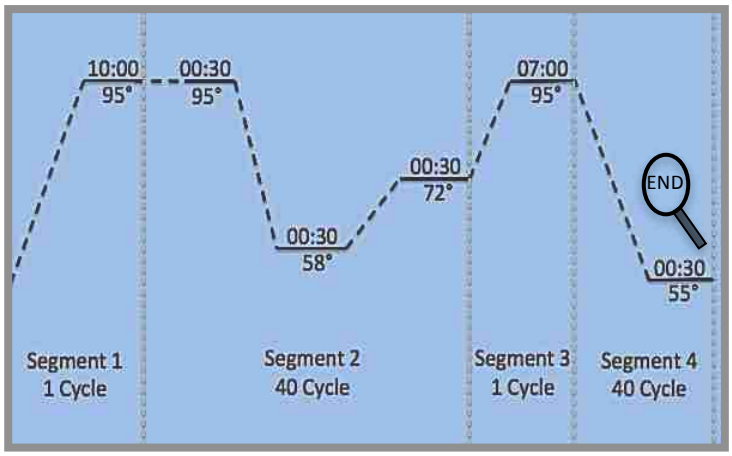

Figure 2.2 RT-PCR Thermal Profile.

This study of RT-PCR amplifications (Stratagene, Mx4000) were carried out in 25µL of 1X PCR buffer II pH 8.3 (BioLabs Ipswich, MA), 2.5 mM $MgCl_2$, 200 µM dNTPx, 1 µM forward and reverse primers, 1.25 units of DNA polymerase (AmpliTaq Gold Polymerase, BioLabs), 0.1ng of 100ng of template DNA (ATCC, MCF7 - Homo sapiens) and enough nuclease-free H_2O (Sigma-Aldrich, W4502) to make a total reaction of 25µL. The PCR primer sequences (Integrated DNA Technologies, Inc.) are as follows: Forward - 5′ ACT TCA CCC GAC GCT TAG 3′; Reverse - 5′ CAG ACA AAC CTT GGG AAG AT 3′; PCR product size 152 (bp) after extension, Homo sapiens. In PCR, the reaction cocktail was first heated to 94ºC for 10 minutes to activate the Amplitaq gold enzyme. After a 30 s denaturation step at 94ºC, the cocktail was subjected to 40 thermal cycles, annealing step at 58ºC for 30 s, and extension step at 72ºC for 30 s. Following the thermal cycling, the reaction mixture was maintained at 95ºC for an additional 7 min to allow complete extension of all RT-PCR products. The PCR products were cycled at 95ºC to 55ºC 40 times to insure proper hybridization.

2.3 Ligase Detection Reaction (LDR)

The LDR (which process was outlined in section 1.7) was chosen as a means of discrimination for this work. By process of traditional bench top chemistry a thermal cycler (Eppendorf, New York) performed LDR on human genomic DNA (ATCC, MCF7 - Homo sapiens) at copy numbers between 15-3,090 and at the primer concentration of 100 pM (Integrated DNA Technologies, Inc.) through isothermal zones poised at 65ºC for annealing/ligation and 94ºC for denaturing (see Figure 2.3). The subjected reaction mixture consisted of 2 units/mL of thermo-stable DNA ligase, 20 mM Tris-HCl (pH 7.6), 25 mM potassium acetate, 10 mM magnesium acetate, and 1 mM NAD+ cofactor (New England, BioLabs), 10 mM dithiothreitol and nuclease-free H_2O for a total volume of 10 µL. It is important to note that this same LDR technique can be employed for the probing and discrimination of RNA target sequences, unlike the conventional gene expression method RT-qPCR.

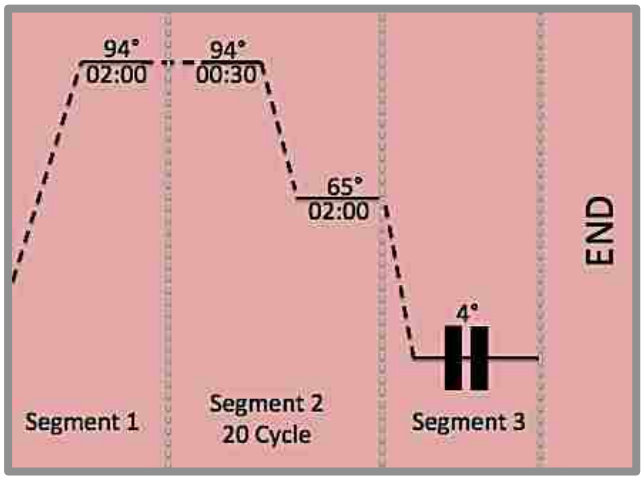

Figure 2.3 LDR Thermal Profile.

2.4 LDR Primers and Molecular Beacon Design

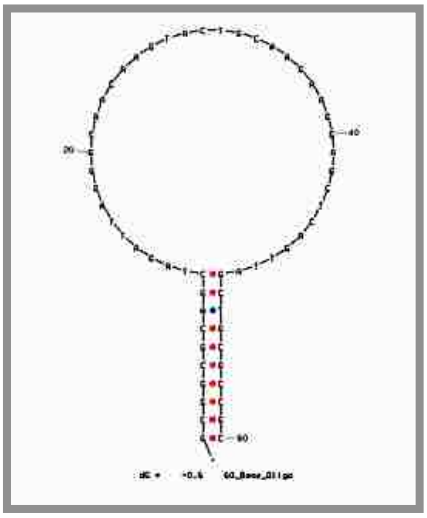

Figure 2.4 LDR Primers and reverse Molecular Beacon Designed to undergo FRET.

The AMPH gene sequence specific LDR primer (Integrated DNA Technologies, Inc.), which will give way to the production of rMBs for SMD (as seen in figure 2.4 above), are synthesized as such: 5'- /5Cy55/GCG GCG CAG CTA GAT TAG GGC AAC AAG TAC-3';5'-/5Phos/TGC AAG AAG GAG CTC AGT TAG CTG CGC CGC/3Cy5Sp/ -3' (primer length should between 17-30 bases long not including tail sequences to specificity). In regard to the LDR primer modeling, the acceptor functioning primer was composed by a 20-base loop and a 10-base stem, with the 10-base arm 5'-end labeled with Cy5.5. The 30-base donor functioning primer, which contained a 20-base loop and a 10-base stem, was phosphorylated at its 5'-end and at the 3'-end was labeled with Cy5. The two stem sequences were designed to be complementary to each other, but not to the target gene sequence, should be 80-90% G-C to T-A to increase rMBs T_m. This T_m increase of stem is due to the stronger bond formed by G-C's triple bond Watson-Crick base pairing interactions and in turn makes sure the loop base sequence's T_m is lower then the stem's T_m, which is essential when considering detection variable. The research shows that when the formation of stem-hairpin loops (rMB) is thermodynamically favored over

loop-target hybridization (at a temperature of 75ºC), the resulting formation generates FRET response from the rMB and no FRET from unligated primers. It is important to make sure the FRET's T_m is high such that when self-dimer temperature is exceeded, mRNA and ligase primer interactions are present during the temperature set for Single Molecule Detection (SMD) thermal profile operations.[12]

2.5 Microfluidic Chip Design and Fabrication

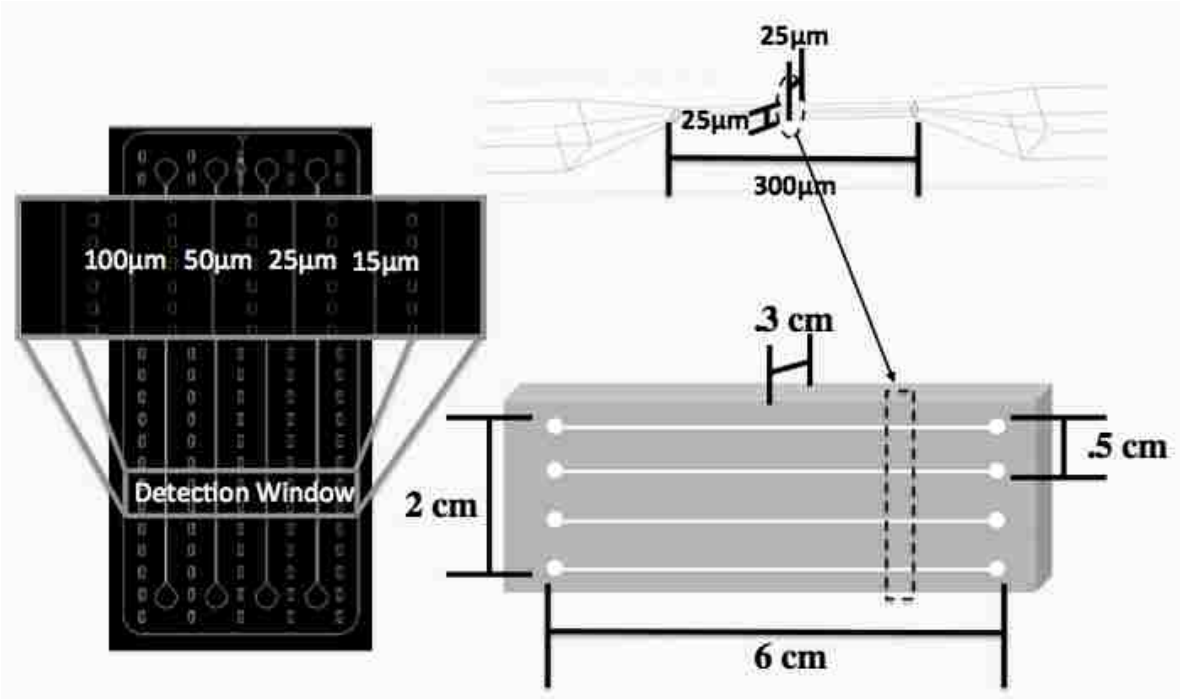

Figure 2.5 Microfluidic chip AutoCAD Design that illustrates a chip model that has multiple detection zones in the dimensions of 100µm x 100µm, 50µm x 50µm, 25µm x 25µm, and 15µm x 15µm respectfully.

In order to fabricate the chip, microfluidic channels were hot embossed into a 5013-L COC substrate (0.5 cm thickness, TOPAS Advanced Polymers GmbH) using a high precision micro-milled brass master and hydraulic press (PHI Precision, City of Industry, CA) supplied with homemade vacuum chamber. Micro-milling of the master was performed with 50 to 500 mm diameter solid-carbide milling bits (McMaster-Carr or Quality Tools, Hammond, LA) at 40,000 rpm using KERN MMP 2522 CNC milling machine (KERN Micro-und Feinwerktechnik

FmbH). Hot embossing was achieved by pressing a headed (170°C) metal master into a polymer substrate for 210 s at 62 psi pressure. The polymer substrate was then cooled below the liquid-glass transition state (T_g) of the polymer and separated from the molding master. The chip was cut to final size of 3 cm x 7 cm and the holes for fluid s were drilled see Figure 2.5. Further optimization and fabrication included O_2 plasma modification and UV modification. The microfluidic channels were formed by thermal fusion bonding of a thin (0.25μm) COC coverslip (GoodFellow, Oakdale, PA) to the embossed COC substrate. For the microfluidic chip assembly, the devices were clamped between two glassplates and placed in a convection oven at 132°C for 15 min for annealing. Reviewing the T_g and identifying the inflection temperature as seen in Figure 2.6 realized the annealing parameters. For sample injection, the system was enclosed using a 21cm capillary (O.D. 363nm; I.D. 75nm), which was attached by applying epoxy to the chip/capillary joint.

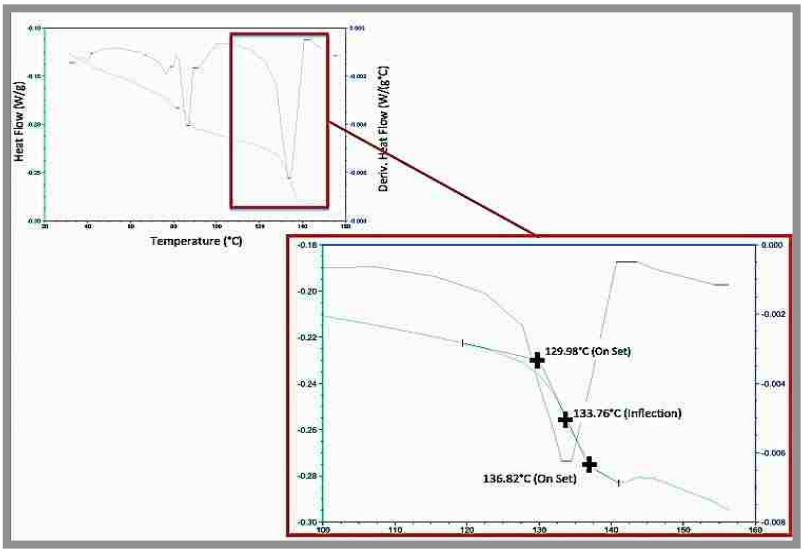

Figure 2.6 Plot illustrating the measuring of the amount of energy needed to melt the COC polymer sample to identify the T_g.

The plastic material cyclic olefin copolymer (COC) is seen to be a useful substrate material for fabricating microfluidic devices due to its low cost, ease of fabrication, excellent optical properties, and resistance to many solvents.

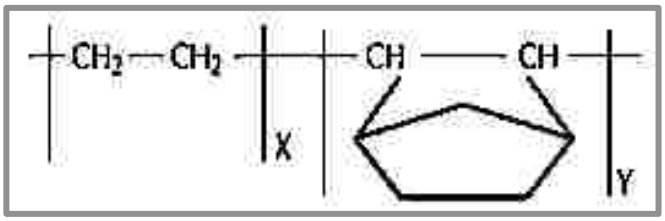

Figure 2.7 The employed polymer is a cyclo olefin copolymer (COC) copolymerized from norbornene and ethylene using a metallocene catalyst. This polymer has a very low auto-fluorescence, which is the natural emission of light by biological entities. COC has a high moisture barrier, excellent chemical resistance, high heat resistance and long shelf life, which makes it a perfect subtract for this work.

2.6 Instrument Design

SMD Instrument Design. The hardware was designed to not only perform the SMD, but also control temperatures for the biochemical reaction. There were five major sections associated with the hardware: (1) photon detection, (2) laser diode control, (3) high voltage, (4) microfluidic channel temperature control, and (5) data acquisition. The components and layout of the system are presented in Figure 2.8.

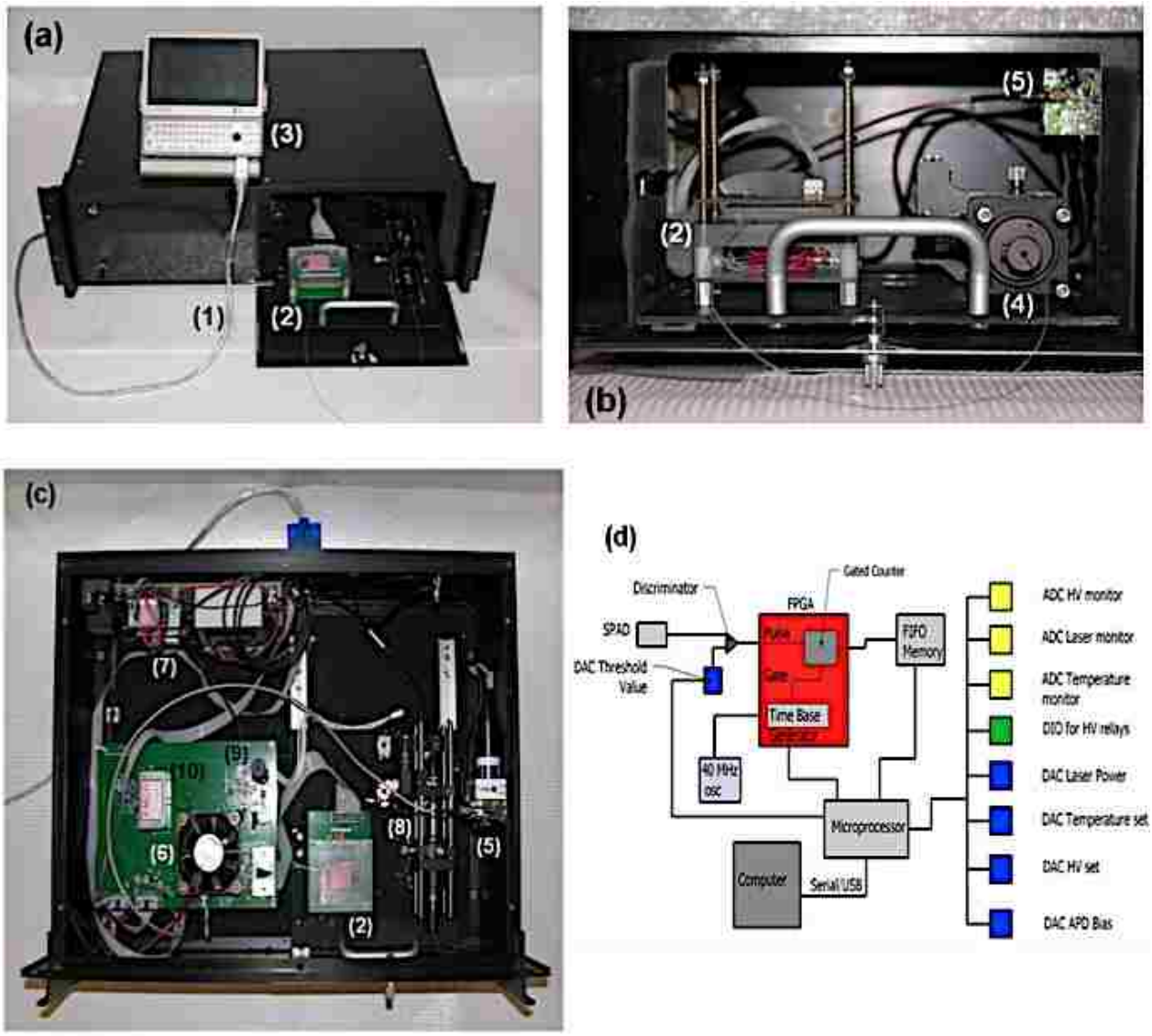

Figure 2.8 (a) Picture of the compact SMD instrument connected to a mini-computer for data collection and instrument control. (b) Access panel for loading sample into the microfluidic chip and connecting the collection fiber optic to the fiber U-bench, which contained optical fibers and was interfaced to the SPAD. (c) Inside the compact SMD instrument showing the arrangement of the VCSEL, SPAD, FPGA and other peripheral electronics. (d) Schematic of the FPGA that was used for data acquisition and single-photon processing. The FPGA counted signals from the SPAD and output information to the first-in first-out (FIFO) memory. (1) – USB interface cable to the controlling computer; (2) – microfluidic chip sitting atop a mounting stage, which is accessed through a drawer that slides out from the main instrument case; (3) – controlling computer; (4) – fiber bench with optical cable connected to the fluidic chip; (5) – SPAD with integrated fiber optic; (6) – cooling fan for the FPGA, which is located underneath this fan; (7) – various power supplies; (8) – fiber bench with optical filters; (9) – VCSEL with integrated fiber; and (10) – electrophoresis power supply to actuate fluids electronkinetically.

An Opnext HL6385DG vertical cavity surface emitting laser (VCSEL) diode was used as the excitation source with a lasing wavelength of 642 nm. To minimize output power fluctuations, a highly stable constant current source was designed to provide up to 280 mA drive current to the laser. The laser diode was connected to an SMA housing for interfacing a fiber optic to it, which also contained a built-in pin diode for laser power monitoring. At 250 mA drive current, the laser output from the coupling fiber optic was ~24 mW. Conditioning electronics were designed to convert the pin diode output to a 0-5 V signal that was directly proportional to the laser diode output power. An optical fiber was coupled to the SMA housing using an SMA connector and was a 10/125μm (SMF-28-10, Thorlabs) single-mode fiber. The distal end of this fiber was sealed using epoxy glue into a guide channel embossed into the fluidic chip.

The photon counting system used a PCDMini single photon avalanche diode, SPAD (SensL, Cork, Ireland), which was directly coupled to a fiber optic (200/230 μm BFH48-200, ThorLabs). The PCDMini measured 1½" x 1½" and had an integrated Peltier cooler. The PCDMini possessed a high single photon quantum efficiency between 650-700 nm (>23%) and an extremely low dark count rate (~10 cps). The maximum acceptable count rate of the SPAD was determined to be 5M cps (See Supporting Information, Figure S1).

Collection of the fluorescence photons was achieved using a high NA (0.48) multimode fiber (200/230 μm BFH48-200, Thorlabs) that was sealed within the fluidic chip and oriented at 90° with respect to the excitation fiber. The distal end of the collection optical fiber was spliced into an OFR fiber port (PAF-X-5, Thorlabs) for free beam-to-fiber coupling that allowed placement of the appropriate optical filters for the emission and then coupling back into the fiber optic cable interfaced to the SPAD. In this way, the fiber connected to the SPAD did not need to be replaced every time the fluidic chip was changed.

To minimize dead time and conserve board space, the photoelectrons generated from the SPAD were processed using a custom programmed field programmable gate array (FPGA). The FPGA (XCR3256XL-12TQ44I, Xilinx Inc., San Jose, CA) was a surface mount 144-pin device programmed using the ISE Webpack software, version 7.1. The design used a JTAG interface for in-circuit programming so that the FPGA code could be loaded or modified on the target board without the need to remove the FPGA chip for updating. The SPAD produced a TTL pulse that was sent to the FPGA, which was used for processing the TTLs from the SPAD. A diagram of the electronic components including the FPGA operation is shown in Figure 1(d). The FPGA was integrated into the SMD instrument as a single-photon counter with a unique dual gated counter configured in a "ping-pong" format to give virtually zero dead time (50 ns) between output counts to the first-in first-out (FIFO) memory.

Finally, communication between the microcontroller and the analog system used 12-bit A/D and D/A converters via an I2C serial bus. Data transmission between the control board and the computer was via the standard USB port. Custom software was written in-house using LabView and installed on a mini computer (OQO, Marlton, NJ) for end user control.

2.7 Microfluidic Chip Optimization

The prescribed optimized chip was fabricated out of the polymer COC, and then embossed at CAMD. The chip design applied four different detection zone dimensions: 100µm x 100µm, 50µm x 50µm, 25µm x 25µm, and 15µm x 15µm, respectfully, as seen in Figure 2.5. Each of the four-channels began uniformly with a dimension of 100µm x 100µm and then tapered into the desired detection window parameters. To optimize these various channel dimensions, studies investigated the probing of genomic DNA, for the target gene sequence of AMPH and the florescent events produced by applying the LDR-spFRET technique.

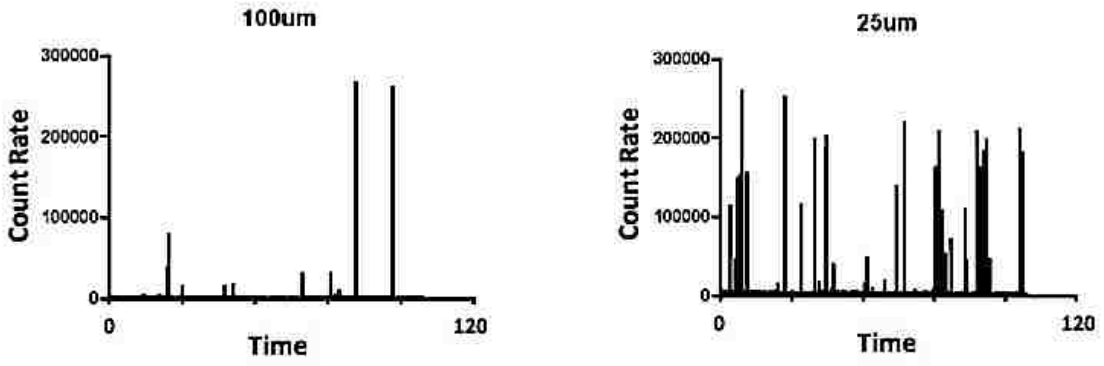

Figure 2.9 shows the increase of fluorescent events and their intensity, in equivalent LDR-spFRET product dilutions, which have been subjected to SMD methodology.

When reviewing the data for the different detection zones, there is an increase of real-time fluorescent events as indicated in Figure 2.9. In addition to the increase of events and intensity, which is contributed to the change in concentration detectable in the defined, probe volume. The sampling efficiency shows improvement due to the probing volume being manipulated my enforced smaller dimensions of the microfluidic channels; which shows more detection of rMB events in dimension with smaller detection windows.

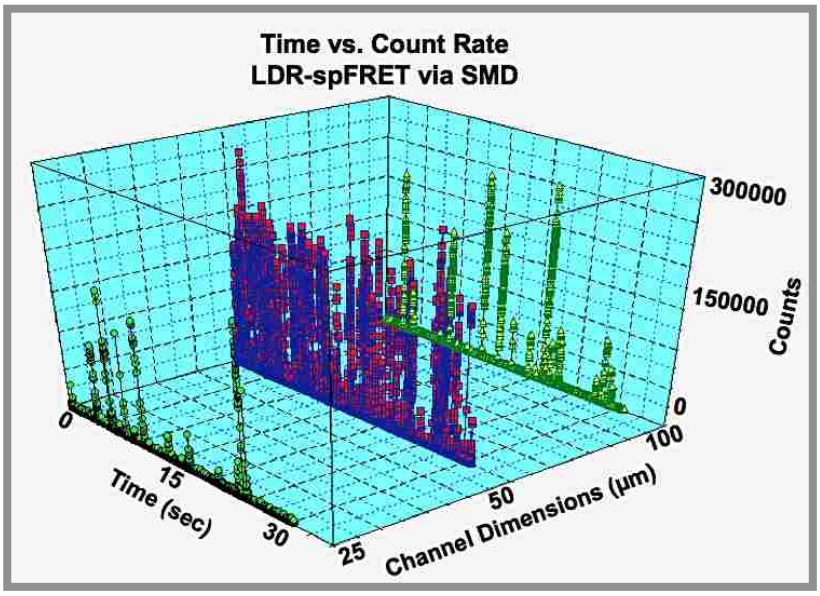

Figure 2.10 shows an increase of fluorescent events and their intensities, in equivalent LDR-spFRET product dilutions for channel dimensions 50 µm to 100 µm via SMD, but decreases when sample is detected in 25µm.

When optimizing the microfluidic device, the consideration of polymer surface chemistry must be taken into account. If the sample/polymer interaction does not amplify the detection method's figures of merit a surface modification maybe advantageous. This modification was done to negate any sample and polymer reaction causing substrate adhesion. If this adsorption occurs we see a dramatic decrease of fluorescent events during SMD. To limit this occurrence, which can arise during experimental analysis on involved surfaces such as: the inner parts of the injection syringe, capillary and microfluidic channel, the COC's surface chemistry required modification. The modification optimizing was deemed beneficial into increase the COC's surface chemistry hydrophilic nature. We know for prior studies that DNA is a hydrophilic molecule, in turn making the LDR-spFRET products hydrophilic molecules.

The modification of the microfluidic chip was realized when the loss of samples on the microfluidic channel walls was hypothesized from data illustrated in Figure 2.10. This defect can have great impact on the quality of biological sample preparation and detection conditions. It has been observed that DNA can bind to polymers, and that the interaction of DNA with channel walls can induces a change of conformation, which can go as far as complete denaturation. The choice of a polymer with low binding adsorption quality is therefore of crucial importance. The LDR-spFRET products seem to have an affinity to the polymer walls; this inherited issue is due to the nature and chemistry the rMBs mimic (e.g DNA or RNA).

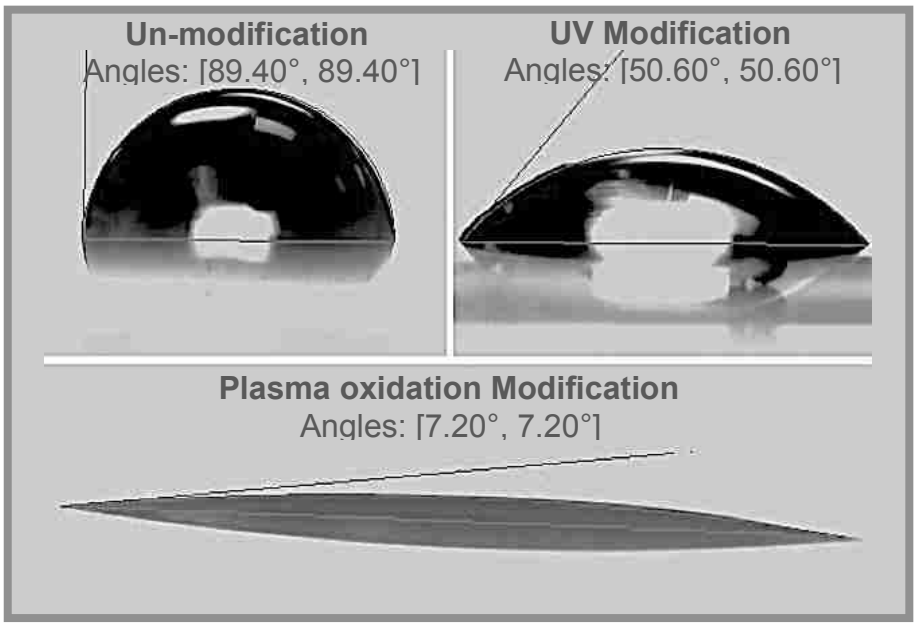

Figure 2.11 The calculated angle shown is determined by the interactions across the three interfaces. This test is illustrated with a small liquid droplet resting on a flat horizontal solid surface. The Young's relation or Wetting, which observes the ability of a liquid to maintain contact with a solid surface, determines the droplets shape.

The COC surface modification optimizing applied adaptation procedures such as UV and O_2 plasma modifying. We learn that after UV modification there is an increase of carboxyl groups on the polymer's surface. Furthermore, the concentration of ether and carbonyl groups (C-O-C and C=O) increased on polymer surface after O_2 plasma modification; however, the percentage of the carbon atoms in C-C groups was reduced at the surface after exposure. To further understand the UV and O_2 plasma modification, an analysis of the hydrophilic nature of the COC's surface chemistry, a measurement of the contact angle was employed. This depicts the angle at a liquid/surface interface as seen in figure. The image reveals that after undergoing O_2 plasma modification, the contact angle decreases substantially. This is due to the formation of the COC's surface hydrophilicity in respect to the functional groups each modification provokes, see figure 2.12.

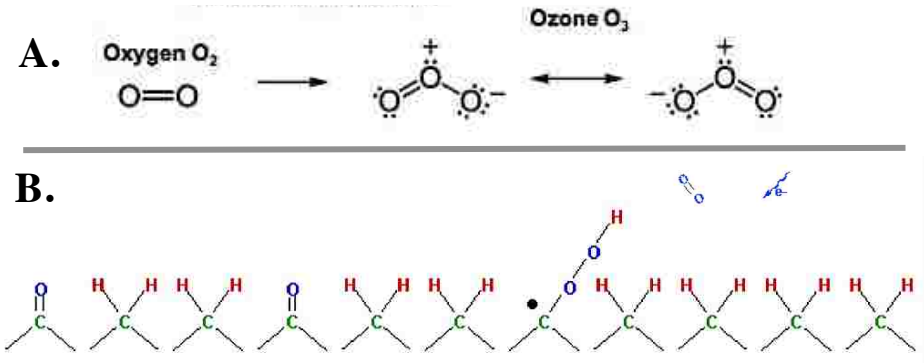

Figure 2.12 (A.) The surface activation is characterized by the modification of chemical surface properties which is based on chain scission, the formation of functional groups, and cross-linking on the surface based on plasma generated components mainly UV radiation, charged particles (ions), and radicals, which in turn reacts using an oxygen molecule to producing hydro-peroxides, ketones, aldehydes, carboxyls, hydroxides, and ester groups. **(B.)** O_2 plasma modification - The reaction is initiated with atomic oxygen, which abstracts a hydrogen atom from the surface. This result in a free radical on the surface, which in turn can react with an oxygen molecule to producing hydro-peroxides, ketones, aldehydes, carboxyls, hydroxides, and ester groups. The plasma oxidation results furthermore in breaking the polymer chains and material removal. A specific surface functionalisation is possible under precise control of the reaction conditions.

2.8 RT-PCR Data

For the RT-PCR genomic DNA analysis, we first ran the sample cocktail on the multiplex quantitative (Stratagene Mx4000) PCR system and confirmed the PCR product assembly via agarose gel electrophoresis (Figure 2.13).

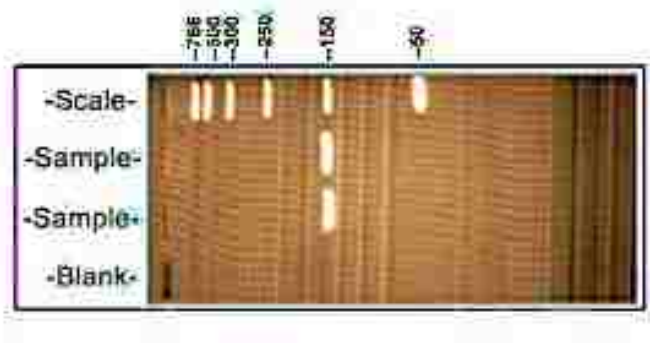

Figure 2.13 Agarose gel electrophoresis using 1.8% TBE (Tris-Borate-EDTA) Human genomic cDNA and PCR primer assembly to form products (152 bp), running at a constant voltage of 200 volts.

After loading the sample into individual wells with a pipet at a total volume of 5 µL. Then place into gel apparatus, connect the leads so that the red (positive) lead is at the end of the gel to which the DNA will migrate and the black (negative) lead is at the end of the gel

containing the wells, running at a constant voltage of 200 volts. When the blue tracking dye (which runs in these gels along with a DNA fragment) has migrated about 75% of the distance to the end of the gel (60-90 minutes) stop correct. Carefully transfer the gel into a plastic dish and add staining solution to cover the gel. Visualize the DNA with UV light.

The amplification plot below (Figure 2.14) shows and defines the fluorescence signal versus cycle number of the samples. In the initial cycles of the RT-PCR, there is little change in fluorescence signal, which defines the baseline for the amplification plot. An increase in fluorescence above the baseline indicates the detection of accumulated RT-PCR product. A fixed fluorescence threshold of 0.50 was set above the baseline. The parameter Ct (threshold cycle) is defined as the fractional cycle number at which the fluorescence passes the fixed threshold. We indicate that at a higher genomic DNA concentration, the initial amount of the genomic DNA (copy number), the sooner accumulated product is detected in the RT-PCR process as a significant increase in fluorescence, and the lower the Ct value. A CT value in the exponential phase, where the threshold is picked, there is a linear relation between log of the change in fluorescence and cycle number and the reaction components are not limiting (Figure 2.14).

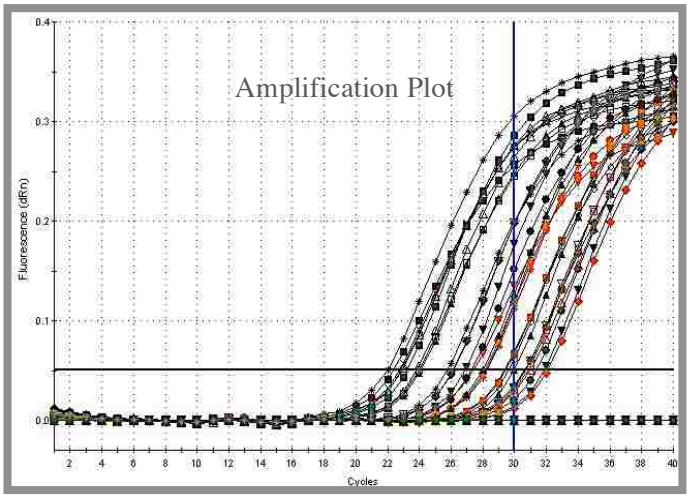

Figure 2.14 RT-PCR Amplification plot of Human genomic DNA diluted in a 10-fold dilution series (copy numbers 0; 22.8; 45.6; 91.2; 228; 456; 912; 2280; 4560; 9120) and amplified using SYBR Green I.

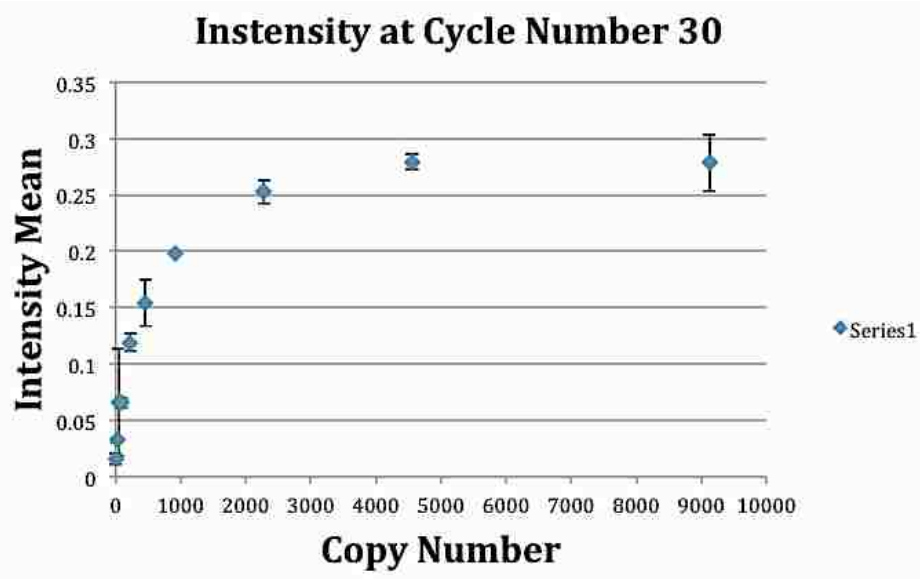

Figure 2.15 (a.) Above. A calibration curve showing the various fluorescence intensities in correlation to the genomic DNA (copy number dilutions) employed (i.e. 0; 22.8; 45.6; 91.2; 228; 456; 912; 2280; 4560; 9120). **Figure 2.15 (b.) Below.** A standard curve was derived from the serial dilutions in a customary manner. Relative concentrations were expressed in arbitrary units. Logarithms (base 10) of concentrations were plotted against crossing points. Least square fit was used as the standard curve.

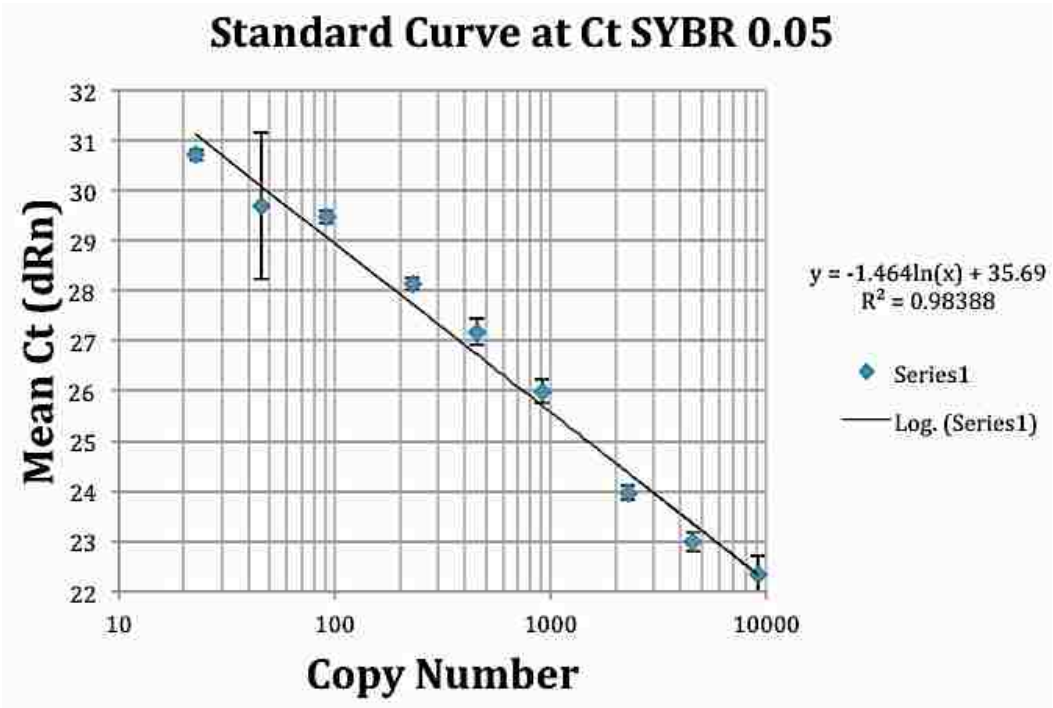

2.9 LDR-spFRET via SMD Data

In the single-molecule detection experiments, tapered detection window with smaller dimensions were designed and fabricated in the micro-channel for fluorescence measurement. This dimension change was completed in order to capture more photo burst events of the rMB generated from LDR. Test results using LDR products of different copy numbers showed good correlation between the detected numbers of photon burst and input cDNA copy number in the 100x100 μm channel. Data was generated utilizing two new chips with straight channels containing 100x100 μm and 25x25 μm detection windows, to compare the sensitivity between detection windows. The COC substrate was treated by means of the oxygen plasma by placing in oven (Harrick Plasma Cleaner/Sterilizer PDC-3XG) for ~2 minutes before closing the channels by annealing. Then, after connecting the capillaries, the chip was rinsed with IPA and buffer before use (Figure 2.16).

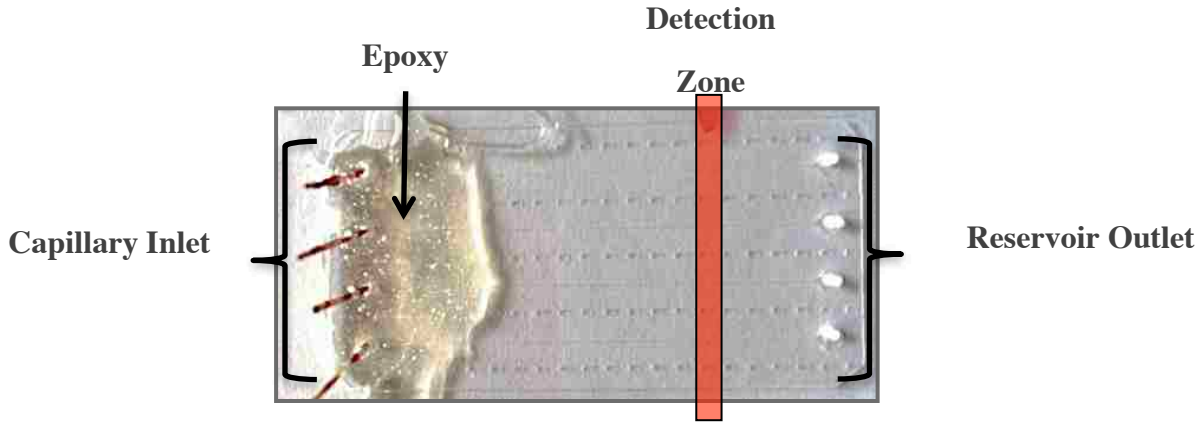

Figure 2.16 Optimized microfluidic chip, which put to use Polymer COC; 25X25 μm channel detection window; Pumping injection method; O_2 plasma modification.

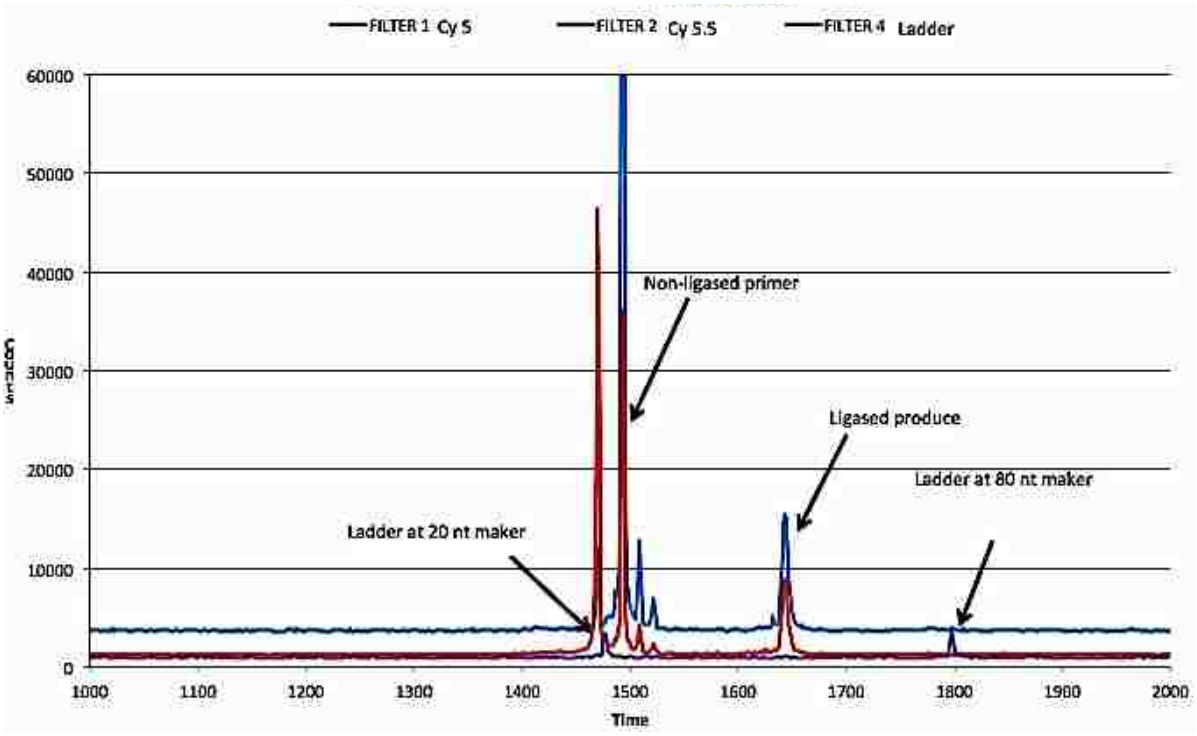

Figure 2.17 Beckman Coulter GenomeLab Plot of LDR-spFRET products. The above graph is showing at ladder marker labeled for 20 nucleotides, we see large peaks characteristic of the non-ligased primers. Furthermore, the data illustrates peaks between 1600-1700 time (min) characteristic of ligased products

The LDR was run 20 cycles in the thermal cycler using cDNA as the template to generate the molecular beacon for single-molecule measurement. To confirm formation of LDR product after thermal cycling a capillary gel electrophoresis (CGE) was done via Beckman Coulter GenomeLab, which is a GeXP Genetic Analysis System that is fully automated that employs an array of coated capillaries, novel infrared dyes, an optimized linear polyacrylamide gel (LPA) and comprehensive informatics which fully automates the processes of DNA sequencing, gene expression and fragment analysis. The results of the CGE plot can be seen in Figure 2.17. The result shown in the following plot, illustrates the optimized chip data recovered (Figure 2.18).

In this plot, the lower curve shows the relationship between the number of detected photon bursts and the input cDNA copy number detected on the 100X100 μm channel, and the upper curve shows the 25X25 μm channel. The input cDNA copy number was varied from 300

to 30,000. In the 25X25 μm channel, the detected photon bursts range from 13 to 630. In the 100X100 μm channel, the detected photon bursts range from 0.7 to 64. This suggested that many more single molecule events could be registered in the 25X25 μm detection channel than in the 100X100 μm detection channel, and the smaller detection channel offered a better sensitivity in the single-molecule measurement. The sample with 30 copies of cDNA was measured in both 100X100 μm and 25X25 μm channels, but unfortunately there were no photon bursts observed.

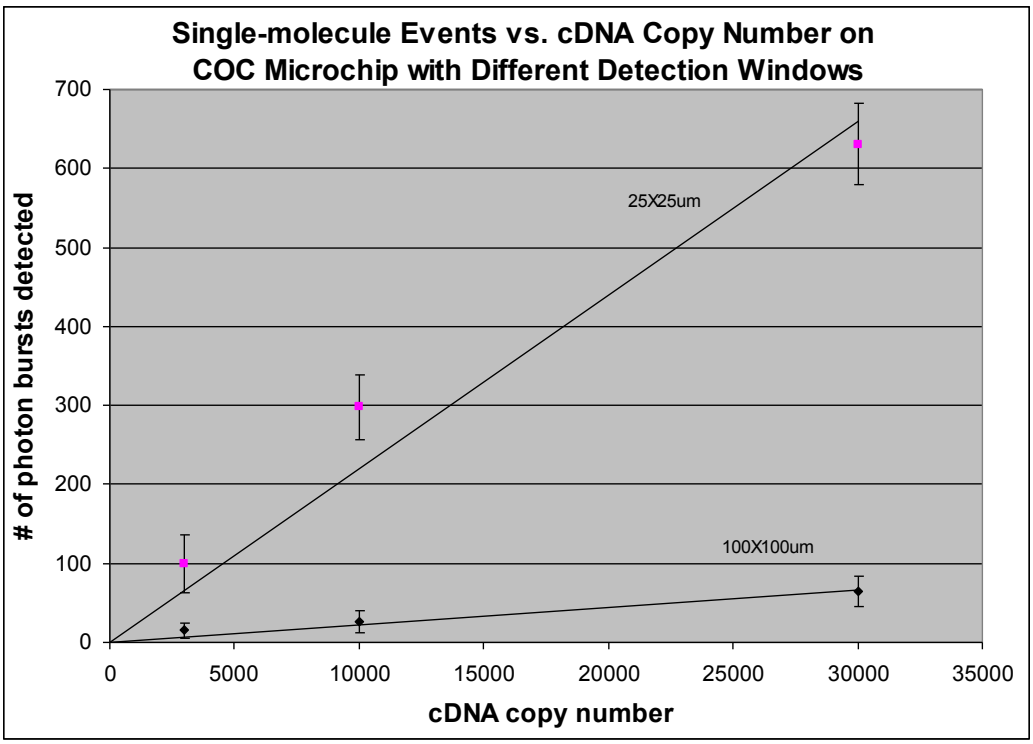

Figure 2.18 Calibration plot of channel dimensions at various copy numbers dilutions presented by plotting the number of photon events versus the copy number.

2.10 References

1. Whiteley, W.; Tseng, M. C.; Sandercock, P., Biomarkers in the Diagnosis of ischemic Stroke- a Systematic Review. *Stroke* **2008**, 39 (10), 2902-2909.

2. Reynolds, M.A.; Kirchick, H. J.; Dahlen, J. R.; Anderberg, J. M.; McPherson, P. H.; Nakamura, K. K.; Laskowitz, D. T.; Valkirs, G. E.; Buechler, K. F., Early Biomarkers of Stroke. *Clinical Chemistry* **2003**, 49 (10), 1733-1739.

3. Samowitz, W. S., Curtin, K., Schaffer, D., Robertson, M., Leppert, M., and Slattery, M.L., Relationship of Ki-Ras Mutationsin Colon Cancers to Tumor Location, Stage, and Survival: A Population-Based Study. *Cancer Epidemiol Biomarkers Prev* **2000**, 9, 1193-1197.

4. Neely, L.A.; Patel, S.; Garver, J.; Gallo, M.; Hackett, M.; McLaughlin, S.; Nadel, M.; Harris, J.; Gullans, S.; Rooke, J., A Single-Molecule Method for the Quantitation of Micmrna Gene Expression. *Nat Methods* **2006**, 3 (I), 41-46.

5. C. A. J. Hoeve .,Theory of polymer adsorption at interfaces, Journal of Polymer Science Part C: Polymer Symposia 1971 Volume 34, Issue 1, pages 1–10

6. Lin, Y. C.; Jen, C. M.; Huang, M. Y.; Wu, C. Y.; Lin, X. Z., Electroporation Microchips for Continuous Gene Transfection. *Sensors and Actuators B-Chemical* **2001**, 79 (2-3), 137-143.

7. Barany, F.; Widmann, M.; Wilson, W. J.; Czajka, J.; Luo, J.; Batt, C. A., Ligase Chain Reaction (Lcr)--Overview and Applications. *PCR Methods and Applications* **1994**, S51- S64.

8. Khanna, M., Park, P., Zirvi, M., Cao, W., Picon, A., Day, J., Paty, P. and Barany, F., Multiplex Pcr /Ldr for Detection of K-Ras Mutations in Primary Colon Tumors. *Oncogene* **1999**, *18,* 27-38

9. Dahlgren, N.; Ahmed, N.; Davalos, A.; Hacke, W.; Millan, M.; Muir, K.; Roine, R. O.; Toni, D.; Lees, K. R.; Investigators, S., Thrombolysis with Alteplase 3-4 Center Dot 5 H after Acute Ischaemic Stroke (Sits-Istr): An Observational Study. *Lancet* **2008**, *372* (9646), 1303-1309.

10. Rosamond, W.; Flegal, K.; Furie, K.; Go, A.; Greenlund, K.; Haase, N.; Hailpern, S.M.; Ho, M.; Howard, V.; Kissela, B.; Kittner, S.; Lloyd-Jones, D.; McDermott, M.; Meigs, J.; Moy, C.; Nichol, G.; O'Donnell, C.; Roger, V.; Sorlie, P.; Steinberger, J.; Thorn, T.; Wilson, M.; Hong, Y.; Arner Heart Assoc Stat Comm, S., Heart Disease and Stroke Statistics - 2008 Update - a Report from the American Heart Association Statistics Committee and Stroke Statistics Subcommittee. *Circulation* **2008**,117 (4), E25-El46.

11. Furlan, A.; Higashida, R.; Wechsler, L.; Gent, M.; Rowley, H.; Kasc, C.; Pessin, M.; Ahuja, A.; Callahan, F.; Clark, W. M.; Silver, F.; Rivera, F.; Investigators, P., Intra-Arterial Prourokinase for Acute Ischemic Stroke - the Proact **Ii** Study: A Randomized Controlled Trial. *Jama-Journal of the American Medical Association* **1999,** *282* (21), 2003-2011.

12. Wabuyele, M. B.; Farquar, H.; Stryjewski, W.; Hammer, R. P.; Soper, S. A.; Cheng, Y. W.; Barany, F., Approaching Real-Time Molecular Diagnostics: Single-Pair Fluorescence Resonance Energy Transfer (spFRET) Detection for the Analysis of Low Abundant Point Mutations in K-Ras Oncogenes. *JACS* **2003**, 6937-6945.

CHAPTER 3 – DESIGN AND DEVELOPMENT OF A FIELD-DEPLOYABLE SINGLE-MOLECULE DETECTOR (SMD) FOR THE ANALYSIS OF MOLECULAR MARKERS

3.1 Introduction

While many have demonstrated the utility of fluorescence-based single-molecule detection (SMD) for several different types of molecular assays,[1-10] the transitioning of SMD into routine clinical measurements has not occurred to-date in spite of its inherent advantages. The advantages afforded by SMD specifically for molecular assays includes, elimination of processing steps in multi-step assays (for example, eliminates the need for amplification steps, such as PCR), reduces the processing time to realize near real-time readout, exquisite analytical sensitivity due to the use of molecular (i.e., digital) counting, and ultra-low limits-of-detection (single-molecule level). In addition, SMD can generate quantitative data without the need for generating calibration plots when the sampling efficiency of single molecules is near unity.

The major bottleneck toward realizing the wide-spread use of SMD into many applications has been limitations imposed by the equipment required to make these measurements, typically consisting of large continuous or pulsed lasers, an extensive array of opto-mechanical components and expensive photon transducers, such as CCDs or channel plates.[11, 12] In fact, most single-molecule measurements are made using laser confocal microscopes due to the ultra-small probe volume they generate providing high signal-to-noise ratios (SNR) for individual molecules and the excellent light gathering ability of the isotropic emission they can produce when using a high numerical aperture microscope objective.

Another bottleneck for transitioning SMD into routine use is the extensive amount of sample preparation that is required prior to carrying out the fluorescence measurement. For example, clinical samples, such as blood, urine, cerebral spinal fluid, saliva, *etc*., typically

require extensive amount of pre-processing to isolate the target molecules to minimize matrix interferences during the single-molecule measurements. For example, many biomarkers such as DNAs and RNAs, are encased within the cellular and nuclear envelopes and therefore, must be released via cell lysis prior to analysis. Also, once lysed, the targets must be isolated using for example solid-phase extractions to eliminate potential interferences in the downstream processing steps and/or interferences during the fluorescence SMD.

There have been a few reports focused on simplifying some of the operational components associated with SMD, for example miniature power supplies developed by Erickson.[13] Giudice *et al*. also reported a photon counting module using Si avalanche photodiodes[14] and several groups have also reported SMD for lab-on-a-chip (LOC) devices with potential field-use applications.[15-19] However, the literature is currently devoid of any reports detailing the development of a compact and simple SMD instrument, including the processing electronics, opto-mechanics, excitation source and photon transducer, that can provide processing of input samples and the subsequent detection of single molecules using laser-induced fluorescence for potential point-of-use measurements.

The evolution of equipment such as light emitting diodes, laser diodes, optical fibers, and gradient refractive index lenses has important applications to SMD.[20] Laser diodes are available in a wide range of wavelengths and offer reduced sizes compared to other lasers, such as air-cooled argon, Ti-sapphire, or helium-neon lasers. Furthermore, many different optical components allow for the control and shaping of the excitation source to create the necessary photon flux to provide near optical saturation for generating high signal-to-noise ratios for SMD. On-chip lenses have also been demonstrated to create high photon densities.[21-23] Waveguides are another important optical component that can be integrated into microfluidic devices for both

illumination and emission collection for SMD. Recently, Yin and coworkers demonstrated anti-resonant reflecting optical waveguides (ARROW) for single-molecule fluorescence correlation spectroscopy (FCS) in a microfluidic format.[16] The compact planar opto-fluidic devices were able to generate small excitation volumes (~fL) and signals coupled to external optical fibers for both excitation and detection. A sacrificial layer process on a silicon nitride substrate fabricated the ARROWs with silicon dioxide layers serving as the core.

The drawback to most of the aforementioned approaches was the increased complexity associated with the fabrication of the fluidic chip making it difficult to realize low-cost disposable platforms appropriate for diagnostic applications. Therefore, simple and low-cost optical components incorporated into the microfluidic chip with minimal fabrication steps would be highly advantageous for clinical diagnostics. Seo *et al*. demonstrated a 2D planar lens in PDMS to focus light from an LED into a fluidic channel.[22] They designed single and multi-element lenses to effectively shape the excitation beam to increase the resulting fluorescence intensity from fluorescent nanospheres. The lenses were fabricated in the same step used to fabricate the microfluidic channels. However, the 2D lenses only focused the light in one dimension. The direct integration of fiber optics into micro-capillary electrophoresis devices has been previously demonstrated in the literature as well.[21, 24-33]

When fibers are integrated into microfluidic devices, they can act as waveguides to deliver excitation light to a defined location of the device in a well-controlled volume, producing high photon irradiances. The illumination volume is set by the core diameter of the fiber optic as well as the acceptance angle of the fiber with typical diameters ranging from 4 μm to 1 mm. Fiber optics can also act as collection optics. In a method called “butt-end fiber coupling,” a fiber was placed against a diffuse light source and collected the light from an area of radius *r* and solid

angle defined by the numerical aperture (NA) of the fiber.[34] The maximum collection efficiency of a fiber optic cable is achieved by directly integrating the fiber optic into the microfluidic chip butting the end to the excitation zone. The NAs of optical fibers (NA 0.12 to 0.22) are generally lower than a microscope objective typically used in SMD experiments, but high NA fibers are also available (NAs ~0.48).

The requirement for a small footprint SMD instrument not only includes the opto-mechanical components, but consideration to the data processing electronics as well. Field programmable gate arrays (FPGA) offer a number of advantages compared to standard printed circuit boards for the processing of electronic signals generated from photon transducers (see Supporting Information, Table S1).[35] The integration of FPGA into microfluidic devices has not been extensively reported, except for one clinical application.[36] However, no reports have appeared in which an FPGA was used for SMD.

Another issue associated with the utilization of SMD for clinical applications has been the inability of the SMD equipment to prepare samples prior to the optical measurement. Microfluidics offers the possibility of generating systems appropriate for point-of-use analyses that can provide full automation of the sample processing pipeline.[17] Coupling microfluidics to SMD offers the capability to generate sample-processing pipelines that reduce processing time through the elimination of processing steps and eliminate the need for operator intervention. In addition, the small sample volume requirements associated with microfluidics are compatible with SMD. Therefore, the use of SMD coupled to microfluidics can produce systems with unique capabilities that can be used for potential point-of-use applications.

SMD of bacteria based on the use of genomic probes offers the potential for fast, sensitive analysis with minimal amounts of false positive results. For example, Castro *et al*. demonstrated a technique for the rapid detection of specific nucleic acid sequences in unamplified DNA samples from *Bacillus anthracis*.[37] [38] They demonstrated the ability to detect 100 amol of target DNA at a SNR of 3 in 200 s and the assay showed good specificity, even in the presence of an excess of *B. globigii*. In addition, Peng *et al*. used single-pair fluorescence resonance energy transfer following a ligase detection reaction to detect bacterial species with high specificity and sensitivity.[39] The authors reported the ability to identify Gram(+) from Gram(-) bacteria in 2.6 min with single copy limit-of-detection. While the aforementioned papers are excellent examples of using SMD for the rapid reporting of various bacterial species, the hardware used for the measurements were poised on optical tables and in some cases, used mode-locked lasers and microchannel plates with time-correlated single photon counting electronics for processing the photoelectron events. Thus, the SMD hardware was not conducive to point-of-use operation.

In this paper, we describe the hardware and fluidic components necessary for a molecular analysis system that was configured in a compact, and potentially field-deployable format capable of performing SMD for the determination of Gram positive/negative status of bacteria as an example. The system consisted of the opto-mechanics coupled to a microfluidic chip with the interface consisting of fiber optics integrated to the fluidic chip. The processing electronics were based on an FPGA design. The system could detect fluorescence signatures from single molecules and also, could prepare the sample prior to the SMD.

3.2 Experimental

SMD Instrument Design. The hardware was designed to not only perform the SMD, but also control temperatures for the biochemical reaction. There were five major sections associated with the hardware: (1) photon detection, (2) laser diode control, (3) high voltage, (4) microfluidic channel temperature control, and (5) data acquisition. The components and layout of the system are presented in Figure 3.1.

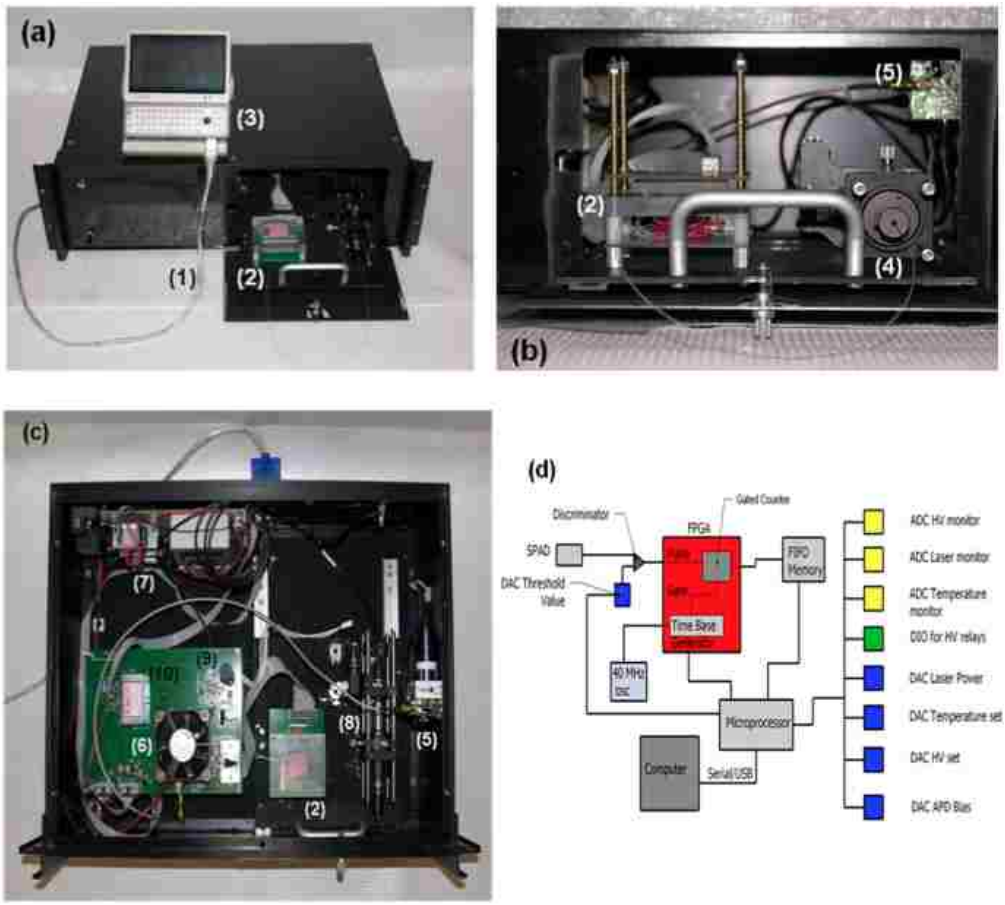

Figure 3.1 (a) Picture of the compact SMD instrument connected to a mini-computer for data collection and instrument control. (b) Access panel for loading sample into the microfluidic chip and connecting the collection fiber optic to the fiber U-bench, which contained optical fibers and was interfaced to the SPAD. (c) Inside the compact SMD instrument showing the arrangement of the VCSEL, SPAD, FPGA and other peripheral electronics. (d) Schematic of the FPGA that was used for data acquisition and single-photon processing. The FPGA counted signals from the SPAD and output information to the first-in first-out (FIFO) memory. (1) – USB interface cable to the controlling computer; (2) – microfluidic chip sitting atop a mounting stage, which is accessed through a drawer that slides out from the main instrument case; (3) – controlling computer; (4) – fiber bench with optical cable connected to the fluidic chip; (5) – SPAD with integrated fiber optic; (6) – cooling fan for the FPGA, which is located underneath this fan; (7) – various power supplies; (8) – fiber bench with optical filters; (9) – VCSEL with integrated fiber; and (10) – electrophoresis power supply to actuate fluids electronkinetically.

An Opnext HL6385DG vertical cavity surface emitting laser (VCSEL) diode was used as the excitation source with a lasing wavelength of 642 nm. To minimize output power fluctuations, a highly stable constant current source was designed to provide up to 280 mA drive current to the laser. The laser diode was connected to an SMA housing for interfacing a fiber optic to it, which also contained a built-in pin diode for laser power monitoring. At 250 mA drive current, the laser output from the coupling fiber optic was ~24 mW. Conditioning electronics were designed to convert the pin diode output to a 0-5 V signal that was directly proportional to the laser diode output power. An optical fiber was coupled to the SMA housing using an SMA connector and was a 10/125 μm (SMF-28-10, Thorlabs) single-mode fiber. The distal end of this fiber was sealed using epoxy glue into a guide channel embossed into the fluidic chip.

The photon counting system used a PCDMini single photon avalanche diode, SPAD (SensL, Cork, Ireland), which was directly coupled to a fiber optic (200/230 μm BFH48-200, ThorLabs). The PCDMini measured 1½" x 1½" and had an integrated Peltier cooler. The PCDMini possessed a high single photon quantum efficiency between 650-700 nm (>23%) and an extremely low dark count rate (~10 cps). The maximum acceptable count rate of the SPAD was determined to be 5M cps (See Supporting Information, Figure S1).

Collection of the fluorescence photons was achieved using a high NA (0.48) multimode fiber (200/230 μm BFH48-200, Thorlabs) that was sealed within the fluidic chip and oriented at 90° with respect to the excitation fiber. The distal end of the collection optical fiber was spliced into an OFR fiber port (PAF-X-5, Thorlabs) for free beam-to-fiber coupling that allowed placement of the appropriate optical filters for the emission and then coupling back into the fiber optic cable interfaced to the SPAD. In this way, the fiber connected to the SPAD did not need to be replaced every time the fluidic chip was changed.

To minimize dead time and conserve board space, the photoelectrons generated from the SPAD were processed using a custom programmed field programmable gate array (FPGA). The FPGA (XCR3256XL-12TQ44I, Xilinx Inc., San Jose, CA) was a surface mount 144-pin device programmed using the ISE Webpack software, version 7.1. The design used a JTAG interface for in-circuit programming so that the FPGA code could be loaded or modified on the target board without the need to remove the FPGA chip for updating. The SPAD produced a TTL pulse that was sent to the FPGA, which was used for processing the TTLs from the SPAD. A diagram of the electronic components including the FPGA operation is shown in Figure 1(d). The FPGA was integrated into the SMD instrument as a single-photon counter with a unique dual gated counter configured in a "ping-pong" format to give virtually zero dead time (50 ns) between output counts to the first-in first-out (FIFO) memory.

Finally, communication between the microcontroller and the analog system used 12-bit A/D and D/A converters via an I2C serial bus. Data transmission between the control board and the computer was via the standard USB port. Custom software was written in-house using LabView and installed on a mini computer (OQO, Marlton, NJ) for end user control.

Microfluidic Chip Fabrication. Figure 2a shows the design of the microfluidic chip, which consisted of a single channel that had a width of 50 μm and a depth of 120 μm. The excitation fiber conduit, which was embossed into the fluidic chip, was 120 μm wide with a depth of 120 μm. The collection conduit was 220 μm wide and 220 μm deep. The excitation and detection geometry is shown in Figure 2b, which consisted of a four-way intersection.

A detailed description of the microfluidic chip fabrication protocol is described elsewhere[40] and a brief description is given in the Supporting Information (Figure 3.2). The microfluidic channels were enclosed by thermal fusion bonding a thin (0.25 mm) PMMA

coverslip (GoodFellow, Oakdale, PA) to the embossed PMMA substrate following insertion and gluing of the fiber optics to the substrate. For thermal fusion bonding, the microfluidic chip assembly containing the fibers was clamped between two glass plates and placed in a convection oven at 107°C for 20 min.

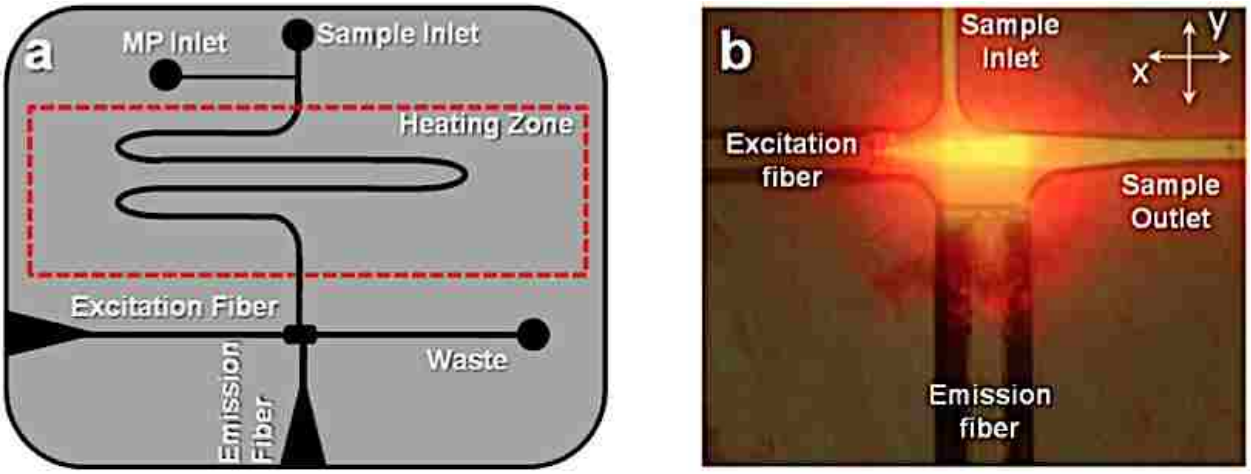

Figure 3.2 (a) Design of the polymer-based microfluidic chip with integrated fiber optics for delivering excitation light to the chip and collecting the resulting emission. The fibers were placed in guide channels embossed into the chip to allow exact placement during chip assembly and were oriented at 90° with respect to each other. The chip also contained a backside heater to control the temperature for hybridization-based assays. (b) Fluorescence image of the field-of-view of the excitation and emission fibers showing the intersection of the optical paths, which defined the probe volume, which was determined to be 98 pL in this case. The chip was filled with Alexa Fluor 660 dye to generate the necessary image.

Chemicals and Materials. Borate buffer was prepared by dissolving the desired amount of sodium borate (Sigma Chemical) into nanopure water secured from a Barnstead Nanopure Infinity System (Model D8991, Dubuque IA). The pH (pH 8.5) was adjusted by the addition of concentrated HCl. The buffer was diluted to a final concentration of 50 mM and filtered with a 0.2 μm filter before use. Bovine serum albumin (BSA) from Sigma was added to the buffer (0.1 mg/mL) to reduce surface non-specific interactions. Alexa Fluor 660 and Dark Red fluorescent FluoSpheres (diameter = 0.2 μm) were both purchased from Invitrogen (Eugene, Oregon). The fluorescent spheres were sonicated and diluted in the borate buffer to yield the desired

concentration. The fluorescent dye was diluted in buffer to yield a final concentration of 2.0 fM. Concentrations were selected to keep the occupancy probability below 1.0% to minimize the probability of photon bursts arising from ≥2 molecules occupying the probe volume simultaneously.

Oligonucleotides used to probe for the bacterial genomes and generate molecular beacons (MPs) were purchased from Integrated DNA Technologies (Coralville, Iowa) with a custom sequence (5'-GCACGAAAGCCTGACGGAGCAACGCCGCGTGAGTGATGACGTGC-3', where the underline section designates the complementary stem sections of the MP). The 5' end was modified with a TYE 665 fluorescent dye and the 3' end was modified with Iowa Black RQ-Sp quencher. The MB sequence was designed to probe for the presence of DNA encoding for ribosomal RNA (rRNA) related to the Gram(+) gene.[41] **The MBs were diluted in 50 mM borate buffer with BSA to a concentration of 0.5 nM.** Two bacterial strains, *Staphylococcus aureus* subsp. Aureus (ATCC 700699) and *Escherichia coli* (ATCC 700926) were investigated in this study and the genomic DNA for each strain was acquired from ATCC (Manassas, VA).

Flow Velocity Modeling. A computational fluid dynamic (CFD) simulation was run using ANSYS Fluent 12.0 software. The general-purpose preprocessor for CFD analysis was done with Gambit 2.0, which created quad element meshing with 80,000 nodes. The input volume flow rate for these simulations was 0.05 mL/h.

3.3 Results and Discussion

The diameter of the excitation optical fiber coupled to the microfluidic chip as well as the fiber's divergence served in determining the irradiance and the probe volume size. Reductions in the core diameter of the excitation fiber led to an increase in the irradiance producing better signal-to-noise ratio for the single-molecule measurements, but also reduced the excitation volume, consequently, a reduction in the single-molecule sampling efficiency.[42] On the other hand, increasing the diameter of the collection fiber along with its numerical aperture and reductions in its distance from the emitting source (i.e., single molecule), increased the amount of fluorescence processed by the system during the residence time of the molecule within the excitation volume.

The effective field-of-view of the collection fiber overlaid with the excitation fiber's field-of-view should define the probe volume. Ideally, this volume should be minimized to reduce noise generated from scattering photons produced from the solvent; however, larger collection fibers allowed for more efficient gathering of the fluorescent photons as noted above. To visualize the field-of-views of the excitation fiber and collection fiber, we filled the microfluidic device with Alexa Fluor 660 and launched laser light into both fibers. We then collected two images using a microscope equipped with a CCD camera; (1) Fluorescence generated by the excitation fiber only; and (2) fluorescence generated by the collection fiber only. An overlay image was also produced from images (1) and (2) (see Figure 2(b)). The overlap area of the resulting fluorescence produced from both fiber optics defined the effective probe volume. The cross section of the excitation fiber image produced a diameter of 10 μm due to its low divergence because this was a single mode fiber (cross sectional area = 7.85 x 10^{-7} cm^2). With this cross section, the 24 mW output power from the optical fiber generated an

irradiance of ~10^{23} photon cm^{-2} s^{-1}. This is a reasonable fluence because it generated an excitation rate, k_a ($k_a = \sigma I$, σ is the absorption cross section, cm^2, and I is the laser fluence, photons cm^{-2} s^{-1}) near optical saturation ($1/\tau_f$, where τ_f is the fluorescence lifetime of the dye).[43]

The probe volume was calculated from the $1/e^2$ diameter of the laser emanating from the fiber (~25 μm) and the collection fiber (observation length = 200 μm) and was determined to be 9.8 x 10^{-11} L or 98 pL. This probe volume was used to select the concentration for the SMD experiments so that the occupancy (molecules/probe volume) probability could be adjusted to minimize contributions of double occupancy within the data stream.

The probe volume was configured at a right angle with respect to the sample input into the probe volume with the two fiber optics meeting at a four-way junction to keep the emission fiber close to the excitation fiber to improve the fluorescence collection efficiency. Due to the irregular shape of this detection geometry, we performed simulations to map the flow vectors as the fluid moved through the probe volume and subsequently into the waste reservoir (see Figure 2(b)). The simulation results indicated a decrease in the linear velocity as the solution entered the wider channel region as expected. The velocity through the probe volume showed minor linear velocity changes, however, the paths through the probe volume were distinct. We categorized these different paths into three types; (1) perpendicular to the excitation axis; (2) diagonal to the excitation axis; and (3) parallel to the excitation axis. We overlaid the CFD simulation results with the trapezoid-shaped (black outline, see Figure 3(a)) probe volume. The corresponding path lengths across the probe volume for these 3 types were 50, 75, and 200 μm, respectively. These differences may result in different transit times for molecules adopting a trajectory as it moves through the probe volume. The consequence of this is that a broad range of photon burst peak

heights would be generated even when operating under a condition where photobleaching is negligible.[44]

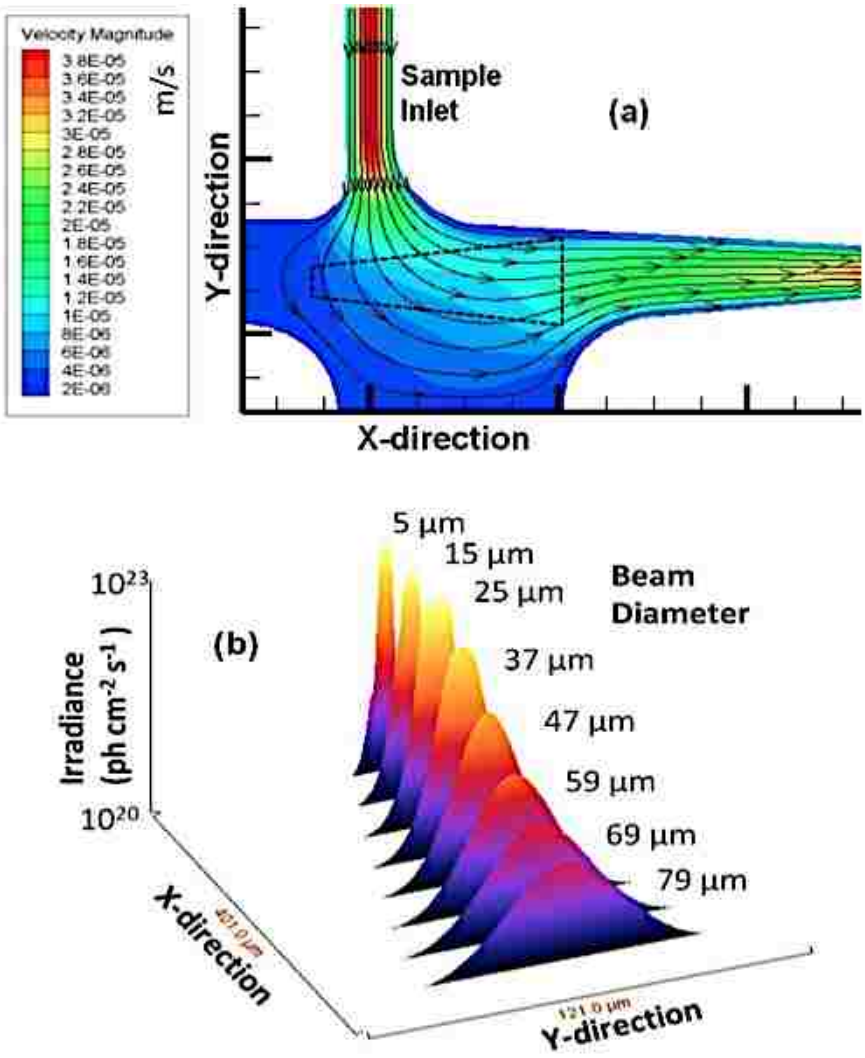

Figure 3.3 (a) Simulation of the flow velocities and flow vectors of the fluid as it moved from the input channel into the detection zone (units are m/s). The simulation was run using Fluent software with quad elements meshing and 80,000 nodes performed in Gambit. An outline of the probe volume as determined from Figure 1 (b) is shown as well (black dotted line). (b) 3D surface plot of the detection zone versus the irradiance experienced by single fluorescent entities as they traverse through the probe volume. The irradiance decreased as the beam expanded and thus, single fluorescent entities traveling along the edges of the Gaussian intensity profile show reduced photon fluxes.

The distribution of the irradiance as a function of channel position was also plotted versus the irradiance (photon cm^{-2} s^{-1}) and is shown in Figure 3(b) with 8 cross sections taken. As can be seen, moving away from the terminal end of the excitation fiber, the irradiance decreased, which

will reduce the SNR in the single-molecule measurement. From these results, it was apparent that the perpendicular flow path resulted in the best SNR of the three flow paths due to the higher irradiance it afforded. Additionally, the perpendicular path occurred closer to the emission fiber terminal end and was centered over this fiber, which would result in a higher collection efficiency of the resulting fluorescence photons.

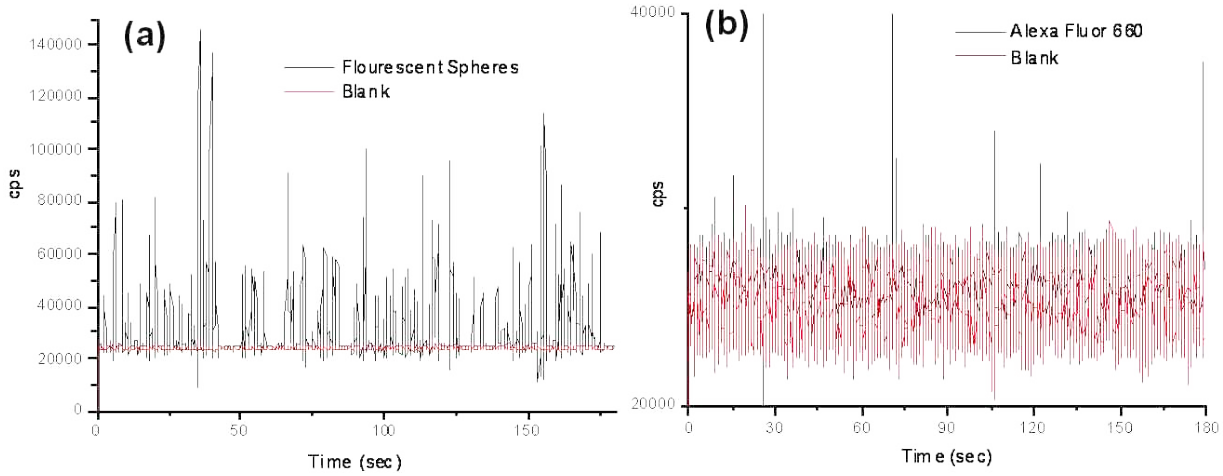

Figure 3.4 Photon burst data collected using the compact, field deployable SMD instrument. The red trace shows the blank and the black trace is the data with fluorescent beads or dye seeded into the buffer. (a) Plot of photon bursts generated from fluorescent microspheres. (b) Single Alexa Fluor 660 dye molecule burst data.

To evaluate various operational parameters associated with this SMD instrument, we used fluorescent microspheres as the probes due to their bright fluorescence signatures resulting from a high load of dye per bead and the lack of photobleaching they demonstrate. A dilute solution of microspheres (3.1 x 10^6 particles/mL) was used, which had a single particle occupancy probability of 0.3 based on the measured probe volume. The spheres were pumped through the microfluidic channel using a syringe pump at a flow rate of 0.05 mL/h (linear flow rate ~0.096 cm/s at 120 μm x 120 μm channel cross section). Figure 4(a) presents a trace of the photon bursts versus time for these microspheres as well as a blank. We were interested in understanding the distribution in the amplitudes of these bursts and whether the probe volume shape, which was defined by the overlap of the excitation and collection fibers, as well as the

various paths taken by the molecules (or microspheres) would affect the variance in this distribution, especially when compared to conventional confocal excitation geometries.

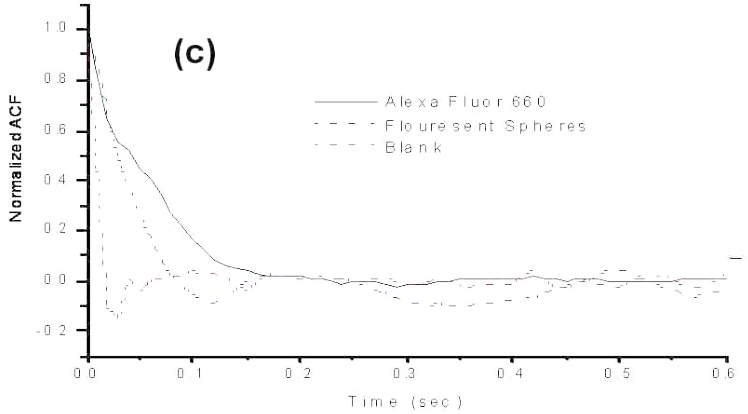

Figure 3.4 (c) Autocorrelation analysis was performed on the blank, fluorescent spheres and Alexa Fluor 660 dye molecule solutions. The fluorescent microspheres and the Alexa Fluor dye molecules showed transit times of 49 ms and 53 ms, respectively, using the same flow rate.

For typical confocal laser-induced fluorescence (LIF) single-molecule detectors, the collimated laser beam is tightly focused to a diffraction-limited spot with the $1/e^2$ beam waist defining the excitation volume and whose intensity distribution has a Gaussian profile. When a single fluorescent molecule is brought into this excitation volume, a photon burst is produced due to repetitive cycling of the fluorophore from the ground to excited state with subsequent relaxation back to the ground state accompanied by photon emission. The magnitude of the burst is directly proportional to the local photon density experienced by the molecule during its passage through the laser. The distribution pattern of the photon burst amplitudes can thus serve as an indicator of the intensity profile the molecules take through the excitation volume. In order to examine if the irregular shape of the probe volume arising from the dual optical fiber configuration had any effect on the photon burst distribution of single-molecule events, we ran a control experiment by hydrodynamically driving the fluorescent beads through a microchannel and histogramming to produce a photon burst distribution using a confocal LIF SMD instrument described elsewhere[45] and compared these results to the dual-fiber arrangement.

Photon burst intensity distribution plots for both the confocal and dual-fiber SMD instruments were built from the raw trace data. In the single particle detection using the confocal setup, the fluorescent beads were diluted to a concentration of ~6 X 10^5 particles/mL to keep the occupancy probability low and the solution was driven through the microchannel at a flow rate to give a similar linear velocity as that for the dual-fiber arrangement (~0.096 cm/s). The trace data for the photon bursts from the single fluorescent beads detected using the confocal setup is shown in Figure 5(a). In order to discriminate real photon burst events from background fluorescence fluctuations (i.e., false positives), a threshold level of 3,000 cps was used. A histogram was constructed from this photon burst data and is shown in Figure 5(c). In this plot, the photon burst magnitude was binned with an increment of 5,000 cps above the threshold level and each bin was normalized to the total number of photon burst events. We found that the photon burst distribution was best fit to a single exponential function (see Figure 5(c)). The reduced χ^2 value of the least square fit was 9.5 X 10^{-4} and the R^2 value was 0.97. From the actual trace data, the average photon burst intensity for the confocal excitation volume was 11,000 ± 12,400 cps. However, we should note that the distribution depicted in Figure 5(c) represents a truncated Gaussian due to the fact that events were only counted when their maximum exceeded the threshold condition.

The photon burst trace data of the fluorescent beads detected using the dual-fiber instrument is shown in Figure 5(b). A threshold condition of 40,000 cps was set as the discriminator threshold in this case to minimize false positive events. A histogram was built from the photon burst trace data and is shown in Figure 5(d). The photon burst intensity distribution was also best fit to a single exponential function with a reduced χ^2 of 1.12 x 10^{-4} and a R^2 value of 0.997. The average photon burst intensity was 65,800 ± 23,700 cps.

Using the histogram data depicted below in Figures 5(c) and (d), we overlaid a Gaussian function on these exponential functions and from these distributions, determined the standard deviations and relative standard deviations (RSD) for the burst amplitudes. For the confocal system, the standard deviation was 2,970 cps with an RSD of 27% while for the dual fiber arrangement; the standard deviation was 23,880 cps with an RSD of 37%.

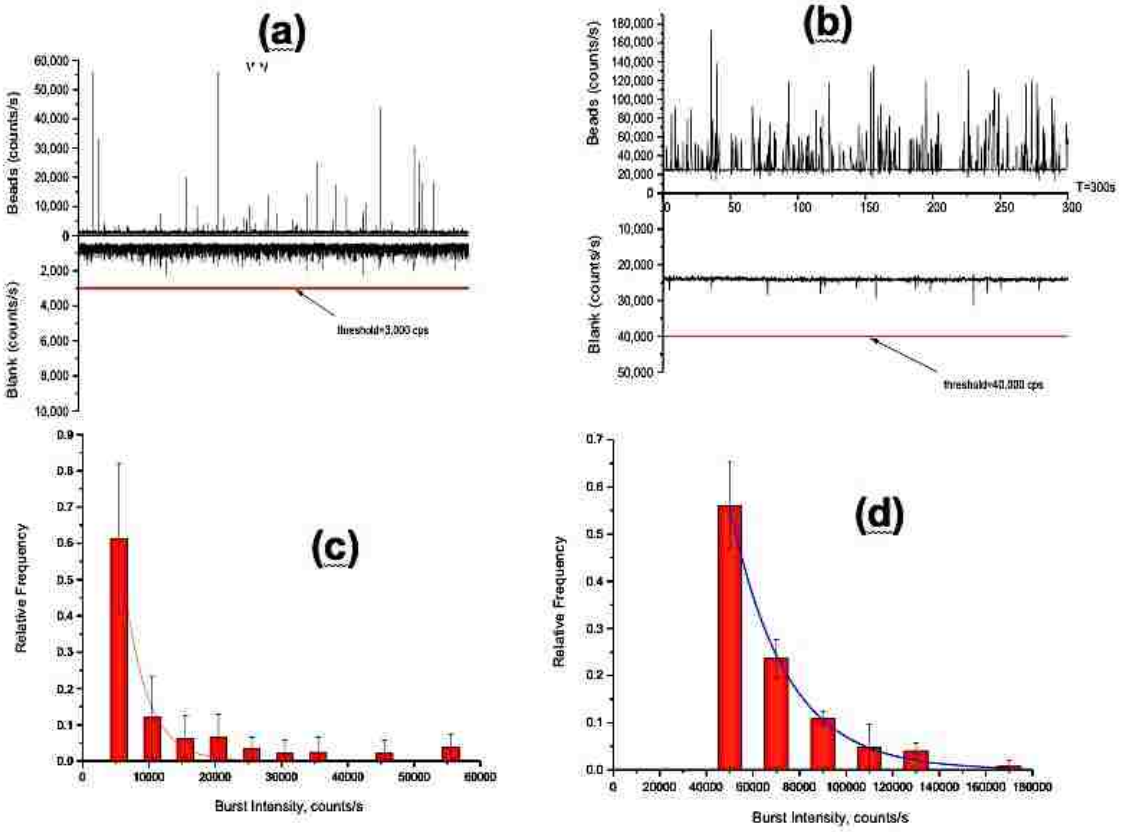

Figure 3.5 (a) Trace data of photon bursts detected using a confocal LIF setup. A threshold level of 3,000 cps was set to discriminate true single particle events against background fluorescence fluctuations. (b) Trace data of photon burst data detected using the compact SMD instrument. In this case, a threshold level of 40,000 cps was set to discriminate single particle events against background fluorescence fluctuations. (c) Histogram of photon burst intensity constructed from data set in (a) using the confocal LIF setup. The accepted photon bursts were compiled into bins of 5,000 cps. (d) Histogram of photon burst intensity from data set in (c) using the compact SMD instrument. The data in this case were accumulated into bins of 20,000 cps.

The average photon burst intensity for the dual-fiber system was higher than that of the confocal setup due to the fact that the residence time of the fluorescent microspheres in the dual fiber arrangement were longer than the confocal system (transit time for dual fiber arrangement ≈

49 ms; transit time for confocal arrangement ≈ 15 ms). However, the relative standard deviation of the burst distribution was larger for the dual-fiber arrangement because of the multiple paths the beads can travel when moving through the excitation volume (see Figure 3(a)).

Single-fluorophore detection. The SMD system was also analyzed for its ability to detect single-fluorophore molecules (see Figure 4(b)). In this case, we chose Alexa Flour 660 due to its high quantum yield and favorable photostablity.[46] The dye was diluted to a concentration of 2 fM, which corresponded to a single-molecule occupancy probability of 0.12. The solution was pumped through the microfluidic chip at the same volume flow rate as that of the microspheres (0.05 mL/h). The fluorescent dye showed a drop in SNR compared to the microspheres, which was anticipated due to the high load (1.1×10^5 fluorescein equivalents per microsphere) of fluorescent dyes on each microsphere. Using a blank sample with no fluorescent molecules set a discriminator level. The discriminator level was set such that no signal from the blank exceeded the discrimination level keeping the false positive rate near 0. The single-molecule data showed photon burst signals above the background when a discrimination level of 32,000 cps was selected for the Alexa Fluor dye. From the data trace shown in Figure 4(d), 48 single-molecule photon burst events were detected.

The autocorrelation functions were derived for the blank, fluorescent spheres and the Alexa Fluor dye solutions and are shown in Figure 4(c). The differences in the autocorrelation function (ACF) from the blank and the fluorescent samples indicated that single molecule events were being detected due to the presence of a non-random component in the ACF. Analysis of the full width at half height of the non-random component in the ACF yielded transit times of 49 ms for the microspheres and 53 ms for the fluorescent dyes. The ACF did not show evidence of the longer transit time components (78-208 ms) associated with some of the flow paths shown in

Figure 3(a), but, the ACF is a weighted average with the weighting factors emanating from the number of events as well as their intensity (i.e., number of fluorescent photons comprising the burst).[43] In addition, the transit time is not just a function of the flow velocity of the particles and the size of the probe volume, but also the bleaching lifetime,[12, 44] and therefore, these longer transit time components may not have been observed due to bleaching artifacts and/or molecules following paths that produce lower numbers of fluorescent photons due to the lower irradiance (see Figure 3(b)). However, the transit time calculated using the ACF did show close agreement with that calculated from the linear flow velocity and the average $1/e^2$ radius of the probe volume.

Gram(+) bacterial detection using single MBs. A calibration curve was constructed from oligonucleotides ranging in concentration from 0.5 to 10 fM that were prepared by adding different concentrations of target DNA sequences (synthetic complementary DNA sequence to the loop section of the MB) to a 0.5 nM solution of the MB. The MB and DNA targets were incubated for 5 min and then loaded into a 500μL syringe and pumped through the optical fiber chip at 0.01 mL/h (see Figure 3.6). Peaks above the discriminator threshold were counted as events and divided by the time of the experimental run (1 min) with the number of events plotted versus the concentration to construct a calibration curve, which is shown in Figure 7(a). The data points were fit to a linear function ($y = 3 \times 10^{-16}x + 4.0 \times 10^{-16}$) with an R^2 value of 0.97. Table 2 in the Supporting Information provides information on the calculation of the sampling efficiency (13.6%) for this system as well as the detection efficiency.

The identification of *S. aureus* was then performed using DNA extracted from 2,000 cells, which was then mixed on-chip with a 0.5 nM solution of the MBs in 50 mM borate buffer (pH 8.5). The solutions were pumped through the chip at 10μL/h and maintained at a

temperature slightly below the T_m of the loop/DNA complement to minimize formation of mismatches. As a negative control, DNA from *E. coli* was also extracted and mixed with the MB solution. *S. aureus* showed multiple events above the discriminator level (28,000 cps) due to the loop structure of the MB hybridizing to a complementary sequence contained within the genome of *S. aureus*, whereas the *E. coli* sample showed no events above this level. The events from the *S. aureus* predicted a DNA concentration (derived from the calibration curve) of 1.3 x 10^{-15} M. Based on the DNA copy number sampled during the experiment, more than one copy of the gene was present in each cell. If 20 copies of the gene were present in each cell, the data secured from the calibration curve would be in good agreement to that predicated on the input copy number. Kim *et al*. demonstrated that the copy number of the 16S ribosomal gene varies from 1 to 15.[47]

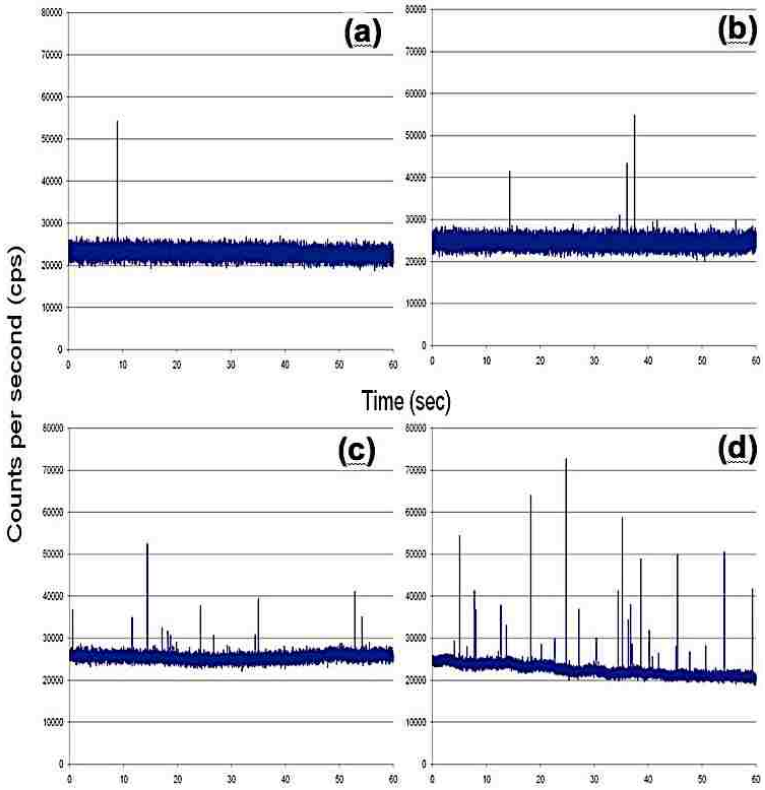

Figure 3.6 Complementary DNA was mixed with 0.5 nM of the MBs and pumped through the microfluidic chip at 0.01 mL/h. The target concentrations used in this case were; (a) 5.0 x 10^{-16} M; (b) 1.0 x 10^{-15} M; (c) 5.0 x 10^{-15} M; and (d) 1.0 x 10^{-14} M.

The limit-of-detection for this system is basically a single copy of DNA, indicating that the cell detection limit is 1 cell. However, the ability to detect a single copy depends on the single-molecule sampling efficiency to be near unity and the sampling throughput is relatively high. The sampling throughput is set by the linear velocity and the input volume requiring sample, with higher linear velocities increasing the throughput but dropping the single-molecule SNR due to reduced transit times limiting the amount of photons extracted from the molecule.[43] Also, larger probe volumes can enhance the sampling throughput, but this can reduce the SNR in the SNIMD measurements because of larger scattering contributions to the background.

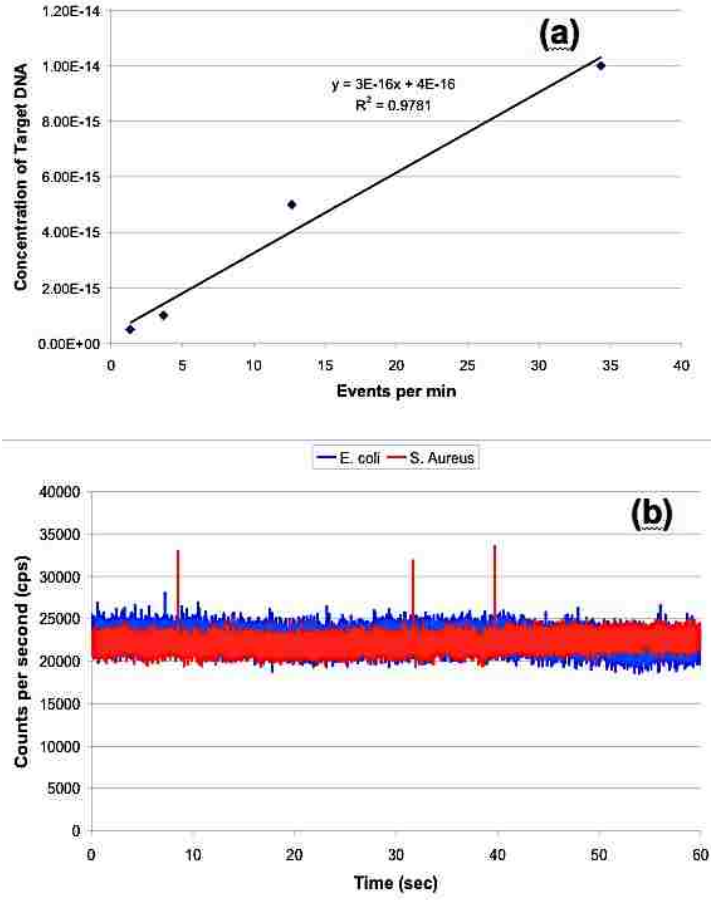

Figure 3.7 (a) Calibration curve generated from the data shown in Figure 6. The data points were fit to a linear function; $y = 3 \times 10^{15} x - 0.9291$, with $R^2 = 0.97$. (b) rDNA extracted from 2,000 *S. aureus* cells (Gram (+)) and mixed with the 0.5 nM MB solution. As a control, DNA from *E. coli* (Gram(-)) was extracted and mixed with the MB solution as well. The *S. aureus* showed 3 events above the discrimination level whereas the *E. coli* showed no events above this level.

3.4 Conclusions

We have demonstrated the ability to detect single molecules using a small footprint instrument coupled to microfluidics that will find applications where point-of-use measurements with near real-time results are required. In addition, the optical train consisting of integrated fiber optic cables to the microfluidic for both excitation and emission minimized end user optical alignment, which significantly reduced operator expertise requirements; only insertion of the cable termini into SMA connectors was required to install a new chip. Also, the implementation of a FPGA in conjunction with a diode laser and SPAD significantly reduced the instrument footprint compared to conventional single-molecule optical components and data processing electronics. As a demonstration of the utility of this instrument for analyses using SMD, MBs were designed to probe bacterial cells for the gene encoding the Gram(+) identity using *S. aureus* and *E. coli* as models.

In the current format, the target cells were isolated, lysed and the genomic DNA purified off-chip. However, we can envision adding additional fluidic sample processing modules to the existing microfluidic to provide the ability to fully prepare the sample prior to performing the single-molecule measurement. For example, we can select cells,[48-50] lyse the selected cells either chemically or electrically, isolate the target materials using solid-phase extraction,[51-53] and then perform the molecular reactions on the purified material.[54-56] This will create a fully integrated system to accept a variety of input samples, for example clinical samples used for *in vitro* diagnostics, prepare the samples and then perform SMD without requiring significant operator intervention or large amounts of operator expertise.

3.5 References

1. Gell, C.; Sabir, T.; Westwood, J.; Rashid, A.; Smith, D. A. M.; Harris, S. A.; Stockley, P. G. *Journal of Molecular Biology* **2008**, *384*, 264-278.

2. Haupts, U.; Rudiger, M.; Ashman, S.; Turconi, S.; Bingham, R.; Wharton, C.; Hutchinson, J.; Carey, C.; Moore, K. J.; Pope, A. J. *Journal of Biomolecular Screening* **2003**, *8*, 19-33.

3. Hintersteiner, M.; Auer, M. In *Fluorescence Methods and Applications: Spectroscopy, Imaging, and Probes*; Wolfbeis, O. S., Ed., **2008**; Vol. 1130, pp 1-11.

4. Kang, S. H.; Kim, Y. J.; Yeung, E. S. *Analytical and Bioanalytical Chemistry* **2007**, *387*, 2663-2671.

5. Moore, K. J.; Turconi, S.; Ashman, S.; Ruediger, M.; Haupts, U.; Emerick, V.; Pope, A. J. *Journal of Biomolecular Screening* **1999**, *4*, 335-353.

6. Neely, L. A.; Patel, S.; Garver, J.; Gallo, M.; Hackett, M.; McLaughlin, S.; Nadel, M.; Harris, J.; Gullans, S.; Rooke, J. *Nature Methods* **2006**, *3*, 41-46.

7. Qiu, H.; Ferrell, E. P.; Nolan, N.; Phelps, B. H.; Tabibiazar, R.; Whitney, D. H.; Nalefski, E. A. *Clinical Chemistry* **2007**, *53*, 2010-2012.

8. Wang, L.; Xu, G.; Shia, Z. K.; Jiang, W.; Jin, W. R. *Analytica Chimica Acta* **2007**, *590*, 104-109.

9. Wu, A. H. B.; Fukushima, N.; Puskas, R.; Todd, J.; Goix, P. *Clinical Chemistry* **2006**, *52*, 2157-2159.

10. Wabuyele, M. B.; Farquar, H.; Stryjewski, W.; Hammer, R. P.; Soper, S. A.; Cheng, Y. W.; Barany, F. *J. Am. Chem. Soc.* **2003**, *125*, 6937-6945.

11. Shera, E. B.; Seitzinger, N. K.; Davis, L. M.; Keller, R. A.; Soper, S. A. *Chem. Phys. Lett.* **1990**, *174*, 553-557.

12. Soper, S. A.; Shera, E. B.; Martin, J. C.; Jett, J. H.; Hahn, J. H.; Nutter, H. L.; Keller, R. A. *Anal. Chem.* **1991**, *63*, 432-437.

13. Erickson, D.; Sinton, D.; Li, D. Q. *Lab Chip* **2004**, *4*, 87-90.

14. Giudice, A.; Ghioni, M.; Biasi, R.; Zappa, F.; Cova, S.; Maccagnani, P.; Gulinatti, A. *J. Mod. Opt.* **2007**, *54*, 225-237.

15. Agrawal, A.; Zhang, C. Y.; Byassee, T.; Tripp, R. A.; Nie, S. M. *Anal. Chem.* **2006**, *78*, 1061-1070.

16. Yin, D. L.; Deamer, D. W.; Schmidt, H.; Barber, J. P.; Hawkins, A. R. *Opt. Lett.* **2006**, *31*, 2136-2138.

17. Dittrich, P. S.; Manz, A. *Anal. Bioanal. Chem.* **2005**, *382*, 1771-1782.

18. Yan, F.; Vo-Dinh, T. *Sensors and Actuators B-Chemical* **2007**, *121*, 61-66.

19. Mechery, S. J.; Zhao, X. J. J.; Wang, L.; Hilliard, L. R.; Munteanu, A.; Tan, W. H. *Chemistry-an Asian Journal* **2006**, *1*, 384-390.

20. Verpoorte, E. *Lab Chip* **2003**, *3*, 42N-52N.

21. Camou, S.; Fujita, H.; Fujii, T. *Lab Chip* **2003**, *3*, 40-45.

22. Seo, J.; Lee, L. P. *Sensors and Actuators B-Chemical* **2004**, *99*, 615-622.

23. Roulet, J. C.; Volkel, R.; Herzig, H. P.; Verpoorte, E.; de Rooij, N. F.; Dandliker, R. *Anal. Chem.* **2002**, *74*, 3400-3407.

24. Chabinyc, M. L.; Chiu, D. T.; McDonald, J. C.; Stroock, A. D.; Christian, J. F.; Karger, A. M.; Whitesides, G. M. *Anal. Chem.* **2001**, *73*, 4491-4498.

25. Bruno, A. E.; Maystre, F.; Krattiger, B.; Nussbaum, P.; Gassmann, E. *Trac-Trends in Analytical Chemistry* **1994**, *13*, 190-198.

26. Deng, J. J.; Huang, Y. T. *J. Lightwave Technol.* **1998**, *16*, 1062-1069.

27. Galarza, M.; De Mesel, K.; Baets, R.; Martinez, A.; Aramburu, C.; Lopez-Amo, M. *Appl. Opt.* **2003**, *42*, 4841-4846.

28. Galarza, M.; De Mesel, K.; Verstuyft, S.; Aramburu, U.; Lopez-Amo, M.; Moerman, I.; Van Daele, P.; Baets, R. *J. Lightwave Technol.* **2003**, *21*, 269-274.

29. Hubner, J.; Mogensen, K. B.; Jorgensen, A. M.; Friis, P.; Telleman, P.; Kutter, J. P. *Rev. Sci. Instrum.* **2001**, *72*, 229-233.

30. Litchinitser, N. M.; Abeeluck, A. K.; Headley, C.; Eggleton, B. J. *Opt. Lett.* **2002**, *27*, 1592-1594.

31. Ren, K. N.; Liang, Q. L.; Yao, B.; Luo, G. O.; Wang, L. D.; Gao, Y.; Wang, Y. M.; Qiu, Y. *Lab Chip* **2007**, *7*, 1574-1580.

32. Xiang, Q.; Hu, G. Q.; Gao, Y. L.; Li, D. Q. *Biosens. Bioelectron.* **2006**, *21*, 2006-2009.

33. Soper, S. A.; Ford, S. M.; Xu, Y. C.; Qi, S. Z.; McWhorter, S.; Lassiter, S.; Patterson, D.; Bruch, R. C. *Journal of Chromatography A* **1999**, *853*, 107-120.

34. Dharmasiri, U.; Witek, M. A.; Adams, A. A.; Osiri, J. K.; Hupert, M. L.; Bianchi, T. S.; Roelke, D. L.; Soper, S. A. *Anal. Chem.* **2010**, *82*, 2844-2849.

35. Lorenz, M. G.; Mengibar, L.; Entrena, L.; Sanchez-Reillo, R. In *Field-Programmable Logic and Applications, Proceedings*; Cheung, P. Y. K., Constantinides, G. A., DeSousa, J. T., Eds., 2003; Vol. 2778, pp 220-229.

36. Chowdhury, S. R.; Chakrabarti, D.; Saha, H. *Microprocessors and Microsystems* **2008**, *32*, 107-120.

37. Castro, A.; Okinaka, R. T. *Analyst* **2000**, *125*, 9-11.

38. Castro, A.; Williams, J. G. K. *Anal. Chem.* **1997**, *69*, 3915-3920.

39. Peng, Z.; Soper, S. A.; Pingle, M. R.; Barany, F. *Analytical Chemistry* **2010**, *82*, 9727-9735.

40. Hupert, M. L.; Guy, W. J.; Llopis, S. D.; Shadpour, H.; Rani, S.; Nikitopoulos, D. E.; Soper, S. A. *Microfluidics and Nanofluidics* **2007**, *3*, 1-11.

41. Ojo, K. K.; Tung, D.; Luis, H.; Bernardo, M.; Leitao, J.; Roberts, M. C. *FEMS Microbiology Letters* **2004**, *238*, 411-416.

42. Emory, J.; Soper, S. A. *Anal. Chem.* **2008**, *80*, 3897-3903.

43. Soper, S. A.; Mattingly, Q. L.; Vegunta, P. *Anal. Chem.* **1993**, *65*, 740-747.

44. Soper, S. A.; Nutter, H. L.; Keller, R. A.; Davis, L. M.; Shera, E. B. *Photochem. Photobiol.* **1993**, *57*, 972-977.

45. Peng, Z.; Soper, S. A.; Pingle, M. R.; Barany, F.; Davis, L. M. *Anal Chem*, *82*, 9727-9735.

46. Panchuk–Voloshina, N.; Haugland, R. P.; Bishop–Stewart, J.; Bhalgat, M. K.; Millard, P. J.; Mao, F.; Leung, W.-Y.; Haugland, R. P. *J. Histochem. Cytochem.* **1999**, *47*, 1179-1188.

47. Kim, J.-s.; Wang, N. *BMC Research Notes* **2009**, *2*, 37.

48. Adams, A. A.; Okagbare, P. I.; Feng, J.; Hupert, M. L.; Patterson, D.; Gottert, J.; McCarley, R. L.; Nikitopoulos, D.; Murphy, M. C.; Soper, S. A. *J. Am. Chem. Soc.* **2008**, *130*, 8633-8641.

49. Dharmasiri, U.; Balamurugan, S.; Adams, A. A.; Okagbare, P. I.; Obubuafo, A.; Soper, S. A. *Electrophoresis* **2009**, *30*, 3289-3300.

50. Dharmasiri, U.; Balamurugan, S.; McCarley, R. L.; Spivak, D.; Soper, S. A. *Electrophoresis* **2009**, *30*, 3289-3300.

51. Xu, Y. C.; Vaidya, B.; Patel, A. B.; Ford, S. M.; McCarley, R. L.; Soper, S. A. *Anal. Chem.* **2003**, *75*, 2975-2984.

52. Witek, M. A.; Llopis, S.; Wheatley, A.; McCarley, R.; Soper, S. A. *Nucleic Acids Research* **2006**, *34*, e74.

53. Witek, M. A.; Hupert, M. L.; Park, D. S. W.; Fears, K.; Murphy, M. C.; Soper, S. A. *Anal. Chem.* **2008**, *80*, 3483-3491.

54. Hashimoto, M.; Chen, P. C.; Mitchell, M. W.; Nikitopoulos, D. E.; Soper, S. A.; Murphy, M. C. *Lab Chip* **2004**, *4*, 638-645.

55. Chen, J. F.; Wabuyele, M.; Chen, H. W.; Patterson, D.; Hupert, M.; Shadpour, H.; Nikitopoulos, D.; Soper, S. A. *Anal. Chem.* **2005**, *77*, 658-666.

56. Hashimoto, M.; Hupert, M. L.; Murphy, M. C.; Soper, S. A.; Cheng, Y. W.; Barany, F. *Anal. Chem.* **2005**, *77*, 3243-3255.

CHAPTER 4 – DISCUSSIONS, CONCLUSIONS AND FUTURE WORKS

4.1 Discussions

In regard to the gene expression analysis of the AMPH gene, we are able to quantify and illustrate the amount of applied biological material to probing methods such as RT-qPCR and LDR-spFRET for plotting of calibration curves: copy number vs. fluorescence intensity, and copy number vs. number of single-molecule events for RT-qPCR and LDR-spFRET, respectfully. From this calibration plot we learn the methods detection limits, quantification parameters, and the techniques sensitivity. With this information we can compare and contrast the two methods to investigate the validity of the techniques as it relates to gene expression profiling.

For the proposed system to be realized, the utilization of analytical methods that show superior probing and detection capabilities is beneficial. The experimental data recovered in this work parallels gene expression profiling's conventional method RT-qPCR, with the proposed method LDR-spFRET (figure 4.1). This is accomplished by observing the gene AMPH, probing in an indistinguishable sequence area, and applying copy number concentrations in a congruent sequence area and applying copy number concentrations in a congruent fashion.

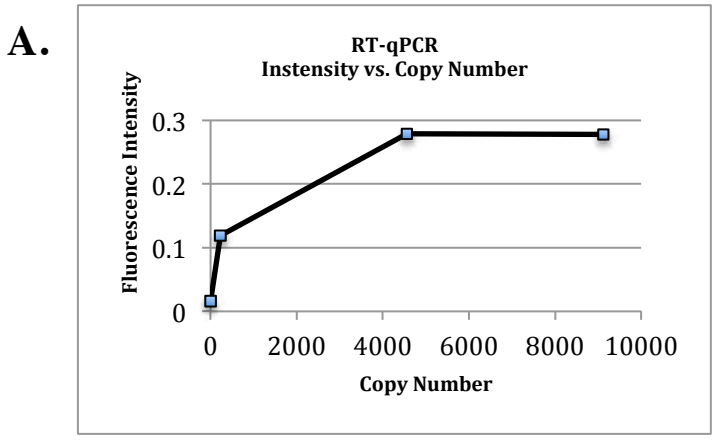

Figure 4.1 (A.) Calibration plots for the merit comparing of methods RT-qPCR.

B.

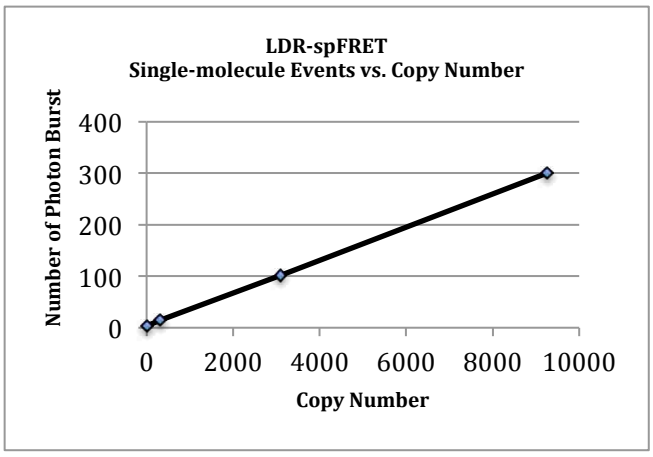

Figure 4.1 (B.) Calibration plots for the merit comparing of methods LDR-spFRET. Figure 4.1 (A., B.) The probing primers are both located in the same 152 (bp) gene sequence succession of the AMPH biomarker target. The biological samples were both at copy number concentration between 0-10,000. The experiment tests were replicated three times and plotting at their means.

Chapter 1 outlines the differences in RT-qPCR and LDR-spFRET, including the primer makeup, amplification and detection methods. When comparing the calibration plots of SMD via LDR-spFRET and RT-qPCR, we can ascertain that the linear nature of the plots directly correlates with the respected methods amplification process. LDR's method of sample probing depicts a linear progression. Conversely, the exponential amplification of the PCR method illustrates a curve, which emulates the nature of the sample probing process; a rapid exponential growth that then gives way to linearity limits due to enzyme and dye consumption. Furthermore, it has been realized that the amplification process is not necessary for SMD via LDR-spFRET. This, theoretically, negates the need for multiple thermo cycling to ensure linear amplification and real time quantification of targeted gene sequences. This factor makes the evolution of gene expression profiling by means of SMD via LDR-spFRET an advantageous and novel approach.

The recovered data points, which render the limit of linearity, demonstrated through experimental means constructs the graph in figure's 1.0 calibration plot of RT-PCR and deems it necessary to investigate the dynamic range. This can then be then used to correlate the sensitivity

merit in comparison the to the SMD technique. The lack of the linearity limits as defined in the nature of LDR's amplification process makes the calibration plot exploitable at all points. In this respect the utilization of all data points defining the graph/slope will be investigated to gage the sensitivity of the method, unlike PCR, where the dynamic range's slope is referenced for method sensitivity.

LOQ for RT-PCR: is dependent on the assay, in combination with the master mix and real-time PCR instrument. In regard to PCR it is noted that the mandate of an optimized assay-system is needed to detect a few copies (1-10 c/rxn) or a few hundreds with a higher reproducibility. Moreover, if the desired detection is less than 10 (or 100) copies, multiplication of replicates (of at least 5-10) must occur. However, this is only possible if the assay has been optimized, a high-quality qPCR instrument is available, and a high-quality master mix from one of the two market leaders (Roche and ABI) is being used. These aspects make the assay costly and not available to all researchers (e.g. labs with cost constraints). These parameters are not characteristic of LDR. Multiplying replicates, in theory, should not be necessary and SMD gives the ability to detect one copy number in a sample with the utilization of microfluidics in combination with LDR-spFRET. The instrumentation that SMD uses is not as contingent upon the master mix quality, due to the theoretical sampling efficiency of the instrumentation's probing volume and LDR's target gene discriminating parameters employed during SMD, which should theoretically illustrate a LOD, a single molecule. This work demonstrates that the quantification reliability; cost factors, biological sampling validity, and time elements are superior in regard to SMD.

4.2 Conclusions

In Conclusion, the sensitivity and versatility of single-molecule detection can eliminate steps required in multistep assays, in turn reducing analysis time. The present work shows, the means to eliminate PCR amplification by implementing a ligation assay directly on genomic DNA for gene expression profiling. Furthermore, thermal cycling can be negated due to high sensitivity yield by single-molecule detection. The specificity of the ligase enzyme applied to LDR gene probing coupled to spFRET of rMB's provided near real-time gene expression profiling even when the copy number of target sequences are as low as 300 copies.

While the conventional method PCR has drawn researchers to invest time in trying to reduce the processing time associated with PCR, the ability to perform analysis directly on genomic DNA and/or RNA using single-molecule detection possesses other unique advantages. Some advantages include: improved quantification using digital molecular counting for real-time readout, reduced reagent requirements, and elimination of post-PCR purification/isolation steps. This assay configuration will find novel applications where rapid low-volume sampling biological analyses are required.

4.3 Future Works

Introduction. Currently, no molecular diagnostic exists for stroke. The hypothesis is to develop a molecular diagnostic strategy including the biomarker panel, assay approach and the necessary hardware, for the point- of-care (POC) diagnosis of ischemic and/or hemorrhagic stroke, using mRNA expression profiling directly from whole blood with a processing time <20 min to accommodate effective therapeutic treatment of this disease. A fluidic bio-processor fabricated in polymers via micro-replication technology will provide autonomous sample processing and will be comprised of a fluidic motherboard possessing task-specific modules. The

sample-processing pipeline will be streamlined to generate a rapid assay turn-around-time affected using microfluidics and single-molecule detection. The output of the clinical sample processing will be molecular beacons undergoing single pair Fluorescence Resonance Energy Transfer (spFRET) that are digitally counted to provide exquisite analytical sensitivity.

Background. Stroke results from the occlusion or rupture of a blood vessel in or around tissue in the brain leading to this tissue being deprived of its blood supply. Stroke is a leading cause of death and disability in the United States. The two types of stroke - ischemic stroke (80-85%) resulting from vessel occlusion, and hemorrhagic stroke (15-20%) resulting from vessel rupture - cannot be differentiated on clinical grounds and furthermore, 30% of patients presenting stroke-like symptoms do not have stroke at all. It is imperative that stroke diagnosis be made quickly and accurately because ischemic and hemorrhagic strokes have different treatments and there is only a short time window for effective treatment. Current stroke diagnoses require the patient to be transported to a hospital and undergo a brain scan, usually with computed tomography (CT), which are very sensitive for the detection of hemorrhagic stroke but less so for ischemic stroke in the first hours of a stroke event; this typically delays therapy from starting for ~60 min upon arrival of the patient to a hospital. The current intravenous treatment for ischemic stroke (recombinant tissue plasminogen activator, rt-(PA)), reaches only 2% of patients and is absolutely contraindicated in hemorrhagic stroke. Delay in diagnosis is a major reason that this treatment reaches so few patients. Furthermore, the earlier treatment starts, the better the outcome. New approaches for speeding up and improving the accuracy of ischemic and hemorrhagic stroke diagnoses are therefore much needed to accommodate therapy. The purpose of this proposal is to develop a novel technology platform for the rapid and point-of-care (POC) molecular diagnosis of stroke using mRNA biomarkers.

Research Design and Methods. We will develop a simple flow-through modular fluidic bio-processor made from polymeric materials via replication micro-technologies to analyze the molecular content of PBMCs for the expression level of mRNAs that provide diagnostic information for ischemic and/or hemorrhagic stroke in a turn-around-time (TAT) less than 20 min. The fluidic bio-processor (see Figure 4.3.) accepts the input sample (whole blood), clears the blood of RBCs, neutrophils and platelets to produce the PBMC fraction, thermally and/or chemically lysis the PBMCs, isolates the total RNA using SPE, reverse transcribes the mRNAs into cDNAs, performs an LDR on the cDNAs using primers that carry reporter sequences for the target and readout of successful ligation events using spFRET. The use of spFRET obviates the need for a PCR step, which not only reduces processing time, but also produces exquisite analytical sensitivity.

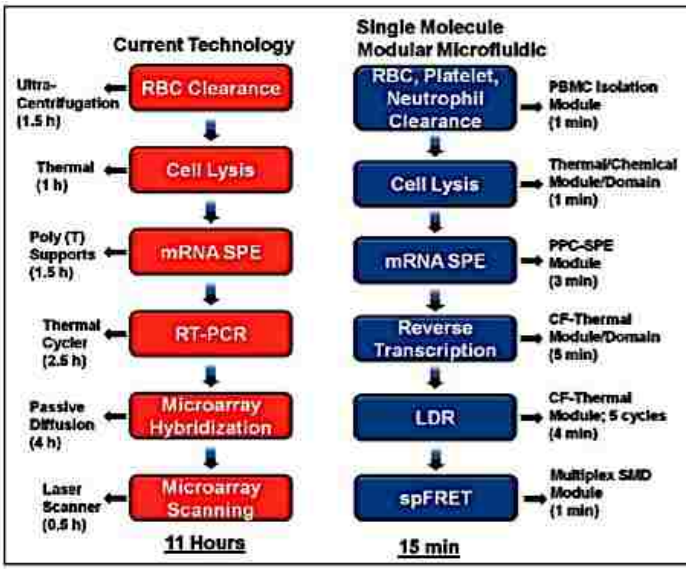

Figure 1. Processing pipelines using a conventional bench-top strategy for processing mRNAs specifically for obtaining expression data and the processing pipeline that will be employed in this POC system for the rapid reporting of mRNA signatures associated with stroke. In addition, the associated processing times for each step of the conventional and proposed methods for mRNA analysis is provided. The sample input for this system is whole blood, which is first subjected to a clearance step to isolate PBMCs (1 min) and then, thermal/chemical cell lysis (1 min), isolation of the RNAs using solid-phase extraction (3 min), reverse transcription (5 min), ligase detection reaction (4 min) and spFRET readout (1 min), producing a turn-around-time of ~15 min. The Research Design and Methods section will provide a description of each processing step and the fluidic device for its implementation.

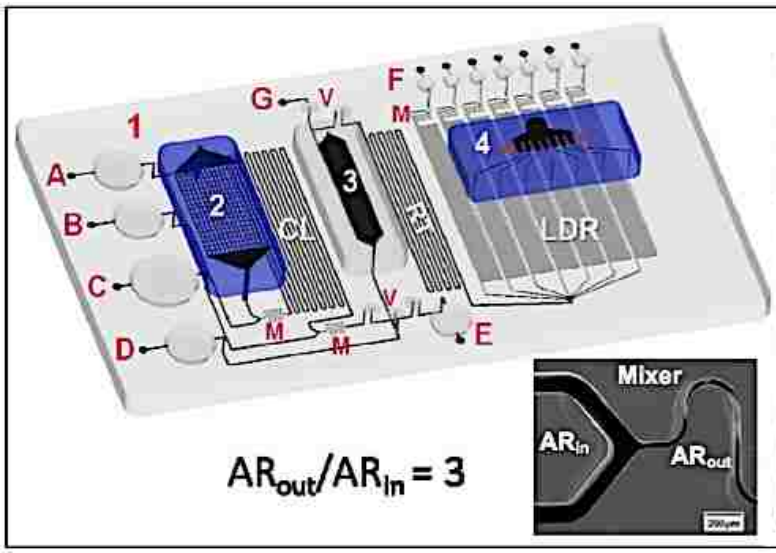

Figure 7. Fluidic bio-processor for the analysis of mRNAs in PBMCs. The fluidic bio-processor has 3 modules that are used for cell selection (depletion of RBCs, neutrophils and platelets), (**2**) SPE isolation/purification of RNA (**3**) and spFRET readout (**4**). These modules are "plugged" into a fluidic motherboard (**1**) that also contains thermal domains for performing cell lysis (**CL**), reverse-transcription (**RT**) and LDR (**LDR**). Heating of the thermal reaction domains are carried out by placing the fluidic bio-processor on Cu blocks set at the necessary temperatures. Also shown are locations of on-chip valves (**V**) pumps (**A-F**) and high-aspect ratio mixers (**M**). A – sample input; B – lysing buffer; C – SPE buffer; D – ethanol; E – RT cocktail; F – LDR cocktail; G – connection to off-chip vacuum pump.

Through this dialysis we will be able to correlate between normalized gene expression and hyper gene expression because of a stroke. Using these bio-makers will help differentiate between the two types of strokes and in turn potentially save a significant number of lives. While the proposed system is targeted for field diagnosis of stroke using mRNA biomarkers, the system can be envisioned for other applications as well that require quantitative expression analysis of mRNA. In the case of stroke diagnoses, the fluidic bio-processor can be configured to detect other biomarkers necessary for the diagnoses, such as serum proteins, without requiring hardware reconfiguring.

VITA

Brandon M. Young was born on February 5, 1985, in Rock Hill, South Carolina, United States of America (USA) and was raised in East Cleveland, Ohio from the age of two. He enrolled in Cleveland State University, Cleveland, Ohio, USA, in 2002 during his senior year of high school for post-secondary enrollment. From 2003-2007 he attended Bowling Green State University, Bowling Green, Ohio, USA where he earned dual Bachelor of Science degrees in chemistry and biology. For his master degree study in chemistry, he enrolled in Louisiana State University, Baton Rouge, Louisiana, USA where he earned his Master of Science degree in chemistry in December of 2011. In August of 2011, with the financial support from the Department of Chemistry of The University of North Carolina at Chapel Hill Chapel Hill, North Carolina, USA he begin his doctoral degree study in chemistry and studied under the guidance of Professor Steven A. Soper's research group to continue his work in analytical chemistry with an emphasis in biomedical engineering.